Response to Reviewers

Dear Yves,

Thank you for your comments on the initial draft that improved its clarity. We also greatly appreciate the extensive and thoughtful comments of the two reviewers that identified additional points of confusion. We have used the extra time you have given us to thoroughly revise the article. We have attempted to address the reviewers' comments while trying to simplify and improve the clarity of the remainder of the article. (As an example, we combined Figs. 9 and 10 to facilitate the comparison of the globally averaged mineral fractions of each experiment.)

One consequence of the extensive revisions is that a version showing the contrast of the original and revised articles is so marked up as to obscure the specific changes made in response to the reviewers. (Both latexdiff and Adobe Acrobat Pro gave marked-up changes that were similarly tangled and confusing.) As an alternative, our response to each of the reviewer comments below contains a precise reference to a page number or section of the revised article where a change was made. (Where the change is limited to a sentence or two, we simply quote the change in our response.) We think these references will make it clear how we have attempted to improve the article in response to the reviewers' comments.

Best wishes,

Ron Miller
Jan Perlwitz
Carlos Peréz García-Pando

Reviewer 1:

This article provides a detailed treatment of the partitioning of minerals into dust aerosols at emission, which is critical for capturing the many mineralogy-dependent impacts of dust, for instance on radiation, biogeochemistry, and clouds. The methodology developed in this work is described in detail, is (mostly) well justified (where possible; sometimes experimental constraints are not available), and assumptions and weaknesses of the approach are discussed in detail.

The methodology draws partly from the recent previous study of Scanza et al. (2015). In essence, it partitions minerals in the soil into suspended dust aerosols using brittle fragmentation theory for D<20 um, extended to D=50 um by the detailed measurements of Kandler et al. (2009). This empirical extension is necessary because the soil mineralogy in Claquin et al. (1999) and Nickovic et al. (2012) is described in terms of clay (D<2 um) and silt (2<D<50 um). Combined with several other improvements, for instance in the treatments of iron oxide and quartz, the methodology in this study is advanced over that in Scanza et al. (2015). As such, this article makes an important step in progressing dust cycle models, and therefore makes a substantial contribution to the field. I anticipate that I can recommend the article for publication, after the following comments have been addressed:

We appreciate the thoughtful comments, which have helped us to clarify and correct some important points.

The authors description of the brittle fragmentation theory (Kok, 2011) is not quite correct. Contrary to what is stated on p.3503, this theory does not reconstruct the aggregated soil size distribution. Brittle fragmentation theory does not need (or assume) a particular undisturbed soil size distribution, and in fact hypothesizes that the emitted dust size distribution is independent of the aggregated soil size distribution. This confusion is repeated at several places in the article, and I think in the companion article as well, and it should be corrected throughout.

Thanks for this correction. As the reviewer notes, the theory provides the size distribution of the emitted dust aggregates without reconstructing the distribution of the original undisturbed soil. The cumulative term accounts for the range of indivisible scales within the soil. For the materials used to test brittle fragmentation theory in a laboratory, this scale corresponds to a single value that is on the order of the crystal dimension. In contrast, dust particles are comprised of aggregates of different sized particles that are approximately irreducible during mobilization and fragmentation. The cumulative integral sums over the range of indivisible scales identified from the fully dispersed soil. Aggregates formed from smaller irreducible particles will obey the scale-invariant power law of brittle fragmentation across a larger range of emitted particle diameters. The cumulative basically acts to attenuate this power law at the smallest sizes that is beneath the indivisible scale of the the larger irreducible particles. Conversely, the emitted distribution exceeds this power law at larger silt sizes because aggregates are comprised of particles with nearly the entire range of indivisible scales. (The reviewer describes this equivalently, saying that aggregates at a certain diameter are comprised of all the particles with indivisible scales below that diameter: eq. 3, Kok PNAS 2011).

All this is now described in Sect. 2.1.2 (especially p. 12), and additional corrections are scattered throughout the revised article.

If I understand the methodology correctly, the authors are assuming that, except for iron

oxides, each aerosol is composed of an individual mineral, even when it is an aggregate.
Yes. We are interpreting the mineral fractions within each size category as the mass available for combination with other minerals. The size category corresponds to the dimensions of the aggregate rather than the diameter of the individual minerals contributing to the aggregate. This interpretation is consistent with the size distribution of each mineral measured by Kandler et al. (2009), where particle size refers to the aggregate.
This interpretation allows for an economical representation of mineral aggregates. The economy results from the fact that we don't explicitly track individual aggregates. Instead, we represent the minerals as an external mixture, assuming that they all have identical (or approximately identical) removal rates. The mineral fractions are interpreted as an average over all particles within the size category. Only for iron oxides do we explicitly represent mineral combinations. This is now discussed explicitly and in detail on p. 9 (last paragraph) through the end of the subsection.
That is, they scale the production of aggregated silt-sized aerosols of a given mineral by the prevalence of clay-sized particles of that same mineral. I would think that, in reality, the probability that a clay-sized particle ends up in a silt-sized aggregate depends on (among many other factors) on the fraction of other small (clay- sized?) particles in the soil, not just of the same mineralogy. Why did the authors make this assumption, and how do they expect it to affect their results? Some justification needs to be provided. Does this simplification explain some of the disagreements with measurements?
According to eq. 3 of Kok (PNAS 2011), the number of aggregates of diameter D scales with the volume fraction of indivisible particles with sizes below or equal to size D. The physical interpretation of this equation does not depend upon the identity of the minerals forming the aggregates, so we apply it to each mineral separately. Our application to individual minerals is consistent with the method used by Scanza et al. (2015). This is described in p. 18 ("We also assume that the emitted mass fraction of each mineral n at silt sizes consists of two contributions from the wet-sieved soil . . . ")
I also have a few minor comments:
Line 24-25 on p. 3500: The cohesive forces actually increase with particle size (e.g., Shao and Lu, 2000). What the authors probably mean to say here is that the cohesive forces per unit weight (or per unit surface area, which is more relevant for particle lifting) decreases with particle size.
We have revised our discussion to incorporate this qualification along with a citation to: Shao, Y., and H. Lu (2000), A simple expression for wind erosion threshold friction velocity, J. Geophys. Res., 105(D17), 2243722443, doi:10.1029/2000JD900304.
In Section 2.1.1 (p. 8): "Larger soil grains or aggregates are more easily lifted because this cohesion can be overcome by the wind stress acting over a larger area (Iversen and White 1982; Shao and Lu 2000."
Line 17 on p. 3503. Sow et al. (2009) actually argue that the size distribution depends significantly on wind speed. In addition to Gillette et al. (1974), better references here would be Shao et al. (2011) and Kok (ACP, 2011). Please correct that here and in the companion article (if appropriate).
We have incorporated this clarification in Sect. 2.1.2 (p. 11): "However, measurements suggest that for the smallest particles that are transported globally, the emitted size distribution is approximately independent of wind speed and soil properties (Gillette et al., 1972, 1974;

Gillette, 1974; Kok, 2011a, Shao et al., 2011)."

Line 25 on p. 3503. Reconstructing the aggregated soil size distribution from the fully dispersed one is very difficult and Im not aware of any theoretical models for this. I looked at the cited Shao (2001), but could find no reference to such a model. If this reference does present the (otherwise reasonable) assumption that the amount of aggregation scales with the clay fraction, can you provide a page number?

Our citation of Shao was based upon a misinterpretation of the cumulative integral of the fully dispersed size distribution, as described above. The lesson we are now deriving from Shao's Figure 4a is that clay size particles in the fully dispersed soil were originally present as aggregates at much larger diameters (between roughly 20 and 300 um). These aggregates are large enough to be entrained directly into the saltating layer by the drag of the wind. According to brittle fragmentation theory, the emitted size distribution includes aggregates that would be destroyed during measurements of the fully dispersed soil.

The assumption that the amount of emitted aggregates scales with the fully dispersed clay fraction derives from eq. 3 of Kok (PNAS 2011). It reflects the effect of the cumulative integral when considering different soil textures (and therefore different distributions of indivisible scales).

We have corrected the discussion in Sect. 2.1.2 (especially p. 12) to reflect these points.

I think d is a confusing variable name for the mass fraction, as many readers will inherently associate this with particle diameter. I suggest using a different variable name.

This is a good suggestion. We have replaced "d" (intended to indicated dust) with "a" for aerosol (in contrast to "s" for soil). This necessitated finding another variable name for soil type. We now refer to soil type and texture, respectively, using "α" and "β". (c.f. Table 5)

Since there are no strong constraints on the global dust emission rate, I think it makes little sense to force the total emission rate equal to some somewhat arbitrary figure (2224 Tg/year in this case). For future studies, I would suggest setting the dust emission proportionality constant either by forcing the global dust AOD to some constant value (since we do have constraints on that), or by calibrating to some observational data set such as AERONET.

Our original submission unintentionally gave the impression that we had some reason for choosing 2224 Tg of global annual emission. In fact, this value was a historical accident. Our comparison to observations is based upon mineral *fractions* that are independent of the global annual emission, and thus, we made no effort to adjust the global value. In the revised version (Sect. 2.2.3), we are explicit that the value of 2224 Tg is irrelevant to our comparison, which does not depend upon a particular value (p. 27, top).

Nonetheless, the reviewer raises a more general question about how to compare two simulations in a meaningful way. Despite identical global emission, the SMF and AMF experiments have emitted size distributions that are markedly different. Thus, the experiments have different particle lifetimes and thus different aerosol loads, resulting in different degrees of fidelity to observations. For this comparison, we agree with the reviewer that we should separately calibrate the global emission of each experiment using observations. Unfortunately, it is beyond the scope of this study to simulate the radiative effects of the different minerals (including their individual contributions to the total dust AOD). We have kept this caveat in mind in Section 4, where we compare the AMF and SMF size distributions and lifetimes.

Im a bit confused by the term accreted. Is this the same as aggregated? Can you give exact definitions of both terms?

We recognize the potential confusion identified by the reviewer. We were attempting to avoid confusing the aggregation of minerals with iron oxides with our frequent references to disaggregation of clays by wet sieving. In the revised version (top of Sect. 2.2.2, p. 22, top), we explicitly note that we are using two distinct terms to discourage this association.

Why does this article include a comparison to data at Tinfou, Morocco when part 2 contains an extensive evaluations against measurements? I think this needs some justification at the beginning of section 4.5.

We have two reasons for bundling the comparison of the size distribution at Tinfou to this article (that is otherwise a model description). First, the measurements at Tinfou are exceptionally detailed, allowing a more extensive model evaluation than is permitted by the other observations that are compared in the companion article. However, our main reason is that the comparison highlights some limitations of our method, and the need for future improvements. We felt that this discussion fit best in this article, whose focus is on the method. In the revised version (Sect. 4.5, p. 38 bottom), we try to motivate this organization. Nonetheless, we acknowledge that this is a somewhat arbitrary choice.

Figure 15: keeping the color scheme consistent for panels e-h would make the figure more readable.

We think this is generally good practice, which we have applied to the preceding figures (formerly Figs. 11-14, now Figs. 10-13). The problem for this particular figure is that quartz and iron oxides have a much smaller range of values compared to the ranges for feldspar and gypsum. We were not able to figure out how to choose a color scale that can incorporate both ranges while showing regional variations in detail for all minerals. In response to the reviewer request, we instead note explicitly in the figure caption for Fig. 14 (the former Fig. 15) that the color scale varies among the minerals.

Reviewer 2

The paper documents and preliminary evaluates the new methods of explicit calculation of dust aerosol mineral composition incorporated in the GISS ModelE. That was never done in full scale so far and is of great importance as dust mineralogy and chemical composition defines radiation effects of dust particles, their impact on atmospheric chemistry, and clouds. Currently models calculate dust size distribution but assume globally uniform mineral composition of dust particles. The authors show that the proposed approach gives results consistent with a few available observations of dust mineralogy. However, the simulations in this study do not account for radiative feedback of aerosols. It would be interesting to provide more detailed evaluation that would estimate the new approach from this point of view. The paper is well written and could be published after minor corrections.

At present, we don't account for radiative effects, whose representation within the model would require additional development and assumptions (about mixing rules and particle morphology, for example). Nonetheless, we agree that this will be a useful direction for future work, especially given the abundant measurements and retrievals of aerosol radiative diagnostics like optical thickness. (We are explicit about our neglect of radiative effects at the end of Sect. 2.3 at the top of p. 28.)

P. 3500, L 27-29: please clarify the sentence.

We have tried to make clear that the smaller soil particles that become aerosols are bound tightly to the soil by cohesive forces, and are unlikely to be lifted directly by the force of the wind. Instead, these smaller particles enter the atmosphere either because of the impact of a larger particle (whose kinetic energy overcomes the cohesive force) or because a larger particle disagregrates into a collection of smaller particles.

On p. 8, we write "Most of the smaller particles that are transported globally are entrained into the atmosphere during the fragmentation of aggregates that are bombarded by larger particles, or else are large enough to be lifted directly by the wind and disintegrated through repeated collisions (Shao et al., 1993; Kok, 2011b; Marticorena, 2014)."

P. 3504, L 5: You mean below 20 micron?

We have rewritten this section (2.1.2) to provide a more precise description of brittle fragmentation theory. According to this theory (Kok PNAS 2011), soil aggregates are distintegrated by repeated collisions resulting in particles with diameters that are almost entirely below a scale λ. Kok estimates this scale to be around 12 um, while noting that is an approximate upper bound. In our model, we assume that brittle fragmentation is the process that controls emission for particle diameters up to around 20 um.

In the revised version, we have elaborated our discussion of brittle fragmentation theory to address these points. This discussion starts on p. 11. At the bottom of p. 13, we note our assumption that "The specific range of validity is below 20 um."

P. 3505, L 1-2: Could you give a reference here?

This model behavior described by this sentence is noted to be consistent with the size distributions of each mineral in Fig. 1, which we note throughout the article is derived from measurements by Kandler et al. (2009).

P. 3506, L 10-18: Validity of the approach

At the end of Sect. 2.1.2 (last paragraph on p. 14 to the end of the section), we discuss approximations involved in our use of an empirical distribution to prescribe the size distri-

bution of emission within the silt size range. As noted in the text, we can only demonstrate the validity of this approach by using a more complicated model of emission that explicitly represents saltation and sandblasting. However, we note that the increase of emission with particle diameter is likely to be a robust consequence of the decreasing threshold for emission with diameter: "The increase of the emitted silt fraction with increasing particle size (Fig. 3, second panel from left) is probably a robust consequence of the wind speed threshold for emission that decreases with diameter within this size range (Iversen and White, 1982b)."

P. 3506, L 21-25: What would be if we take an external mixture?

We don't understand this comment. We are treating the different minerals as an external mixture. We have provided an expanded discussion of this point in Sect. 2.1.1 (the last paragraph on p. 9 through the end of the section).

P. 3509, (8): No, if (8) satisfies, then (6) will satisfy. Not vice versa.

We believe that any two of the three equations (6)–(8) are sufficient to establish the third.

P. 3509, (9) and (10): It is the same assumptions as in GOCART scheme.

On p. 13, we extend the comment of the reviewer to note that many current models of dust emission specify the emitted size distribution to be spatially uniform.

"The prescription of an emitted size distribution that is independent of location is shared by studies of the global dust cycle that do not resolve mineral variations (e.g. Miller et al., 2006; Albani et al., 2014). This approach has also been used by Scanza et al. (2015) to account for the effect of brittle fragmentation upon the aerosol mineral composition."

We reiterate this point on p. 18 in the context of the two equations cited by the reviewer. "As noted above, the assumption of an emitted size distribution that is spatially uniform is shared by many models, including those with uniform or else varying mineral content (e.g. Miller et al., 2006; Scanza et al., 2015)."

P. 3509: (11) just defines the amount of clay particle aggregated to silt sizes. What was the reason to talk about corrected size distributions? Are they consistent?

The reviewer is correct. We are 'correcting' the size distribution of the wet-sieved soil to create the aggregates that would be emitted after brittle fragmentation. This is consistent with the representation of Kok (PNAS 2011) that is described in Eqs. (1) and (2). However, instead of using a cumulative integral like Kok (Eq. 2), we restore the aggregates using a heuristic representation whereby the emitted silt includes a contribution from clay particles in the wet-sieved soil.

This is expressed on p.18 just above Eq. (13): "We also assume that the emitted mass fraction of each mineral n at silt sizes consists of two contributions from the wet-sieved soil. The emitted fraction combines soil mass at silt sizes along with clay particles whose aggregates were broken during wet sieving. This is expressed by Eq. (2), but we represent reaggregation more simply by augmenting emission at silt sizes in proportion to the fractional abundance of clay particles in the fully dispersed soil:"

P. 3510, L 21: Change predominately to predominantly

Done.

P. 3520, L 10-11: It is difficult to believe that this distribution is invariant.

We share this reservation for the larger size particles that are not subject to brittle fragmentation, and note this point explicitly. However, it is difficult to assess how much the distribution varies, given the paucity of size-resolved concentration measurements for individual minerals. As noted above, we discuss this approximation more fully in Sect. 2.1.2

(last paragraph on p. 14 to the end of the section).
P. 3531, L 23-26: It is consistent with the larger radiation effect of coarse fraction in comparison with a fine dust fraction discussed in the literature.
Our point here is that an increase at one size has to be compensated by a decrease at another, because the emitted size distribution of silt is based upon a normalized distribution derived from measurements. We have tried to express this more clearly in the final paragraph of Sect. 4.5 (p. 40).
P. 3532, L 24: Change crytalline to crystalline
Done. (Despite the kind efforts of the reviewers, we have probably introduced other typos during revision :)

Additional Comments by Zhang Xuelei, 1 March 2015

Here, I have four viewpoints for the authors and the editor to improving this paper.

1. Mineral composition has questions. This manuscript adopted the relative volume abundance of minerals deduced from single particle analysis to calculate the mass distribution as a function of particle size for common airborne minerals in Figure 1. The original data is from Table 1 of Kandler et al. (2009) with identified specific mineral phases. In Kandler et al. (2009) used the method in Kandler et al. (2007) to classified the mineral phases, but this method only identified the whole silicate (which could not further classified as illite, kaolinite and chlorite) and Kandler (2009) also written as All silicates except quartz are sorted into the silicates class, as the different silicate minerals cannot be distinguished from each other reliably by the elemental composition only. in section 4.3.2.1 line 11-14. The content of Table 1 in Kan2dler (2009) is low quality and unusable. This question directly influence the second challenge mentioned in Page 3501.

We agree that Kandler et al. assign identical size distributions to phyllosilicates and feldspars (as we noted in our original submission). We disagree that this makes Kandler et al.'s measurements 'low quality and unusable'. In general, the quality of measurements is meaningfully assessed only with respect to their specific application. Our application is to partition the silt fraction given by Claquin et al. (1999) into the size categories used by our transport model. We speculated in our original submission how the contrast between the size distribution of phyllosilicates and feldspars would alter our results. (In the revised version, we have expanded our discussion of the implications of any contrast. See the final paragraph of Sect. 4.5, p 40, along with the final paragraph on p. 42.). However, the commenter does not explain why this contrast would undermine any of our main conclusions.

2. iron oxides: The reported hematite abundances in Table 1 of Kandler et al. (2009) were obtained from the measured content of elemental Fe by EDX, and then each value multiply 20 percent. Thus, the result is almost similar values (0.5 percent-0.8 percent) in different size bins. To my experimental experience, the size of hematite particle is presented as particles less than 10 um. But the iron-rich particles indentified by individual particle analysis actually are the assemble of hematite, goethite, wuitite and so on. These iron-rich particles is the so called pure crystalline form and as an external mixture with other minerals. For hematite with nanometer sizes which attached to phyllosilicates is hard to be identified by individual particle analysis, and this attachment is also the external mixing. Because the internal mixing is meaning that a small particle was coated or partly immersed into a larger particle. Once nano-sized hematite particles attached to phyllosilicates would not effectively change size of silicates. The volume contribution is mainly from the iron-rich particles with micrometer sizes. As mentioned above, the usage of volume fraction of hematite in Fig. 11 of Kandler et al. (2009) is more plausible for calculation in Fig 1 of this manuscript. 2. The usage of internal mixture and external mixture in this paper is easy to comprehend as terms for calculating the complex refractive indices for optical properties of mineral mixtures.

High resolution images show that aerosols comprised of iron oxides are present as both pure crystals and as accretions on or within other minerals. In our model, we represent both forms because of the potential importance of this distinction to radiative forcing by iron oxides. However, we admit that our treatment is relatively simple in the absence of much guidance from observations. Our general strategy for representing iron oxides is discussed in

Sect. 2.1.1 starting on p. 10.

3. settling speed: As mentioned in page 3519 line 1-3, Settling speeds are proportional to mineral density, and the minerals have nearly identical densities except for iron oxides. Quartz has similar density (2.67 g/cm3) with compare to phyllosilicates (such as Kaolinite with 2.67 g/cm3), this means that both quartz and kaolinite have almost the same settling speed. Phyllosilicates with flake shape is easy fly in air than quartz, and the difference of morphology will obviously affect the settling speed (Li and Osada, 2007). If possible, the effect of morphologies of different mineral particles on their settling speeds should be taken into account in future works.

In general, dust aerosol models do not account for morphology in their representation of gravitational settling, and we have yet to add this effect. We appreciate the reference to Li and Osada (2007), who show that dust particles that most likely originated within Chinese deserts are largely spherical by the time they are observed in Japan. Li and Osada interpret this to mean that variations in particle morphology and their effect upon dry deposition are mainly important only near the source region. We have added this citation and a brief discussion to p. 10.

4. The core of the paper is built on the brittle fragmentation ¿ theory of Kok et al. (2011). **Once the core collapsed, and this manuscript will be collapsed.** *Many models simulate the dust size distribution as a sum of lognormal modes (e.g., Balkanski et al., 2007 and Zhao et al., 2010). This approach is computationally efficient for. . .*

Kandler et al. show that for clay minerals like illite, a large fraction of the aerosol mass is present at diameters larger than 2 μm, even though Claquin et al. (1999) find that within wet-sieved soil samples, clay minerals are present only at smaller sizes. (Kandler et al. use XRD to show that the total mass of clays and feldspars are comparable, so the presence of clay minerals at silt sizes cannot be explained by the misattribution of feldspars, even though the size distributions of the two minerals cannot be distinguished.) These measurements (and observations from other studies cited in the text) point to the need to consider silt-sized aggregates of clay minerals that are emitted as aerosols, but which are not present in measurements of the wet-sieved soil (a point also discussed by Claquin et al. 1999 and Shao 2001). We choose to calculate emitted aggregates using Kok's theory of brittle fragmentation. The commenter subsequently claims that other representations of the emitted size distribution provide a better fit to data, but assessing this claim is beside the point of our article. (In any case, brittle fragmentation theory has been shown to be consistent with a widening set of that have become available after Kok's initial study.) Our interest here is simply to relate the size distribution of the wet dispersed soil to the emitted size distribution. Again, aerosol measurements clearly show the presence of phyllosilicates at silt sizes, and our model needs to reproduce this behavior. We expect other representations of the emitted distribution proposed by the commenter would change our results only quantitatively.

Manuscript prepared for Atmos. Chem. Phys. Discuss.
with version 2014/09/16 7.15 Copernicus papers of the LaTeX class copernicus.cls.
Date: 6 September 2015

Predicting the mineral composition of dust aerosols – Part 1: Representing key processes

J. P. Perlwitz[1,2,*], **C. Pérez García-Pando**[1,2,*], **and R. L. Miller**[2,1,*]

[1]Department of Applied Physics and Applied Mathematics,
Columbia University in The City of New York, New York, USA
[2]NASA Goddard Institute for Space Studies, New York, New York, USA
[*]All authors contributed equally to this article.

Correspondence to: J. P. Perlwitz (jan.p.perlwitz@nasa.gov)

Abstract

Soil dust aerosols created by wind erosion are typically assigned globally uniform physical and chemical properties within Earth system models, despite known regional variations in the mineral content of the parent soil. Mineral composition of the aerosol particles is important to their interaction with climate, including shortwave absorption and radiative forcing, nucleation of cloud droplets and ice crystals, ~~coating by heterogeneous uptake~~heterogeneous formation of sulfates and nitrates, and atmospheric processing of iron into bioavailable forms that increase the productivity of marine phytoplankton. Here, aerosol mineral composition is derived by extending a method that provides the composition of a wet-sieved soil. The extension accounts for measurements showing significant differences between the mineral fractions of the wet-sieved soil and the ~~resulting~~emitted aerosol concentration. For example, some phyllosilicate aerosols are more prevalent at silt sizes, even though they are nearly absent at these diameters in a soil whose aggregates are dispersed by wet sieving ~~during analysis~~. ~~We reconstruct the undispersed size distribution of the original soil that is subject to wind erosion. An empirical constraint upon the relative emission of clay and silt is applied that further differentiates the soil and aerosol mineral composition.~~We calculate the emitted mass of each mineral with respect to size by accounting for the disintegration of soil aggregates during wet sieving. These aggregates are emitted during mobilization and fragmentation of the original undispersed soil that is subject to wind erosion. The emitted aggregates are carried far downwind from their parent soil. The soil mineral fractions used to calculate the aggregates also include larger particles that are suspended only in the vicinity of the source. We calculate the emitted size distribution of these particles using a normalized distribution derived from aerosol measurements. In addition, a method is proposed for mixing minerals with small impurities composed of iron oxides. These mixtures are important for transporting iron far from the dust source, because pure iron oxides are more dense and vulnerable to gravitational removal than most minerals comprising dust aerosols. A limited comparison to measurements from North Africa shows that the ~~extension brings the model into~~model extensions

result in better agreement, consistent with a more extensive comparison to global observations as well as measurements of elemental composition downwind of the Sahara, as described in companion articles.

1 Introduction

Climate perturbations by soil dust aerosols created by wind erosion depend fundamentally upon the physical and chemical properties of the aerosol particles. However, Earth system models typically assume that soil dust aerosols have globally uniform composition, despite known regional variations in the mineral composition of the parent soil. Perturbations by dust to the energy and water cycles depend upon aerosol radiative forcing (Miller et al., 2004, 2014; Perlwitz and Miller, 2010), whose solar component is strongly related to the presence of iron oxides (Sokolik and Toon, 1996, 1999; Tegen et al., 1997; Redmond et al., 2010; Wagner et al., 2012; Moosmüller et al., 2012). Forcing at thermal wavelengths also varies with source mineral content (Turner, 2008). Absorption of solar radiation by dust alters the photolysis of ozone (Bian et al., 2003), while influencing chemical reactions of other trace gases (Goodman et al., 2000; Usher et al., 2003; Chen et al., 2011). The rates of heterogeneous chemical reactions on the dust particle surface that form coatings of sulfate, nitrate, chloride, or organics during atmospheric transport depend on the dust mineral and chemical composition (Dentener et al., 1996; Russell et al., 2002; Bian and Zender, 2003; Krueger et al., 2004; Bauer and Koch, 2005; Sullivan et al., 2007; Matsuki et al., 2010; Rubasinghege et al., 2013). Dust aerosols influence cloud formation (and the associated radiative forcing) by serving as nucleation sites for cloud droplets and ice crystals (Johnson, 1982; Feingold et al., 1999; Sassen, 2002; DeMott et al., 2003; Twohy et al., 2009; Seifert et al., 2010). The nucleation properties of dust depend upon their hygroscopicity and shape ,that in turn depend upon their mineral composition (Frinak et al., 2005; Kelly et al., 2007; Hatch et al., 2008; Ma et al., 2012; Hatch et al., 2014; Zimmermann et al., 2008; Hoose and Möhler, 2012; Murray et al., 2012; Atkinson et al., 2013; Yakobi-Hancock et al., 2013). Bioavailable iron within dust, transported to remote regions and processed during trans-

port (Shi et al., 2011; Takahashi et al., 2011; Ito, 2012), ~~fertilizes~~catalyzes photosynthesis by ocean phytoplankton, ~~influencing~~increasing carbon dioxide uptake and influencing the global carbon cycle (Jickells et al., 2005; Maher et al., 2010; Shi et al., 2012; Schulz et al., 2012). Dust is associated with respiratory and cardiovascular disease, along with epidemics of ~~meningoccocal~~meningococcal meningitis in the African Sahel (Pérez García-Pando et al., 2014a, b), where iron from dust particles may foster bacterial growth and weaken the immune system.

Deriving aerosol mineral composition requires global ~~maps derived from measured regional variations~~knowledge of soil mineral content. Claquin et al. (1999) proposed that the soil mineral fractions are approximately related to the soil type, which is available from global atlases (see also Nickovic et al., 2012; Journet et al., 2014). However, Claquin et al. (1999) noted that the mineral content of the emitted aerosol may differ from that of the parent soil ~~for two reasons~~. ~~First, measurements~~Measurements of mineral fractions are based upon wet sedimentation (or "wet sieving") techniques that disturb the soil sample, breaking aggregates that are found in the original, undispersed soil that is subject to wind erosion. Wet sieving alters the soil size distribution, replacing aggregates that are potentially mobilized as aerosols with a collection of smaller particles (Shao, 2001; Choate et al., 2006; Laurent et al., 2008). ~~Second, certain particle sizes (and the minerals comprising these particles) are preferentially emitted and converted into aerosols.~~ Size-resolved measurements of emission show that silt sizes are ~~emitted~~mobilized in greater proportion compared to clay (e.g. Gillette et al., 1974; Sow et al., 2009; Kok, 2011b). ~~Emission of minerals~~Minerals like phyllosilicates that are commonly ~~found in~~emitted as aggregates will be underestimated where ~~the aggregates are fragmented during~~their size distribution is characterized after wet sieving.

The challenge remains to derive mineral fractions of the emitted dust based upon their fractions measured in wet-sieved soils. Previous attempts to predict the aerosol mineral composition have generally neglected the effects of wet sieving (Hoose et al., 2008; Atkinson et al., 2013; Journet et al., 2014). Calculation of how the particle size distribution and mineral composition of the soil are modified during emission is ~~also~~ complicated (e.g. Shao,

2001; Alfaro and Gomes, 2001; Grini et al., 2002), although recent studies have proposed simplifications (Kok, 2011b; Scanza et al., 2015). Finally, representations of aerosol mineral composition need to account for mixtures of minerals. Examination of individual particles shows that iron, an element that is central to many climate processes, is often found as trace impurities of iron oxide attached to aggregates of other minerals (Reid et al., 2003; Scheuvens et al., 2011; Lieke et al., 2011; Deboudt et al., 2012; Scheuvens and Kandler, 2014).

In this article, we ~~extend previous models~~propose a model of dust mineral composition to address these challenges. Some of the extensions of our model have been introduced previously (Kok, 2011b; Scanza et al., 2015). In Sect. 2, we ~~reconstruct the undispersed soil~~use measurements of the fully dispersed soil to calculate the emitted size distribution of each mineral~~and calculate its modification during emission~~. We also calculate mixtures ~~containing~~of minerals with iron oxides to account for the transport of iron to remote regions. In Sect. 3, we describe simulations with the NASA Goddard Institute for Space Studies (GISS) Earth System ~~ModelE~~ModelE2 that show the effect of our extensions. In Sect. 4, we describe the geographical distribution of emission and surface concentration for each mineral and its mixture with iron oxide, while using an intermediate model version to identify the origin of improved behavior in our new model ~~,~~ that is documented here and in the companion articles. We summarize the new features of our model in Sect. 5.

Our model extensions are motivated by observations. In Sect. 4, we show that our new model is in better agreement with aerosol measurements at a site in North Africa after ~~correcting~~accounting for the effects of wet sieving. Detailed comparison of the model to a broader array of observations is deferred to companion articles. In Perlwitz et al. (2015), we compare our predicted aerosol distribution to a new global compilation of mineral measurements from nearly sixty studies. In Pérez García-Pando et al. (2015), we evaluate our results using observations from the Izaña Observatory, where elemental composition of Saharan dust has been measured for the past decade.

2 The mineralogical dust cycle model

2.1 Overview

2.1.1 Modeling challenges

Our aim is to predict regional variations of aerosol mineral composition as a function of particle size. For comparison, ~~ModelE~~ModelE2 currently predicts the size distribution of dust aerosols, but assumes a globally uniform mineral content (Miller et al., 2006). Regional variations in soil mineral composition lead to variations in dust aerosol composition. However, deriving aerosol mineral content also requires knowledge of how the size distribution of the parent soil ~~along with its transformation~~is transformed during the emission process. Here, we discuss some of these challenges, before describing our algorithm in Sect. 2.2.

Claquin et al. (1999) proposed that soil mineral content is related to the soil type provided by the Digital Soil Map of the World (DSMW), compiled by the Food and Agriculture Organization (FAO) of the United Nations (FAO, 1995, 2007). For the clay-sized fraction of the soil (with particle diameters up to $2\,\mu m$), the DSMW soil type is used to estimate the fractional composition of phyllosilicates (illite, kaolinite and smectite) along with calcite and quartz. Similarly, for the silt-sized soil fraction (with diameters between 2 and $50\,\mu m$), soil type is used to estimate the fractional composition of calcite, quartz, feldspar, gypsum and hematite. These minerals were chosen because of their relative abundance and potential importance to climate and biogeochemical processes, although other minerals are present in arid soils. The relation between soil type and fractional mineral abundance within the clay and silt-size categories is summarized in the Mean Mineralogical Table (MMT; Table 2 from Claquin et al., 1999). Subsequent studies have refined the proposed relation between soil type and mineral composition (Nickovic et al., 2012; Journet et al., 2014). Estimating the soil mineral composition additionally requires information about the fraction of clay and silt-sized particles present at each location, available from global databases of soil texture (Webb et al., 1993; Reynolds et al., 2000; Shangguan et al., 2014).

Claquin et al. (1999) note that their MMT introduces ~~two~~various sources of uncertainty for dust aerosol modeling. First, the relation between mineral composition and soil type is derived from a limited amount of measurements that are particularly scarce in the arid and semi-arid areas that contain dust sources. Second, this relation assumes that regional variations in mineral content within a particular soil type can be neglected. Third, measurements are based on wet sedimentation ("wet sieving") techniques that disturb the soil samples, breaking the aggregates that are found in the original, undispersed soil that is subject to wind erosion. Wet sieving alters the soil size distribution, replacing aggregates with a collection of smaller ~~and relatively loose~~ particles (Shao, 2001; Choate et al., 2006; Laurent et al., 2008). Techniques that minimize the breaking of the aggregates (McTainsh et al., 1997; Marticorena et al., 1997) are available to characterize the size distributions of North African and Chinese soil samples (Chatenet et al., 1996; Mei et al., 2004). However, these measurements remain very limited, are based upon a variety of analytical methods (Laurent et al., 2008), and provide the size distribution of only the bulk soil rather than distinguishing among individual minerals. Wet sieving is also used to characterize the soil texture in global datasets that give the fraction of clay, silt and sand-sized particles at each location (e.g. Shangguan et al., 2014). Claquin et al. (1999) emphasize that differences ~~of~~ in the mineral size distribution between wet-sieved soils and the ~~original undispersed soil that undergoes mobilization~~emitted aerosol particles are potentially important and merit further examination. In the absence of knowledge about this difference, previous studies have assumed that the emitted size distribution of each mineral closely resembles that of the wet-sieved soil (Claquin et al., 1999; Hoose et al., 2008; Atkinson et al., 2013; Journet et al., 2014).

~~Modification of the soil size distribution by~~Differences between the size distribution of the soil after wet sieving and during emission ~~is~~are potentially large. Figure 1 shows the ~~mass~~volume distribution as a function of particle size for common airborne minerals at Tinfou, Morocco during the Saharan Mineral Dust Experiment (SAMUM) campaign of 2006 (Kandler et al., 2009). Calculation of these distributions is described in ~~page 2 of the Supplementand is based upon measurements of collections of aerosol particles that~~

~~are sorted by size~~the Supplement. Each particle consists of a single mineral or aggregates of different minerals. For example, images suggest that iron oxides are consistently present both in pure crystalline form and as small impurities attached to other minerals (e.g. Fig. 2.1f and g of Scheuvens and Kandler, 2014). ~~The measurements are sorted~~Figure 1 distinguishes between conditions of high and low aerosol concentration. The main difference between the two conditions is that larger-sized particles are missing from the low-concentration events (Fig. 1, top row), suggesting that these particles have been removed during gravitational settling following their mobilization at a distant source. In contrast, the presence of larger particles at times of high concentration (Fig. 1, bottom row) suggests that this size distribution is a better indicator of the emitted size distribution.

Figure 1 shows that the mass of ~~phyllosilicates~~phyllosilicate aerosols like illite and kaolinite is ~~predominately~~predominantly within silt particle sizes. That is, ~~the phyllosilicates~~ phyllosilicate aerosols that are nominally "clay" minerals are observed mainly ~~within larger silt-sized aerosols~~at larger silt sizes. This is corroborated by aerosol measurements at other locations where clay ~~particles and~~ aggregates routinely exceed 2 µm in particle diameter (e.g., Leinen et al., 1994; Arnold et al., 1998; Reid et al., 2003; Alastuey et al., 2005; Jeong and Nousiainen, 2014). Wet sieving breaks up these larger particles, and models that do not account for this potentially allow a significant fraction of phyllosilicates to ~~disperse~~travel unrealistically far from their source ~~by underestimating~~as a result of insufficient gravitational deposition. This has implications for the delivery of phyllosilicate iron to fertilize photosynthesis within distant marine ecosystems (Journet et al., 2008).

The presence of significant clay mass at silt diameters argues that aggregates in the original soil ~~size distribution~~ subject to wind erosion ~~is~~are significantly dispersed by wet sieving. The ~~alternation of carbonates and their distribution with respect to size~~alteration of the carbonate size distribution during emission (Caquineau et al., 1998) suggests that they too are modified during the soil analyses used to construct the MMT. An important challenge ~~for modeling the aerosol size distribution~~ is thus to ~~reconstruct the undispersed size distribution of the soil. A related challenge is to represent the modification of this size distribution as soil~~particles are mobilized and converted into aerosols~~calculate the emitted~~

size distribution of each mineral, given that information is only available about the fully dispersed soil .

Direct entrainment by the wind of the smaller ~~dust~~soil particles that travel thousands of kilometers downwind from their source (whose diameters are generally below 20 µm) is ~~small due to the strong cohesive forces binding soil particles into aggregates of larger sizes~~hindered by the cohesive force that binds adjacent particles (Iversen et al., 1976). ~~Paradoxically, larger and heavier~~Larger soil grains or aggregates are more easily lifted because ~~their cohesive forces are small~~this cohesion can be overcome by the wind stress acting over a larger area (Iversen and White, 1982a; Shao and Lu, 2000).

Most of the smaller particles that are ~~dispersed~~transported globally are entrained into the atmosphere during the fragmentation ~~of clay and silt aggregates, either by saltation bombardment by larger sand-sized particles (with diameters between 50 and 2000 µm) or the fragmentation~~ of aggregates that are bombarded by larger particles, or else are large enough to be lifted directly by the wind and disintegrated through repeated collisions (Shao et al., 1993; Kok, 2011b; Marticorena, 2014). Fragmentation is an important source of clay-sized aerosols, although the abundance of phyllosilicate mass at silt sizes in Fig. 1 makes it clear that many soil aggregates are not ~~broken~~completely disintegrated into clay-sized aerosols during mobilization.

An additional modeling challenge is that different minerals may have different size distributions in the soil and may not be equally susceptible to disaggregation and fragmentation during wet sieving and emission, respectively. The size distribution of each mineral in Fig. 1 is normalized with respect to its total volume, allowing comparison of the characteristic particle size between different minerals. For example, Fig. 1 shows that a greater fraction of quartz mass is found at large particle sizes, compared to other minerals. Differences in the aerosol size distribution among minerals may result from contrasting size distributions in the parent soil as well as different aggregation and fragmentation properties of each mineral. A model must account for these contrasts to reproduce observations that far-travelled aerosols are depleted in quartz compared to the fraction of this mineral in the parent soil (Glaccum and Prospero, 1980; Jeong, 2008).

In Sect. 2.2, we describe a method to calculate the mineral composition of soil dust aerosols. We begin by calculating regional variations in the soil mineral content following Claquin et al. (1999), through a combination of an MMT and a global atlas of soil texture. We propose two extensions to address assumptions noted by that study. First, we describe a semi-empirical method ~~to reconstruct the undispersed size distribution of soil particles, prior to the wet sieving, and its modification during emission~~that follows (Kok, 2011b) to calculate the size distribution of emitted minerals based upon measurements of the soil after dispersion by wet sieving. This extension is described in more detail in Sect. 2.1.2.

~~Our second extension is to account for mixtures of different minerals. Individual particles comprising soil dust aerosols are often observed as mixtures of distinct minerals (Kandler et al., 2011; Scheuvens and Kandler, 2014; Jeong and Nousiainen, 2014), whose representation imposes a potentially large computational burden.~~Our second extension is to account for mixtures of minerals that are often observed within a single aerosol particle (Kandler et al., 2011; Scheuvens and Kandler, 2014; Jeong and Nousiainen, 2014). For example, iron oxides are often present as small impurities within other minerals (Kandler et al., 2007; Scheuvens et al., 2011). Representation of mixtures imposes a potentially large computational burden. For example, the number of combinations consisting solely of mineral pairs increases geometrically with the number of represented minerals.

For minerals removed from the atmosphere at the same rate, their combination can be represented as an external mixture, requiring no additional prognostic variables. ~~The rate of aerosol removal is distinguished in part by particle density that controls the speed of gravitational settling. Many minerals commonly observed to comprise dust particles have similar densities, suggesting that external mixing is a reasonable idealization that is attractive for its computational simplicity. (As a caveat, we note that particles of similar density that experience similar rates of gravitational settling may nonetheless be differentiated during wet deposition through contrasts in mineral solubility. We neglect this complexity in the present study.)~~In this case, the mineral fraction at a particular size is interpreted as the fractional mass of that mineral that is present either in pure form or as

an aggregate. In the latter case, it is the diameter of the aggregate that is used to assign a size category. As an example, a 25 % mass fraction of illite in the 4 to 8 µm category means that the particles within this size range consist on average of 25 % illite by mass. (By treating mineral combinations as external mixtures, we do not explicitly track the mass fractions of individual aggregate particles, so a fraction of 25 % at a particular location might represent a combination of particles with 20 % and 95 % illite, for example.) In this example, the particle diameter does not represent the dimension of the aggregated illite, whose diameter is smaller and possibly outside of this size category. Instead, it is the composite particles containing illite (aggregated with other minerals) that have diameters within the 4 to 8 µm size category. This interpretation is consistent with the measurements of Kandler et al. (2009), whose mass fractions represent the contribution of each mineral to particles of a particular size and not the size distribution of individual minerals.

The rate of aerosol removal is distinguished in part by particle density that controls the speed of gravitational settling. Many minerals commonly observed to comprise dust particles have similar densities, suggesting that external mixing is a reasonable idealization that is attractive for its computational simplicity.Mineral fractions also evolve during wet scavenging as a result of contrasts in mineral solubility and during gravitational settling through contrasts in particle shape. We neglect both sources of complexity in the present study, although Li and Osada (2007) suggest that the latter effect is important near source areas.

~~Iron oxides,~~In contrast, iron oxides like hematite and goethite~~, are an exception. Their density is~~ have densities that are twice that of the other minerals, and would thus be removed by gravitational settling within roughly half the distance from their source. ~~However, iron oxides can exist as small impurities that are internally mixed with other minerals (Kandler et al., 2007; Scheuvens et al., 2011). These accretions~~This density contrast means that mineral combinations containing iron oxides cannot be represented implicitly as external mixtures like combinations of other minerals. Iron oxide mixtures must be treated explicitly as separate prognostic variables that are distinct from pure crystalline forms of this mineral. In general, impurities of iron oxides are only a small fraction of the total

particle mass, and only slightly perturb the particle density that is determined primarily by the ~~density of the host mineral~~host mineral (Kandler et al., 2007; Scheuvens et al., 2011). Iron oxides present as a small impurity will travel farther than in their pure, crystalline form.

To our knowlege, measurements of mineral mixtures within individual aerosol particles are mostly anecdotal and provide only limited guidance about the combinations that need to be represented by a global model. In this study, the only combinations we represent explicitly are internal mixtures of iron oxides with another mineral, following Balkanski et al. (2007) and Scanza et al. (2015). ~~This assumes that the former is present in small enough concentration to make a negligible perturbation to the particle density.~~Aggregates of other minerals will be represented implicitly as external mixtures, assuming that the removal rate of each mineral is approximately the same. Our construction of mixtures with iron oxides is described in Sect. 2.2.2. Previous treatments of aerosol mineral content have addressed the role of clays and feldspars as ice nuclei (e.g. Hoose et al., 2008; Atkinson et al., 2013), circumventing the consideration of iron oxide transport and mineral combinations. Our treatment of iron oxide impurities is possibly more speculative and subject to revision than the remainder of our method. Nonetheless, we address ~~their transport because of their~~ transport of this mineral because of its importance for shortwave absorption and deposition of bioavailable iron, even though we don't consider these applications in this study.

Our extensions to Claquin et al. (1999) are semi-empirical~~and based upon limited size-resolved measurements of aerosol minerals. Ultimately, we hope that our semi-empirical approach will be made unnecessary by routine measurements of undispersed soil particle size and a more physically based model of emission. In the meantime, we illustrate the validity of~~, but we evaluate our approach by comparison to ~~an extensive~~ a global compilation of measurements, as described in Part 2 of this article (Perlwitz et al., 2015) and in Pérez García-Pando et al. (2015).

2.1.2 Observational constraints upon the emitted size distribution

The transformation of the particle size distribution of the (undispersed) parent soil into the emitted size distribution is a complicated process that depends upon wind speed and the

physical properties of the soil and land surface (Shao, 2001; Alfaro and Gomes, 2001; Grini et al., 2002; Marticorena, 2014). However, measurements suggest that for the smallest particles ~~(including the far-travelled particles~~ that are transported globally~~)~~, ~~the~~ , the emitted size distribution is approximately ~~invariant,~~ independent of wind speed and soil properties (Gillette et al., 1972; Gillette et al. 1974; Gillette, 1974; ~~Sow et al., 2009~~Kok, 2011a; Shao et al., 2011). ~~The theory of brittle fragmentation suggests that this is likely a robust result, despite the limited measurements of size-resolved emission (Kok, 2011b). We will use this approximate invariance to calculate the emitted size distribution, after reconstructing the distribution of the original, undispersed soil.~~

~~Kok (2011b) provides a theory for the emitted volume as a function of particle diameter D that begins with the size distribution for a soil that is fully dispersed, for example, by wet sieving. First, the size distribution of the undispersed soil, $u(D)$ is approximately reconstructed using a method proposed by Shao (2001), who assumes that the number of reconstructed aggregates with diameter D is proportional to the fraction of wet-sieved particles smaller than D. The qualitative effect of this method is to redistribute the smallest particles in the wet-sieved soil toward larger sized aggregates in the original soil (cf. Fig. 4 of Shao, 2001). Next, the modification during emission of the size distribution of the original soil is calculated assuming brittle fragmentation. This process is assumed to control the emitted size distribution for particle diameters less than roughly 20 μm (Above this diameter, variations in wind speed are expected to have influence.) Within this range, the size distribution of the emitted dust volume (V) is:~~

The theory of brittle fragmentation has been invoked to suggest that this invariance is robust, despite limited measurements of size-resolved emission (Kok, 2011b). In arid soils, mineral aggregates are typically most abundant at diameters between a few tens and a few hundred microns, according to measurements that minimally disturb the aggregates (c.f. Fig. 4a of Shao, 2001). Brittle fragmentation theory proposes that energetic and repeated collisions, in this case between soil aggregates mobilized by saltation, will result in emitted aggregate diameters that are mostly smaller than a scale λ. According to this theory, the number concentration $\mathcal{N}$ of emitted particles varies inversely with the square

of the diameter D:

$$\frac{d\mathcal{N}}{d\ln D} \propto \frac{1}{D^2} \exp\left[-\left(\frac{D}{\lambda}\right)^3\right] \text{ for } D > x_0, \quad (1)$$

where the exponential imposes an upper bound on the emitted size range near diameter λ. The inverse-square dependence in Eq. (1) remains valid for diameters as small as x_0, the "indivisible" scale, where the material properties of the individual particles comprising the aggregates resist further disintegration.

For soil aggregates, Kok (2011b) proposes that there is a range of indivisible scales that is given by the distribution of soil particle diameters D_s after wet sieving, when aggregates have been dispersed and further disintegration is difficult. Then, if $p(D_s)\,dD_s$ is the distribution of wet-sieved diameters, the emitted number concentration is given by:

$$\frac{dV}{d\ln D}\frac{d\mathcal{N}}{d\ln D} = \frac{D}{C_V}u(D)\frac{1}{c_{\mathcal{N}}D^2}\exp\left[-\left(\frac{D}{\lambda}\right)^3\right]\int_0^D p(D_s)\,dD_s \quad (1)\ (2)$$

where ~~$C_V c_{\mathcal{N}}$~~ is a normalization factor. ~~The exponential on the right side of Eq. (1) represents the fragmentation of aggregates during emission. The length scale $\lambda = 12 \pm 1$ µm was obtained by Kok (2011b), who performed a least-squares fit to the few available measurements of the emitted size distribution (Gillette et al., 1972; 1974; Gillette, 1974; Sow et al., 2009), after estimating $u(D)$ from measured size distributions of arid dispersed soils (d'Almeida and Schütz, 1983; Goldstein et al., 2005). The derived value of λ is roughly ten percent of a typical aggregate diameter (cf. Fig. 1), consistent with the assumption that the emitted particles are created by the fracture of aggregates.~~ The effect of the integral in Eq. (2) is to reduce the number concentration at smaller aggregate diameters compared to the inverse-square power law given by Eq. (1). This reduction occurs because emitted aggregates of diameter D can be comprised only of particles with smaller indivisible

scales (given by D_s). Thus, the integral is the product of an inverse-square power-law dependence with the distribution of indivisible scales identified from the wet-sieved soil.

The emitted number concentration in Eq. (2), derived from brittle fragmentation theory is independent of the size distribution of the original, undispersed soil that is subject to wind erosion. The approximate upper bound λ of emitted aggregates is estimated as $12 \pm 1\,\mu m$ by Kok (2011b), who performed a least-squares fit to the few available measurements of the emitted size distribution (Gillette et al., 1972; 1974; Gillette, 1974; Sow et al., 2009), after estimating $p(D_s)\,dD_s$ from measured size distributions of dispersed arid soils (d'Almeida and Schütz, 1983; Goldstein et al., 2005). This value is roughly ten percent of a typical aggregate diameter in the original soil and bounds the diameters of a majority of the particles that are dispersed globally downwind of their source.

~~The~~ Eq. (2) predicts that the volume distribution of emitted aggregates is shifted toward larger diameters, compared to the distribution of the wet-sieved soil, consistent with the measurements shown in Fig. 1. This is illustrated by Fig. 2, where the normalized distribution of emitted volume is shown as a black line~~in Fig. 2~~, derived from the corresponding distribution of the fully dispersed soil shown in orange. In this example, the ratio of clay-sized mass to silt is 0.5 in the fully dispersed soil but only 0.05 after brittle fragmentation and emission of the undispersed soil. (The silt fraction here represents the sum of particle diameters up to 20 µm, below which we assume Eq. ~~1~~2 is applicable.) ~~The redistribution of emitted mass away from clay sizes compared to the fully dispersed soil (the black and orange curves in Fig. 2, respectively) shows that fragmentation of aggregates during emission results in fewer clay-sized particles than breaking of aggregates during dispersion of the soil prior to measurement. The net effect of reconstruction of the undispersed soil combined with fragmentation during emission is to increase the silt-sized fraction at the expense of clay.~~ That is, brittle fragmentation of aggregates during saltation preserves a greater fraction of mass at silt sizes compared to the breaking of aggregates during dispersion of the soil prior to measurement.

The dotted curve in Fig. 2 shows the contribution to silt emission from ~~clay-sized particles~~ particles with indivisible scales at clay sizes in the fully dispersed soil. This contribution

corresponds to about 45 % of the emitted silt mass. ~~This redistribution is consistent with measured size distributions of concentration, including the nomimal "clay" minerals like phyllosilicates in Fig. 1, whose mass abundance is largest at silt sizes.~~

~~We will follow Claquin et al. (1999) to calculate regional variations in the mineral fractions of the dispersed soil, but augment~~In Sect. 2.2.1, we represent this empirically by augmenting the emitted silt fraction with clay-sized minerals identified in the wet-sieved soil. For example, we assume that phyllosilicates in the parent soil are also emitted at silt sizes even though these minerals are ~~present in~~given by the MMT for the fully dispersed soil only at clay sizes (Claquin et al., 1999). ~~This augmentation crudely represents reconstruction of the original size distribution of the undispersed soil modified by brittle fragmentation during emission (represented by the dotted curve in Fig. 2). We will~~ Wealso use Eq. (~~1~~2), the emitted size distribution derived by Kok (2011b), to specify the relative fraction of emitted clay and silt-sized particles. The prescription of an emitted size distribution that is independent of location is shared by studies of the global dust cycle that do not resolve mineral variations (e.g. Miller et al., 2006; Albani et al., 2014). This approach has also been used by Scanza et al. (2015) to account for the ~~effects of reaggregation and~~effect of brittle fragmentation upon the aerosol mineral composition.

The process of brittle fragmentation that leads to the emitted size distribution in Fig. 2 ~~is expected to be valid for diameters on the order of λ, beyond which the~~creates particles with diameters extending up to approximately λ. We assume that the specific range of validity is below 20 µm. At larger diameters, the emitted size distribution evolves through saltation and sandblasting with a complicated dependence upon wind speed and soil properties (Kok, 2011b). ~~We assume that the specific range of validity extends to 20 µm. This upper bound~~The range of emission by brittle fragmentation is mismatched with respect to the MMT whose silt size category extends to particle diameters up to 50 µm. To ~~constrain the~~calculate the emitted fraction of clay and silt-sized particles over the size range corresponding to the MMT, we need to know the emitted size distribution between 20 and 50 µm. We ~~specify this with the concentration measurements~~obtain this from the normalized volume distribution in Fig. 3 (left panel)~~from~~, measured during the SAMUM campaign in Morocco (Kandler et al.,

2009). (This figure is identical to Fig. 1, but is summed over all minerals and renormalized between 0 and 50 µm, the range of particle diameters corresponding to the MMT.) This figure provides the mass ratio corresponding to particle diameters between 2 to 20 µm compared to diameters between 20 to 50 µm. Combining this ratio with the fraction of clay to silt particles with diameters up to 20 µm provided by Eq. (~~1~~2), equal to 0.05, we calculate that ~~clay particles contribute~~clay-sized particles represent 1.3 % of the total emitted mass for particle diameters up to 50 µm. By combining the size distributions of Kok (2011b) and Kandler et al. (2009) ~~in their regions of respective validity~~at diameters for which they are respectively valid, we arrive at the "corrected" size distribution of emission shown in the second panel from the left in Fig. 3.

By ~~constraining emission with concentration measurements at~~ apportioning silt emission with measurements of the volume fraction after transport to a single location, we are making at least two approximations. ~~First, we are neglecting modification to the emitted size distribution by deposition that preferentially removes larger particles by gravitational settling. We partially account for this removal by using concentration measured only during high-dust events (Fig. 1, bottom row), which we assume correspond to recent emission. (We interpret the presence of large particles with diameters over 100 µm as evidence that deposition has had little time to modify the emitted distribution.)~~ First, we are assuming that the distribution at Tinfou is representative of other sources. The increase of the emitted silt fraction with increasing particle size (Fig. 3, second panel from left) is probably a robust consequence of the wind speed threshold for emission that decreases with diameter within this size range (Iversen and White, 1982a). By neglecting variations in the emitted distribution that result from wind speed, we are assuming that the distribution depends primarily upon each mineral's intrinsic physical characterisitics including its tendency to fragment.~~Second, we assume that the emitted size distribution of each mineral depends primarily upon the mineral's intrinsic physical characterisitics including its tendency to fragment, neglecting a dependence upon wind speed and soil properties that will cause the distribution to vary with location~~. This neglect is less defensible for diameters between 20 and 50 µm (compared to smaller particles for which Eq. (~~1~~2) is a good approximation), but quantifying

the validity of our assumption would require an emission model whose complexity is beyond the goals of the present study. Note that we prescribe an emitted distribution that is normalized over all sizes to remove the influence of the absolute value of emission upwind of Tinfou. Our second approximation is to neglect modification to the emitted size distribution by deposition during transport to Tinfou that preferentially removes larger particles by gravitational settling. We partially account for this removal by using measurements only during high-dust events (Fig. 1, bottom row), which we assume correspond to recent emission. (We interpret the presence of large particles with diameters over 100 µm as evidence that deposition has had little time to modify the emitted distribution.) We assess this approximation in Sect. 4.5.

2.2 Calculating mineral fractions at emission

2.2.1 Algorithm

Here, we describe our calculation of the emitted fraction of each mineral and its particle size distribution. We treat the dust particles as an external mixture of minerals, each corresponding to a separate prognostic variable. We create additional prognostic variables for mixtures of each mineral with iron oxides, where the latter is assumed to be a small fraction of the total particle mass. Calculation of iron oxide mixtures is described separately in Sect. 2.2.2.

We first derive the mineral composition of the fully dispersed soil following Claquin et al. (1999). Their MMT gives $f_n^{\mathrm{c}}(a)$ and $f_n^{\mathrm{s}}(a)$, the mass fraction of mineral n in the clay (0 to 2 µm) and silt (2 to 50 µm) size categories, respectively, as a function of ~~a~~ α, the arid soil type, whose spatial distribution is provided by the DSMW (FAO, 2007) that is integrated into the Harmonized World Soil Database (HWSD FAO/IIASA/ISRIC/ISSCAS/JRC, 2012). (Table 1 describes the data sets used in this study.) For each value of soil type ~~a~~ α (that

implicitly varies with location), the mineral fractions given by the MMT sum to unity:

$$\sum_{n}^{N} f_n^{\mathsf{c}}(a\alpha) = 1 \text{ and } \sum_{n}^{N} f_n^{\mathsf{s}}(a\alpha) = 1, \quad (2)\ (3)$$

For Claquin et al. (1999), only calcite (or more generally, "carbonates") and quartz are present at all particle sizes. Phyllosilicates (illite, kaolinite, smectite) are present only at clay sizes, while feldspar, gypsum and hematite are restricted to silt sizes. Based upon measurements shown in Fig. 1, we assume that each mineral is present within all size categories, so that N, the total number of minerals, equals 8 for both clay and silt-sized particles (Table 2). The ~~iron oxide fraction~~fraction of hematite provided by the MMT was originally derived using soil redness and assigned to the silt size category without reference to its measured size distribution. However, soil measurements show that iron oxides like hematite are present over a range of diameters as small as nanometers (Shi et al., 2012). Following Nickovic et al. (2012), we assume that ~~iron oxide~~hematite is present at both clay and silt sizes, assuming that the clay fraction is identical to the silt fraction provided by the MMT. We assume that the ~~iron oxide~~hematite fraction that is newly introduced at clay sizes occurs at the expense of the phyllosilicate fractions within the MMT. This is partly because iron oxides are a weathering product of phyllosilicates, but in practice this offset causes only a small reduction of the phyllosilicate fraction. ~~The extension of the feldspar and gypsum MMT mineral fractions to clay sizes is described below.~~

To calculate the mineral fractions of the dispersed soil at each location, we specify the fraction of each size category present, provided by the soil texture class ~~b~~β, whose spatial distribution is provided by the FAO/STATSGO soil texture (Table 1). Let ~~$s^{\mathsf{c}}(b)$ and $s^{\mathsf{s}}(b)$~~$s^{\mathsf{c}}(\beta)$ and $s^{\mathsf{s}}(\beta)$ be the mass fractions of clay and silt-sized particles provided by the soil texture triangle for each soil texture class ~~b~~β (Table 3). The clay and silt-size fractions are normalized to sum to unity at each location:

$$s^{\mathsf{c}}(b\beta) + s^{\mathsf{s}}(b\beta) = 1. \quad (3)\ (4)$$

Thus, the soil mass fraction of each mineral in the clay and silt-size categories, s_n^{c} and s_n^{s}, respectively, is given by:

$$s_n^{\mathsf{c}}(a\alpha, b\beta) = s^{\mathsf{c}}(b\beta) f_n^{\mathsf{c}}(a\alpha) \text{ and } s_n^{\mathsf{s}}(a\alpha, b\beta) = s^{\mathsf{s}}(b\beta) f_n^{\mathsf{s}}(a\alpha) \quad (4)\ (5)$$

As a result of Eqs. (23) and (34), the soil mass fractions sum to unity over all sizes and minerals:

$$\sum_n^N (s_n^{\mathsf{c}} + s_n^{\mathsf{s}}) = 1. \quad (5)\ (6)$$

The soil mass fraction of each mineral varies regionally through its dependence upon the arid soil type ~~a~~α (through the MMT that gives the fractional mineral composition of each size category) and soil texture ~~b~~β (that gives the local fractional abundance of each size category). For brevity, we will hereafter omit the dependence of s_n^{c} and s_n^{s} upon ~~a and b~~α and β (and implicitly upon location).

We have derived Eq. (45), the mass fraction of each mineral within the dispersed soil, by applying the method of Claquin et al. (1999) with the extension of hematite to clay sizes following Nickovic et al. (2012). What remains is to specify the *emitted* fraction of each mineral within each size category.

Let ~~d^{c} and d^{s}~~a^{c} and a^{s} be the mass fractions of emitted clay and silt-sized aerosols, respectively, that at each location satisfy:

$$da^{\mathsf{c}} + da^{\mathsf{s}} = 1. \quad (6)\ (7)$$

(The symbols "a" and "s" are chosen to signify the aerosol and soil, respectively.) We further decompose each aerosol mass fraction into contributions from the N minerals. Let ~~d_n^{c} and d_n^{s}~~ a_n^{c} and a_n^{s} represent the contribution of mineral n to the mass fraction of emitted clay and silt-sized particles, respectively:

$$da^{\mathsf{c}} = \sum_n^N da_n^{\mathsf{c}} \text{ and } da^{\mathsf{s}} = \sum_n^N da_n^{\mathsf{s}}, \quad (7)\ (8)$$

that because of Eq. (67) satisfy:

$$\sum_{n}^{N}\left(\underline{d}\underline{a}_n^{\mathsf{c}} + \underline{d}\underline{a}_n^{\mathsf{s}}\right) = 1. \qquad (8)\ (9)$$

That is, the sum of the aerosol mineral fractions over all sizes and minerals equals unity.

As a simple way to account for dispersion in the soil texture measurements and MMT, along with the fragmentation of aggregates during emission, weWe prescribe the mass fraction of the emitted clay-sized particles using brittle fragmentation theory, as described in Sect. 2.1.2 and shown in Fig. 3 (second panel from the left):

$$\underline{d}\underline{a}^{\mathsf{c}} = 0.013. \qquad (9)\ (10)$$

We assume that $d^{\mathsf{c}}a^{\mathsf{c}}$ is independent of location, based upon Kok (2011b), who argues that the black curve in Fig. 2 is a good approximation to measurements of the emitted size fraction for a variety of soils and wind conditions. As a consequence of Eqs. (5) and (10), the emission of clay-sized mineral n (excluding feldspar and gypsum) is:

$$a_n^{\mathsf{c}}(\alpha) = a^{\mathsf{c}} f_n^{\mathsf{c}}(\alpha) \quad \text{where } a^{\mathsf{c}} = 0.013. \qquad (11)$$

Note that for emission at clay sizes, the proportion of minerals is identical to that of the fully dispersed soil and given by the MMT.

Because of Eq. (67), the emitted silt fraction $d^{\mathsf{s}}a^{\mathsf{s}}$ is implicitly determined:

$$\underline{d}\underline{a}^{\mathsf{s}} = 1 - \underline{d}\underline{a}^{\mathsf{c}} = 0.987. \qquad (10)\ (12)$$

As noted above, the assumption of an emitted size distribution that is spatially uniform is shared by many models, including those with uniform or else varying mineral content (e.g. Miller et al., 2006; Scanza et al., 2015).

Our second assumption isWe also assume that the emitted silt fraction d^{s} is a combination of silt-sized particles in the dispersed soil along with aggregates in the

~~original soil that were dispersed into clay-sized particles~~mass fraction of each mineral n at silt sizes (a_n^{s}) consists of two contributions from the wet-sieved soil. The emitted fraction combines soil mass at silt sizes along with clay particles whose aggregates were broken during wet sieving. ~~We represent this restoration of aggregates empirically~~This is expressed by Eq. (2), but we represent reaggregation more simply by augmenting emission at silt sizes in proportion to the fractional abundance of clay particles ~~(s_n^{c})~~ in the fully dispersed soil (s_n^{c}):

$$d a_n^{\mathsf{s}} = \eta(\gamma_n s_n^{\mathsf{c}} + s_n^{\mathsf{s}}). \qquad (11)\ (13)$$

Here, γ_n is a coefficient of proportionality that controls the magnitude of ~~augmentation~~reaggregation and augmentation of the emitted silt fraction for mineral n. For simplicity, we assume that γ_n is identical for all reaggregated minerals, except for feldspar and gypsum, which ~~are~~must be treated separately as described below. The remaining exception is quartz, whose abundance at large diameters in Fig. 1 suggests that it experiences minimal dispersion, which we represent ~~approximately~~ by setting $\gamma_n = 0$. The parameter η is calculated at each location to satisfy Eq. (~~10~~12).

~~As a consequence of Eqs. (4) and (9), the emission of clay-sized mineral n (excluding feldspar and gypsum) is:~~

~~$$d_n^{\mathsf{c}}(a) = d^{\mathsf{c}} f_n^{\mathsf{c}}(a) \quad \text{where } d^{\mathsf{c}} = 0.013. \qquad (12)$$~~

~~Note that reaggregation is assumed to have no effect upon the proportions of minerals emitted at clay sizes, which are thus identical to the soil mineral fractions given by Eq. (4), aside from a multiplicative constant.~~

~~Similarly, the emitted silt fraction of mineral n is~~As a consequence of Eqs. (5) and (13), the emission of mineral n at silt sizes is:

$$d a_n^{\mathsf{s}}(a\alpha, b\beta) = \eta(a\alpha, b\beta)\left[\gamma_n s^{\mathsf{c}}(b\beta) f_n^{\mathsf{c}}(a\alpha) + s^{\mathsf{s}}(b\beta) f_n^{\mathsf{s}}(a\alpha)\right], \qquad (13)\ (14)$$

noting that $\gamma_n \equiv \gamma$, ~~an identical constant~~a constant that is identical for all minerals, except for quartz, for which $\gamma_n \equiv 0$. We have temporarily noted the dependence of the silt fraction ~~d^{s}~~a^{s} upon the local soil type ~~a and texture b~~α and texture β.

Equation ~~13~~14 extends clay-sized minerals like phyllosilicates into the silt-size range, consistent with measurements by Kandler et al. (2009), illustrated in Fig. 1. This extension increases in proportion to the clay fraction of the fully dispersed soil, a heuristic representation of Eq. (2).

Because the total fractional silt emission is assumed to be fixed according to ~~(10)~~Eq. (12)), γ has the effect of reducing the fractional emission of minerals like quartz that are ~~predominately~~predominantly silt-sized in the dispersed soil. We show below and in Part 2 (Perlwitz et al., 2015) that this reduction leads to improved agreement with observations. This fractional reduction of emitted minerals like quartz whose size is largely unmodified by wet sieving is a consequence of the reintroduction of aggregates ~~reconstructed from clay-sized minerals that were originally created by dispersion~~that were destroyed by dispersion but would have been emitted from the original, undispersed soil following brittle fragmentation.

~~To extend feldspar and gypsum emission into clay sizes (motivated by Fig. 1), we start with the mass ratio of clay-sized particles compared to silt particles with diameters less than 20 µm, equal to 0.05, according to Fig. 2 that is based upon (Kok, 2011b). For each mineral, we then use the concentration ratio measured during SAMUM of particle diameter from 2 to 20 µm and 20 to 50 µm (based upon the mass distributions shown in the right two panels of Fig. 3) . This gives:~~

Feldspar and gypsum are observed as aerosols at both clay and silt sizes (Fig. 1). Because of the absence of each mineral at clay sizes within the MMT (Claquin et al., 1999), we cannot specify the emitted clay fraction using Eq. (11). Instead, we assume that the emitted silt mass of each mineral (a_n^{s}) is closely related to its soil mass fraction (s_n^{s}). Then, we calculate the emitted clay mass using its ratio (ψ_n) with respect to the emitted silt mass:

$$d a_n^{\mathsf{c}} = \alpha \psi_n d a_n^{\mathsf{s}} \qquad (14)\ (15)$$

where:

$$d\underline{a}_n^{\mathrm{s}} = \eta(\underline{a}\alpha, b) s^{\mathrm{s}}(b) f_n^{\mathrm{s}}(\underline{a}\alpha) \quad (15)\ (16)$$

~~where~~and n corresponds to feldspar and gypsum. ~~Due to the a posteriori extension of feldspar and gypsum into clay sizes, we proportionally reduce the fractions of illite, smectite and kaolinite in the fraction of clay-sized dust. Note that the derivation of Eq. (14) is identical to the derivation of $d^{\mathrm{c}} = 0.013$, except that the latter uses the measured size distribution summed over all minerals (Fig. 2 , left panel), while the derivation of α_n is based upon the size distribution of either feldspar or gypsum (Fig. 3, right panels).~~The ratio ψ_n is given by the measured volume distribution after adjusting for modification of the emitted size distribution at small diameters during transport to Tinfou. This adjustment is shown in the right two panels of Fig. 3, and its derivation is identical to the calculation of $a^{\mathrm{c}} = 0.013$ (Fig. 3, second panel), except that the latter uses the measured size distribution summed over all minerals (Fig. 3, left panel), while the derivation of ψ_n is based upon the individual size distribution of either feldspar or gypsum (Fig. 1). We proportionally reduce the soil fractions of illite, smectite and kaolinite at clay sizes to compensate for the reintroduction of emitted feldspar and gypsum at this size. (This is an alternative to reducing all the soil mineral fractions at clay sizes. We justify this approximation as a result of the predominance of phyllosilicates at this size according to the MMT.)

The emitted silt particles have diameters ranging between 2 and 50 µm (consistent with the MMT). We distribute each mineral's silt particles over the size categories transported by ~~ModelE~~ModelE2 (Table 4). (Clay-sized particles are transported in a single bin by ~~ModelE~~ModelE2, so distribution within this size range is unnecessary.) We introduce an additional model size category between 32 and 50 µm that is not transported so that the total silt size range within the model and MMT are identical. Let ~~$d^{\mathrm{s}}_{n,k} a^{\mathrm{s}}_{n,k}$~~ be the emitted mass fraction of mineral n within size category k. To distribute the silt mass, we use the normalized mass distribution of each mineral derived from measurements ~~of surface concentration~~ during SAMUM (Kandler et al., 2009), shown in Fig. 4. We define $m^{\mathrm{s}}_{n,k}$ as the mass fraction within size bin k that is normalized for each mineral n over the MMT silt range (between 2

and 50 µm) so that:

$$\sum_{k \in \substack{\text{all silt} \\ \text{size bins}}} m^{\mathsf{s}}_{n,k} = 1 \text{ for each mineral } n. \qquad (16)\ (17)$$

Then, the emitted ~~silt within each~~mineral fraction within each silt size bin k is:

$$d\underline{a}^{\mathsf{s}}_{n,k} = d\underline{a}^{\mathsf{s}}_{n} m^{\mathsf{s}}_{n,k} \qquad (17)\ (18)$$

(The $m^{\mathsf{s}}_{n,k}$ are proportional to the values shown in Fig. 4, but differ slightly because the former are normalized only over the range of silt sizes. In contrast, the values in Fig. 4 include the clay-size bin in their normalization.)

Finally, we renormalize the mass fractions ~~d^{c}_{n} and $d^{\mathsf{s}}_{n,k}$~~ a^{c}_{n} and $a^{\mathsf{s}}_{n,k}$ so that their sum over all minerals and sizes is unity for diameters up to 32 µm. (Silt particles with diameters between 32 and 50 µm are not transported by the model.) This renormalization has the effect of reducing the fraction of quartz ~~fraction~~ compared to the MMT. This is because a greater mass fraction of quartz is measured at diameters above 32 µm, compared to other minerals, according to Fig. 4. For example, quartz has 38 % of its mass between 32 and 50 µm, a significantly larger amount than that of carbonates (23 %), feldspar (30 %) and particularly gypsum (2 %). The shift of quartz aerosols toward larger diameters compared ~~of~~to other minerals results from the larger characteristic particle size of quartz in the parent soil. Thus, the fractional emission of quartz at silt sizes is reduced by two effects compared to the fraction indicated by the MMT: ~~the reaggregation of~~first, the reconstruction of emitted aggregates at silt sizes from wet-sieved clay-sized particles~~and~~, and second, the limited size range of our transport model. The second effect is ~~simply~~ultimately the result of a disproportionate mass of quartz at diameters that are too large to travel far from their source.

Our model generally resembles that of Scanza et al. (2015) although there are differences that illuminate the physical processes represented by both studies. Our ~~method of reaggregation~~calculation of the emitted size distribution Eq. (~~13~~ 14) accounts for local soil texture, reconstructing more ~~aggregates where s_{c}~~silt-sized aggregates where s^{c}, the fraction of clay-sized particles, is particularly large. In contrast, Scanza et al. (2015) assume

a globally invariant size distribution of the wet-sieved soil. In addition, the latter study reconstructs the aggregates of all minerals identically, including quartz, whose reaggregation we neglect due to its presumed mechanical stability and resistance to ~~distinegration during~~disintegration during both brittle fragmentation and wet sieving. ~~This neglect~~The omission of quartz reaggregation reduces the relative fraction of quartz at silt sizes in our model. Finally, we use the measurements of Kandler et al. (2009) to ~~account for the disparity between the size range appropriate for brittle fragmentation theory (diameters less than roughly 20 µm) and the MMT (diameters less than roughly 50 µm)~~truncate the mineral fractions of emitted silt derived from the MMT (representing diameters up to 50 µm) to fit the transport categories of our model (that extend only to 32 µm). In contrast, Scanza et al. (2015) ~~use the entire silt fraction of quartz assigned by the MMT that includes diameters above 20 µm where brittle fragmentation theory is not directly applicable~~apply the entire emitted fraction derived from the MMT to their model transport categories that extend only to 10 µm. This contrast ~~further~~ reduces the relative fraction of quartz transported at silt sizes in our model~~, because a disproportionate amount of quartz given by the MMT is at these larger sizes~~ for two reasons. First, our model emits a larger fraction of quartz at diameters above 10 µm, where the particle lifetime is shorter. Second, our model entirely excludes the fraction of quartz emitted at diameters above 32 µm (where its measured volume fraction is disproportionately large according to Fig. 4).

2.2.2 Transport of iron oxides as internal mixtures

In our model, iron oxides can travel either in pure crystalline form or as an internal mixture with other minerals. (Combinations of the other minerals excluding iron oxides are treated as external mixtures.) Our apportionment of iron oxides combines the two limiting cases considered by Scanza et al. (2015). In that study, iron oxide is treated as either a pure component within an external mixture, or else an internal mixture with phyllosilicates and the other minerals. We refer to the iron oxide within an internal mixture as an “accretion”. (We avoid referring this mixture as an aggregate to avoid confusion with the more general class of aggregated minerals that are subject to brittle fragmentation.)

At each location, Eqs. (~~12~~11) and (~~13~~14), along with (~~14~~15) and (~~15~~16), give us ~~$d^{c}_{n,k}$~~ and ~~$d^{s}_{n,k}$~~ $a^{c}_{n,k}$ and $a^{s}_{n,k}$, including the mass fraction of emitted iron oxide. To create mixtures with other minerals, we ~~will~~ specify the hematite fraction available for mixing along with its mass fraction in each particle. (We describe mixtures in terms of "iron oxides" rather than hematite, whose fraction is provided by the MMT, because our mixing method applies to other highly weathered iron minerals like goethite that are frequently found in aggregation (We describe mixtures in terms of "iron oxides" rather than hematite, whose fraction is provided by the MMT, because our mixing method applies to other highly weathered iron minerals like goethite that are frequently found in aggregation; Lafon et al., 2006; Kandler et al., 2007; Journet et al., 2014.)

To simplify notation, we drop the superscripts in Eqs. (~~12~~11), (~~13~~14), (~~14~~15) and (~~15~~16) that distinguish between clay and silt-sized particles, and denote particle size solely through the k index of ~~$d_{n,k}$~~ $a_{n,k}$. For the GISS ~~ModelE~~ModelE2, $k = 1$ corresponds to the clay-sized fraction, while transported silt sizes correspond to k equal 2 through 5 (Table 4).

We first distinguish between each mineral in its pure and mixed state:

$$a_{n,k} = a^{\text{pure}}_{n,k} + a^{\text{mix}}_{n,k}. \qquad (18)\ (19)$$

For the particular case of iron oxides, we replace the mineral index n with Fe, so that ~~$d_{\text{Fe},k}$~~ $a_{\text{Fe},k}$ denotes the emitted mass fraction of iron oxide in size category k. Then, analogous to Eq. (~~18~~19), iron oxides can be decomposed into pure crystals and impurities mixed with other minerals:

$$a_{\text{Fe},k} = a^{\text{pure}}_{\text{Fe},k} + a^{\text{mix}}_{\text{Fe},k}. \qquad (19)\ (20)$$

We further distinguish the mixture of iron oxide among the remaining minerals ~~as $d^{\text{mix}}_{\text{Fe}|n,k}$~~ (each denoted by the subscript n) as $a^{\text{mix}}_{\text{Fe}|n,k}$, so that the total iron oxide within mixtures is the sum over n:

$$a^{\text{mix}}_{\text{Fe},k} = \sum_{n \neq \text{iron oxide}} a^{\text{mix}}_{\text{Fe}|n,k}. \qquad (20)\ (21)$$

We determine $d a^{\text{mix}}_{\text{Fe}|n,k}$ $a^{\text{mix}}_{\text{Fe}|n,k}$ by first specifying the fraction of emitted iron oxide available for mixing. Define ϵ as the fraction of ~~emitted iron oxide transported~~ iron oxide emitted as pure crystals:

$$d a^{\text{pure}}_{\text{Fe},k} = \epsilon d a_{\text{Fe},k}, \quad (21)\ (22)$$

~~We assume that~~ Micrometer-sized crystalline iron oxide aggregates are typically observed in highly weathered soils that are rich in iron oxides (Chesworth, 2008). Therefore, we assume that the amount of crystalline iron oxides not attached as small impurities to other minerals is proportional to the total iron oxide content of the soil, so that ϵ ~~itself~~ is proportional to the total iron oxide:

$$\epsilon = \epsilon_0 d a_{\text{Fe},k}. \quad (22)\ (23)$$

Then:

$$d a^{\text{pure}}_{\text{Fe},k} = \epsilon_0 d a^2_{\text{Fe},k}, \quad (23)\ (24)$$

and using Eq. (~~19~~20):

$$d a^{\text{mix}}_{\text{Fe},k} = (1-\epsilon) d a_{\text{Fe},k} = (1 - \epsilon_0 d a_{\text{Fe},k}) d a_{\text{Fe},k}. \quad (24)\ (25)$$

Equation (~~22~~23) expresses our assumption that the fraction of pure crystalline iron oxide increases where the total iron oxide fraction is large, a heuristic attempt to account for the weathering that creates iron oxides in the soil. As ~~soil develops~~a soil weathers, more of the primary and secondary Fe-bearing minerals decompose and the iron ~~of their lattice structure~~within the mineral lattices is converted to iron oxides in the soil (McFadden and Hendricks, 1985; Shi et al., 2012). ~~Micrometer-sized crystalline iron oxide aggregates are typically observed in highly weathered soils that are rich in iron oxides (Chesworth, 2008). Therefore, we assume that the amount of crystalline iron oxides not attached as small~~

~~impurities to other minerals is proportional to the total iron oxide content of the soil.~~ In absence of quantitative observational constraints, we simply set $\epsilon_0 = 1$. In the future, ϵ_0 could be prescribed differently or even be a function of other soil properties.

We next assume that iron oxide is mixed with the other minerals in proportion R to the total particle mass:

$$\underline{d}\underline{a}^{\text{mix}}_{\text{Fe}|n,k} = R\left(\underline{d}\underline{a}^{\text{mix}}_{n,k} + \underline{d}\underline{a}^{\text{mix}}_{\text{Fe}|n,k}\right). \tag{25}$$ (26)

We assume that R is a small number so that the iron oxides only slightly perturb the density of the mixture. We set R equal to 0.05, but are aware of only a few measurements that would guide a more precise choice of this parameter. ~~We set R equal to 0.05, and calculate in~~In Sect. 4.4, we calculate that the contribution of aggregated iron oxide to the global dust load is just under 2 %, comparable with the fraction inferred or assumed by other studies (e.g. Sokolik and Toon, 1999; Koven and Fung, 2006; Balkanski et al., 2007; Wagner et al., 2012; Moosmüller et al., 2012). In that section, we suggest that this global fraction is insensitive to our choice of R.

Finally, we assume that the iron oxide available for mixing is distributed among the other minerals in proportion to their mass fraction:

$$\underline{d}\underline{a}^{\text{mix}}_{\text{Fe}|n,k} \propto \frac{\underline{d}\underline{a}_{n,k}}{\underline{\overline{d}}\,\underline{\overline{a}}_k} \tag{26}$$ (27)

where ~~$\overline{d}_k \overline{a}_k$~~ is the mass fraction for each size category summed over all minerals except for iron oxide.

$$\underline{\overline{d}}\,\underline{\overline{a}}_k = \sum_{n \neq \text{iron oxide}} \underline{d}\underline{a}_{n,k} \tag{27}$$ (28)

Equation (~~26~~27) is a reasonable first assumption, although future efforts might construct mixtures by considering whether iron oxides are more likely to be created by weathering of

specific minerals. For example, iron oxides and clay minerals are formed during chemical weathering of parent minerals and are in intimate physical association with each other (Reid et al., 2003; Shi et al., 2012).

As a result of Eqs. (2425) and (2627):

$$\underline{d}\underline{a}^{\mathsf{mix}}_{\mathsf{Fe}|n,k} = \left(1 - \underline{d}\underline{a}_{\mathsf{Fe},k}\right) \underline{d}\underline{a}_{\mathsf{Fe},k} \frac{\underline{d}\underline{a}_{n,k}}{\underline{d}\overline{a}_k} \tag{28} \quad (29)$$

In an appendix, we use these assumptions to derive the emitted mass fraction of iron oxide mixed with mineral n:

$$\underline{d}\underline{a}^{\mathsf{mix}}_{n,k} + \underline{d}\underline{a}^{\mathsf{mix}}_{\mathsf{Fe}|n,k} = \min\left[\frac{\left(1 - \underline{d}\underline{a}_{\mathsf{Fe},k}\right) \underline{d}\underline{a}_{\mathsf{Fe},k}}{R} \frac{\underline{d}\underline{a}_{n,k}}{\underline{d}\overline{a}_k}, \frac{\underline{d}\underline{a}_{n,k}}{1-R}\right]. \tag{29} \quad (30)$$

As shown in the appendix, the second term within the minimum results from the possibility that for small enough mass fractions of accreted iron oxide within each particle ($R \ll 1$), there will be insufficient amounts of mineral n available for combination with the amount of iron oxide specified by Eq. (2425).

The mass fraction of pure, crystalline iron oxide is given by:

$$\underline{d}\underline{a}^{\mathsf{pure}}_{\mathsf{Fe},k} = \underline{d}\underline{a}_{\mathsf{Fe},k} - \min\left[(1 - \underline{d}\underline{a}_{\mathsf{Fe},k})\underline{d}\underline{a}_{\mathsf{Fe},k}, \frac{R}{1-R}\underline{d}\overline{a}_k\right], \tag{30} \quad (31)$$

while the mass fraction of pure mineral n is given by:

$$\underline{d}\underline{a}^{\mathsf{pure}}_{n,k} = \underline{d}\underline{a}_{n,k} - \left(\frac{1-R}{R}\right) \underline{d}\underline{a}^{\mathsf{mix}}_{\mathsf{Fe}|n,k}. \tag{31} \quad (32)$$

According to Eq. (2926), iron ~~oxide is accreted with a host mineral~~oxides are accreted with host minerals within the same size category k. ~~For example, silt-sized mixtures are~~

formed from iron oxide mass in the same size category . This might seem inconsistent, because the accreted iron oxide is assumed to be only a small fraction R of the total particle mass. However, the silt fraction of each mineral measured by Kandler et al. (2009) is the mass fraction within the total *collection of* particles of silt size, and not the fraction of iron oxide particles at this size. That is , at least some of the measured iron oxide mass at silt sizes consists of smaller crystals of this mineral attached to host minerals with silt diameters, as shown by images of single particles (Scheuvens and Kandler, 2014). This follows from our interpretation of $a^{\text{mix}}_{\text{Fe}|n,k}$ as the mass fraction of iron oxides within these particle combinations, whose size category k indicates the diameter of the combined particle. This diameter mainly reflects the contribution of the host mineral n, given our assumption that the fractional contribution R of iron oxide mass to the combined particle is small. The accreted fraction $a^{\text{mix}}_{\text{Fe}|n,k}$ represents the small crystals of iron oxides attached to the host mineral as seen in single-particle images (Scheuvens and Kandler, 2014). We emphasize that these iron oxides available for mixing are not particles themselves with diameters within the size category k. In contrast, the fraction of pure, crystalline iron oxides ($a^{\text{pure}}_{n,k}$) that does not combine with other minerals has a particle diameter within size category k.

Our modeling assumptions leading to Eq. (2930) should be evaluated with more measurements of the size distribution and mixing state of iron oxides in the soil.

2.3 Soil dust tracers in ModelEModelE2

Our model of the emitted mineral fractions has been incorporated into the AR5CMIP5 version of the NASA GISS Earth System ModelE2 (Schmidt et al., 2014) that has horizontal resolution of 2° latitude by 2.5° longitude and 40 vertical layers up to 0.1 hPa. Here, we summarize the dust aerosol module that is largely unchanged since its description in Miller et al. (2006). The values $d_{n,k}a_{n,k}$ give the fractional emission of each mineral within each transported size category. What remains is to calculate the absolute value oftotal emission at each location.

Emission occurs when the surface wind speed w exceeds a threshold w_T. Subgrid variations of ~~w~~wind speed are introduced using a probability distribution ~~$p(w)\,\mathrm{d}w$~~$s(w)\,\mathrm{d}w$ (Cakmur et al., 2004), so that the total emission E at each location is:

$$E = CSZ \int_{w_T}^{\infty} w^2 (w - w_T)\, p(w)\, \mathrm{d}w, \qquad (32)\ (33)$$

where S identifies regions of abundant easily erodible soil particles, and is an updated version of the source map derived by Ginoux et al. (2001). The parameter Z identifies regions of sparse vegetation, where the soil particles are exposed to the force of the wind, and is derived from the climatological annual cycle of surface roughness retrieved from a microwave scatterometer (Prigent et al., 2005). The threshold wind speed w_T in Eq. (~~32~~33) increases with soil wetness q, following Shao et al. (1996):

$$w_T = w_{T,0} \exp(0.7q), \qquad (33)\ (34)$$

where $w_{T,0} = 8\,\mathrm{m\,s^{-1}}$ is the emission threshold of the 10 m surface wind speed for completely dry soil. The ~~value~~parameter C controls the magnitude of the global dust cycle~~, and in the present case is chosen to give global, annual emission for all experiments of 2224 ± 100 Tg for particle diameters up to 32 µm (Table 7). This is within the range of values calculated by recent global models (Huneeus et al., 2011), and remains the case even if our model emission is restricted to smaller diameters (up to 16 µm) that are dispersed farther downwind of their source. Our model evaluation is independent of global emission because the observations consist of mineral fractions (Perlwitz et al., 2015)~~For all experiments, the global, annual emission is 2224 ± 100 Tg for particle diameters up to 32 µm (Table 7). In this and the companion article (Perlwitz et al., 2015), our comparison to measurements is based upon mineral *fractions* that are independent of the value of C. Consequently, the global emission is presented for illustrative purpose only, and we make no effort to adjust C to match any measurements of the dust cycle (cf. Cakmur et al., 2006).

Emission of each mineral is the total emission E from Eq. (~~32~~33) multiplied by the fractions ~~$d_{n,k}$~~$a_{n,k}$ (and their decompostion into pure and mixed states) derived above.

Each mineral is advected using the Quadratic Upstream Scheme (Prather, 1986), which keeps track of nine subgrid-scale moments as well as the tracer mean within each grid box, increasing the effective resolution for transport.

Removal of the mineral tracers from the atmosphere takes place by wet and dry deposition. Dry deposition includes gravitational settling and turbulent deposition in the surface layer. Settling speeds are proportional to mineral density (Tegen and Fung, 1994), whose values are given in Table 8. Note that the minerals have nearly identical densities, except for iron oxides whose density is nearly twice the value of the other minerals. Turbulent mixing near the surface is calculated using the same exchange coefficient as humidity. The calculations of the deposition velocities in the surface layer are based on a "resistance in series" scheme (Wesely and Hicks, 1977; Koch et al., 1999).

Wet deposition occurs through scavenging both within ~~and below clouds~~clouds and below where there is precipitating condensate~~.~~, while aerosols are restored by re-evaporation of cloud droplets and precipitate (Bauer and Koch, 2005; Schmidt et al., 2006). This represents a broader range of scavenging processes than the single scavenging coefficient used by Miller et al. (2006), and is now consistent with the treatment of other aerosol species. Within clouds, dust aerosols are scavenged where they nucleate precipitating cloud droplets. ~~Dust particles are assumed to be 50 % soluble. This scheme is used for the other aerosol species within ModelE2 (Koch et al., 1999), and is more mechanistically based than the single scavenging coefficient used by Miller et al. (2006).~~Nucleation depends upon particle solubility, which is assumed to be 50 % for all minerals throughout the particle lifetime. In a future study, we will represent particle aging, where solubility evolves along the aerosol trajectory as a result of physical and chemical transformations that depend upon mineral composition (cf. Baker et al., 2014).

We also defer calculation of dust radiative forcing and its dependence upon spatial variations in the aerosol mineral composition. This eliminates feedbacks between dust

radiative forcing and emission resulting, for example, from the perturbed surface wind speed or precipitation (e.g., Miller et al., 2014).

3 Model simulations

We evaluate our new approach in comparison to a ~~baseline~~control or "baseline" simulation that assumes the emitted mineral fractions are identical to those of the wet-sieved soil. We conduct a set of simulations with the NASA GISS ~~ModelE~~ModelE2 covering the years 2002 to 2010. This period coincides with a period of detailed measurements at Izaña (Rodríguez et al., 2011), and includes many of the measurements from our global compilation listed in the companion article (Perlwitz et al., 2015). We relax the model winds ~~at each level~~ every six hours toward their NCEP reanalysis values (Kalnay et al., 1996), in an effort to reproduce the observed transport. The winds are relaxed at all levels up to 10 hPa with a globally uniform time scale of 100 s. We also prescribe sea surface temperature and sea ice based upon measurements (Rayner et al., 2003). ~~The prognostic mineral aerosols are assumed to have no radiative effect in the present study. Instead dust radiative forcing is prescribed from a climatological distribution of dust aerosols whose radiative properties are assumed to be regionally invariant (Miller et al., 2006). This eliminates any feedback between radiative forcing by the mineral aerosols and their emission resulting, for example, from the perturbed surface wind speed.~~

Our baseline simulation is referred to as the "soil mineral fraction" (SMF) method, and assumes that the emitted mineral fractions are identical to those of the wet-sieved soil, given by Eq. (~~4~~5). The wet-sieved soil fractions are derived using the MMT of Claquin et al. (1999), augmented by mineral fractions for three additional soil types provided by Nickovic et al. (2012). Following this ~~later~~latter study, iron oxides are extended into the clay-sized category using MMT fractions identical to their values for silt sizes. ~~The emitted silt-sized minerals are distributed over the ModelE size bins according to Eq. (17), whose mass fractions are derived from concentration measurements at Tinfou, Morocco (Kandler et al., 2009).~~However, internal mixtures containing iron oxides are omitted from

this simulation, so that this mineral is removed preferentially as a result of its higher density and rate of gravitational settling. Emission of each of the minerals at silt-sizes is apportioned over the ModelE2 size bins using an identical normalized mass distribution that represents an average over the model minerals observed at Tinfou, Morocco (Kandler et al., 2009), as described in the Supplement. The ratio of emitted clay to silt in the SMF experiment is given by the local soil texture.

Our new approach, hereafter described as the "aerosol mineral fraction" (AMF) method, is described in Sect. 2.2. The emitted mineral fractions are based upon the MMT soil mineral fractions, Eq. (45), modified to account for disaggregation during wet-sieving ~~and fragmentation during emission~~of mineral aggregates that would be emitted during brittle fragmentation of the original undispersed soil. The AMF method extends feldspar and gypsum into the clay fraction using Eqs. (~~14~~15) and (~~15~~16). For the other minerals, clay-sized emission derives from Eq. (~~12~~11); silt-sized emission is taken from Eq. (~~13~~14 ~~), with its allocation into the ModelE silt-size bins according to Eq. (17).~~ Allocation of emitted silt into the ModelE2 size bins is prescribed according to Eq. (18). Mixtures of iron oxides with other minerals are estimated according to Eqs. (~~29~~30)–(~~31~~32).

~~The AMF simulationsset our empirical~~For the AMF simulation, our reaggregation parameter γ is set equal to 2. We performed a simulation with $\gamma = 3.5$ to examine the sensitivity of our results to enhanced reaggregation. In addition, we set $\gamma = 0$ in one experiment to illuminate the physical origin of differences between the AMF and SMF methods. The experiment with $\gamma = 0$ uses an emitted size distribution consistent with measurements and the default AMF experiment, but resembles the SMF method by not reconstructing silt-sized aggregates to undo the effect of wet sieving.

We carried out two more experiments to show the effect of different treatments of iron oxides. The first is the AMF experiment but without accretions of iron oxides ~~within~~with other minerals (denoted by "AMF-NoFeAcc"). The second (denoted as "SMF-NoClayFe") corresponds to the SMF experiment, but without the extension of iron oxides into clay sizes proposed by Nickovic et al. (2012). Our simulations are summarized in Table 9.

4 Results

4.1 Emitted size distribution and implications for long-range transport

We first compare the emitted distributions of ~~dust particles, summed over all minerals and derived from~~ the AMF and SMF experiments ~~along with their impact upon~~ summed over all minerals. This comparison and its implications for long-range ~~transport. This analysis~~ transport helps to understand regional variations of surface concentration for ~~each mineral~~the individual minerals, presented in Sect. 4.3.

Figure 5 displays the ~~emitted mass for each ModelE size bin calculated using~~ fraction of mass emitted at each ModelE2 size bin according to the SMF and AMF methods. ~~For each SMF size bin, emission varies according to the local soil texture. For the AMF method, the size distribution varies additionally due to reaggregation of certain clay-sized minerals. For each size bin, we calculate the distribution of the emitted fraction of each mineral with respect to the 336 combinations of the twelve soil texture categories along with the twenty-eight DSMW soil types included in the MMT. The emitted fractions are weighted by the total emission (at all sizes) to emphasize prolific sources.~~To construct this figure, we calculate the distribution of the emitted fraction within each size bin. The distribution is calculated using the 336 combinations of the twelve soil texture categories along with the twenty-eight DSMW soil types included in the MMT. For each combination of soil type and texture (characterized at the native resolution of the DSMW: $5'$ latitude by $5'$ longitude), emission is normalized so that the sum across all sizes is unity. To form the distribution, each combination at a particular size is weighted by the total emission (summed over all sizes) to emphasize prolific sources. The median emission is marked in the figure by a crossbar with variability ~~indicated by other parameters identified in the caption. Each combination of soil type and texture is characterized at the native resolution of the DSMW ($5' \times 5'$ latitude by longitude)~~among the different soil types and textures indicated as described in the caption.

For each SMF size bin, emission varies according to the local soil texture. For the AMF method, the size distribution varies additionally due to reaggregation of certain clay-sized minerals dispersed in the wet-sieved soil. For ~~each grid box, emission is normalized so that~~

the sum across all sizes (up to 50 µm diameter) is unity, which emphasizes the particle size making the largest contribution to emission. (In the model, normalization extends only to diameters of 32 µm, because model transport is limited to this range.) The median fractional emission of clay-sized particles in the SMF experiment(Figure 5), the median SMF fractional emission is 0.325, which is large compared to the AMF clay-sized fraction of 0.013 that is prescribed and spatially uniform, based upon observations of the emitted size distribution (cf. Eq. 910) and the normalized volume fractions at Tinfou that we assume are universal. The SMF median at each size is a function of the soil texture atlas. For the AMF experiment, the median of the sum of the mass at silt sizes is also spatially uniform by prescription (cf. Eq. 10).At silt sizes, the median of the *sum* of the AMF emission is also spatially uniform by prescription (cf. Eq. 12). Thus, individual silt binsAMF bins at silt sizes exhibit smaller variability, compared to the SMF method, whose silt fraction varies with the local soil texture.

The annual-mean AMF surface concentration for different particle sizes is shown in Fig. 6a, b and c, along with its ratio with respect to the SMF values in Fig. 6d–f. The AMF global mean is 8.27 µg m^{-3}, consisting of 0.47 and 7.79 µg m^{-3} at clay and silt sizes, respectively. The largest concentrations are located near the main source regions, including the Sahara and Sahel, the Arabian Peninsula, and Central Asia, where concentrations can exceed 500 µg m^{-3}. Large amounts of dust are also found in eastern Asia, Australia, and Patagonia, and smaller, yet regionally significant dust concentrations originate from source regions in the Great Plains of North America and Kalahari in southern Africa. The global surface concentration and load in the AMF experiment areis less than half of their corresponding SMF valuesits corresponding SMF value (Table 7, and Figs. 6d, and 7), a reduction that occurs despitecontrast that is also reflected in the aerosol load (Fig. 7). The reduced AMF concentration and load occurs despite the prescription of identical total emission in both simulations (Fig. 8). (See Supplement Figs. S4 to S15 for gravitational settling, dry and wet deposition, and lifetime.) The smaller concentration and load in the AMF experiment results from its different assumption about the emitted size distribution compared to the SMF model. The SMF size distribution is determined by the local soil texture and its specified fractions of clay and silt-sized particles. In contrast, emission of the clay soil frac-

tion is inhibited in the AMF model, an empirical constraint motivated by emission measurements. This results in a greater AMF silt fraction, compared to the SMF model. The larger particles are removed more quickly by gravitational ~~setting~~settling, resulting in a smaller load and surface concentration in the AMF experiment. The reduction of AMF surface concentration compared to the SMF value is smallest over source regions, whereas the largest decreases are observed in remote regions of the tropics ~~where the larger AMF particles have been removed by gravitational~~at the end of long trajectories marked by contrasting rates of settling (Fig. 6d). The ratio of AMF global surface concentration at clay diameters compared to the SMF value is 0.05 (Fig. 6e), comparable to the ratio of clay emission (Fig. 8). This reflects the similar lifetime of clay particles in both experiments, ~~reflecting~~indicating wet removal as the common process that dominates particle removal. At silt sizes, the global AMF concentration is 61 % larger than the SMF value (Fig. 6f), reflecting larger emission at this size in the former experiment. Note that the largest absolute contrasts between the two experiments ~~are~~(not shown) would be found near source regions, where total concentrations are several orders of magnitude higher than in remote regions.

4.2 Emitted mineral mass fractions

Contrasts between the experiments are apparent in the emitted fractions of the individual minerals, shown in Fig. **9**. Within each size bin, distributions are calculated as in Fig. 5. The mass fractions are normalized so that *within each size bin*, their sum over all minerals is unity. This normalization is chosen to show the minerals making the largest median contribution to each size bin. To complement ~~the bin~~these fractions, the magnitude of global annual emission for each mineral and each size bin is shown in Fig. 8.

The SMF method emits clay-sized dust aerosols that are comprised mostly of phyllosilicates with median values of 0.40 for illite, 0.22 for smectite and 0.19 for kaolinite (Fig. **9**, ~~left~~green). SMF phyllosilicates are absent among silt-sized aerosols, which are comprised mainly of quartz and feldspar, whose median values are ~~0.7~~0.70 and 0.21, respectively. In the AMF, the mass fractions of clay-sized phyllosilicates are slightly reduced in comparison to the SMF, offset by increases of feldspar and gypsum (Fig. **9**, ~~right~~orange). However, the

AMF reintroduces ~~phyllosilicates~~phyllosilicate aggregates at silt sizes that are absent in the wet-sieved soil. This reintroduction is in proportion to γ, which is set equal to 2 in our reference AMF simulation. ~~The effect~~A consequence of this reintroduction is to substantially reduce the quartz and feldspar fractions in the silt size range (Fig. **9**). ~~Calcite~~Carbonate fractions at silt sizes are slightly increased compared to the SMF, particularly in the smallest silt-size model bins, due to the prescribed reaggregation of clay-sized soil particles. ~~The use of observations to distribute the mass of each mineral across the silt size bins has significant effects (cf. Eq. (17) and Fig. 4). For example, the quartz fraction is distributed towards the larger silt-size bins, whose short lifetimes prevent significant dispersion downwind of the source region. In contrast, feldspar is enhanced toward the smaller silt size bins, whose shorter lifetime favors longer transport.~~

In the AMF method, the emitted silt mass of each mineral is distributed empirically across the model size categories using the normalized volume fraction derived for each individual mineral based upon measurements at Tinfou (cf. Eq. 18 and Fig. 4). In contrast, silt emission in the SMF method is distributed identically for all minerals using the average normalized distribution. (This is why the SMF emitted fractions in Fig. **9** are identical across all the silt size categories.) This contrast between the methods has significant effects upon the quartz fraction, for example, whose emission in the AMF experiment is distributed towards the larger silt size bins (Fig. 4). Consequently, the truncated fraction of quartz emission with diameters above 32 µm (whose transport is not calculated by the model) is larger in the AMF simulation compared to the SMF method.

Figure ~~10~~**9** (black) displays the emitted mineral fractions for the AMF experiment, but without reaggregation of clay particles ($\gamma = 0$). The ~~distribution of total dust mass~~size distribution of dust mass summed over all minerals in this simulation (not shown) resembles that of our reference AMF simulation (Fig. 6), because it necessarily satisfies Eq. (~~9~~10). However, the effect of $\gamma = 0$ is to preclude the reaggregation of clay soil particles that would otherwise be emitted at silt sizes. The median fractions of quartz and feldspar in the silt size bins are higher than in the AMF experiment due to the absence of reaggregated phyllosil-

icates. This experiment will be used to identify the physical origin of contrasting behavior between the AMF and SMF methods in the companion article (Perlwitz et al., 2015).

4.3 Regional variations of the mineral fractions

4.3.1 Emission

The regional variations of emitted mineral fractions are displayed for illite and kaolinite (Fig. ~~11~~10), quartz and carbonates (Fig. ~~12~~11), and feldspar, gypsum, and iron oxides (Fig. ~~13~~12). The left column shows the AMF emitted fraction, while the right column shows its ratio with respect to the SMF value. These global maps are shown at model resolution ($2^\circ \times 2.5^\circ$ latitude by longitude) and include only regions where dust emission occurs in our model. (Maps covering all soils where the MMT is applicable are provided in Figs. S1–S3 of the Supplement. Note that the extreme values depicted in the box plots in Fig. 9 are smoothed out at the model resolution due to spatial averaging.)

The AMF global fraction of emitted illite is 33 % ~~in the clay size range~~at clay sizes (Fig. ~~11~~10a) and 19 % over all sizes (Fig. ~~11~~10b). The largest fractions are found in Northern Africa (specifically in Erg El Djouf between Mali and Mauritania, the Libyan Desert and the Qattarah Depression in Egypt), the Middle East (southern Saudi Arabia and Mesopotamia), Turkmenistan, the Tarim Basin and the Inner Mongolia deserts in east Asia, southern Australia, and the southern African coastal region. The AMF kaolinite global fraction is 25 % in the clay size range and 15 % for all sizes (Fig. ~~11~~10c and d). In general, kaolinite is largest where the illite fraction is lowest, specifically in the Sahel region, northwestern India, the Kalahari Desert in southern Africa and western Australia.

Illite, kaolinite, and smectite (the latter not shown) are absent at silt sizes in the SMF. The AMF experiment extends these phyllosilicates into the silt size range (the size at which the prescribed fraction of emission is largest according to Fig. 5). This reaggregation is in proportion to their fraction as clay-sized particles in the wet-sieved soil, and results in an average emission increase when summed over all sizes of 27 % compared to the SMF (Fig. ~~11~~10f and h). The global phyllosilicate fraction is decreased at clay sizes compared to

the SMF by roughly 10 % (Fig. ~~11~~**10**e and g) due to the inclusion of feldspar and gypsum by the AMF method.

The AMF global fraction of emitted quartz is roughly 7 % in the clay size range (Fig. ~~12~~**11**a) and 34 % at silt sizes (Fig. ~~12~~**11**b), with the largest values in sandy regions of southern Africa (Kalahari desert), northern Africa (Erg El Djouf between Mali and Mauritania, the Libyan Desert, northern Algeria and the Grand Erg of Bilma in Niger), northwestern India, southern Saudi Arabia, Turkmenistan and the Tarim Basin. Compared to the SMF, AMF quartz fractions are similar for clay sizes (Fig. ~~12~~**11**e) and are lower by half in the silt size range (Fig. ~~12~~**11**f).

The AMF global fraction of emitted carbonate is 5 and 6 % at clay and silt sizes, respectively (Fig. ~~12~~**11**c and d), with the largest values in the North African coastal source regions (Algeria, Lybia and Egypt), Mesopotamia, the southern coast of the Saudi Arabia, the Iran–Afghanistan region, the Ganzu province in China, and the southern coasts of Africa and Australia. Carbonate fractions are low (less than 1 %) in the Sahel and the Kalahari Desert in southern Africa. At the native resolution of the soil texture and type databases, the emitted fractions of clay-sized quartz and carbonate ~~fractions~~ are prescribed to be identical between the AMF and SMF experiments. ~~Small differences at the model resolution arise from interpolation that is weighted by the different clay-sized fractions (Fig. 12e and g).~~ The small differences in Fig. **11**e and g arise when regridding to the coarser ModelE2 resolution. (The emission of each mineral is regridded by averaging over the higher resolution of the soil databases within each ModelE2 grid box. This emission is the product of the mineral fraction and the total clay-sized emission that is summed over all minerals. The clay-sized emission is uniform within the model grid box for the AMF experiment (according to Eq. 10), but varies within this area in the SMF experiment as a result of variations of soil texture, accounting for the contrast in Fig. **11**e and g.)

The AMF global fraction of emitted feldspar is roughly 13 % at both silt and all sizes (Fig. ~~13~~**12**a and b), with the largest values in northern Africa (southern Algeria, northern Mauritania and northern Niger) and south of the Tarim Basin in East Asia. Compared to the SMF experiment, the AMF global silt fraction of feldspar is 45 % lower (Fig. ~~13~~**12**e) due

to the reintroduction of phyllosilicate aggregates, although at all sizes the ~~fraction~~fractional reduction is only 6 % ~~smaller~~ (Fig. ~~13~~**12**f).

Emission of gypsum and iron oxides is comparatively small, with local fractions never exceeding a few percent. The global emitted fraction of iron oxides is nearly identical in the AMF and SMF experiments (Fig. ~~13~~**12**h). This agreement is fortuitous, resulting from the competing effects of reaggregation at silt sizes in the AMF experiment offset by the larger emitted clay fraction in the SMF experiment (Fig. 8). Emission of iron oxides is largest within the Sahel (Fig. ~~13~~**12**d), where dust collected downwind is distinguished by its reddish color (Carlson and Prospero, 1972). Smaller enrichment of iron oxides is seen within the Kalahari Desert of southern Africa, as well as eastern Australia along with the Thar Desert and maritime foothills of the Western Ghats within the Indian subcontinent.

4.3.2 Surface concentration

Figures ~~14 and 15~~**13** and **14** display the global distribution of the annual-average mineral fractions in surface concentration for the AMF, along with their ratio with respect to the SMF fractions.

Attribution of the mineral fractions to contrasts between the AMF and SMF methods is challenging because the fractional surface concentration depends upon the interaction of numerous processes including the size dependence of emission and removal, along with the proximity of sources enriched or depleted in different minerals. Nonetheless, the figures illustrate the effect of some physical assumptions underlying the methods ~~and contrasts between them~~. For example, the AMF kaolinite and iron oxide fractions are large downwind of the Sahel and southern Africa (Figs. ~~14b and 15~~**13**b and **14**c), where the source regions are enriched in these minerals (Figs. ~~11 and 13~~**10** and **12**). Similarly, the fractional concentrations of quartz and feldspar are enriched along the Pacific coast of South America (Fig. ~~15~~**14**a and b), reflecting their origin from local sources, including Patagonia, along with the shielding effect of the Andes that limits transport from Africa. Conversely, the tropical western Pacifc is depleted in quartz and gypsum (Fig. ~~15~~**14**a and d), because emission of these minerals is relatively small upwind over Australia. In general, the concentration of

illite is inversely related to that of kaolinite (Fig. ~~14~~13a and b), reflecting the contrasting weathering processes that create each mineral in the source soil.

Differences between the AMF and SMF methods are also illustrated. Far from source regions, clay-sized particles dominate the concentration. Thus, the difference of the clay-sized fractions of emission determines approximately whether the concentration of a particular mineral in remote regions is larger according to one method. (This relation is approximate, because ~~some clay-sized minerals may be removed preferentially due to the proximity of their sources to regions of enhanced precipitation and wet removal.) For example, the~~ the smallest silt particles have lifetimes that are only slightly shorter.) The clay-sized fraction of phyllosilicates is smaller in the AMF experiment (Figs. **9**), so their ratio with respect to the SMF decreases downwind (Fig. ~~14~~13e–g). This contrast is enhanced by the greater SMF fractional emission of clay particles (Fig. 5) that reduces the offsetting effect of phyllosilicate emission within the smallest silt size category in the AMF simulation. Conversely, the ratios of gypsum and feldspar increase downwind (Fig. ~~15~~14f and h), because clay-sized emission of these minerals occurs only in the AMF experiment. The ratio of AMF quartz also increases downstream (Fig. ~~15~~14e), although attribution is more elusive, because the emitted clay-sized fraction is nearly identical in both experiments. In general, the global-mean ratio of the AMF and SMF fractional concentration for each mineral ~~reflects~~is consistent with the ratio of the two experiments far from the source.

Immediately downwind from a source region enriched in phyllosilicates and iron oxides, the ratio of the AMF and SMF fractional ~~concentrations decrease~~concentration decreases (Figs. ~~14~~13e–g and ~~15~~14g). This is because their emission is peaked toward larger sizes in the AMF experiment, so that the fractional concentration of a particular mineral falls off within a shorter distance of a source region where it is enriched.

4.4 Iron oxides: pure vs. accreted forms

The fraction of the iron oxide in accreted form ~~(based upon column mass)~~ is shown in Fig. ~~16~~15a. The accreted fraction (derived from the aerosol load) is smallest downwind of the Sahel and other source regions enriched in iron oxides (Fig. ~~16~~15a). These minima are

a consequence of our mixing assumption, Eq. (~~22~~23), that increases the fraction of pure crystalline iron oxide where the soil is enriched in this mineral (Fig. ~~13~~12g). The accreted fraction increases downwind as the pure crystalline form is removed preferentially by gravity due to its greater density.

Regions where the soil is enriched in iron oxides correspond to a maximum of accreted iron oxide mass relative to the total dust mass (Fig. ~~16~~15b), even if a larger proportion of this mineral is in pure crystalline form ~~according to Eq. (22) and~~ (Fig. ~~16a~~15a). This is a consequence of our partitioning assumption (Eq. 25) and the small value of $a_{\mathrm{Fe},k}$ that represents the soil fraction of iron oxides. The AMF global mass fraction of accreted iron oxide is 1.82 %, within the range of values typically assumed by models that relate dust radiative properties to (globally uniform) prescribed mineral composition (Sokolik and Toon, 1999; Balkanski et al., 2007). This fraction results from two assumptions in our model: first, that iron oxides are 5 % of the particle mass (Eq. ~~25~~26), and second, that the assumed fraction of accreted iron oxide decreases in enriched soils, according to Eq. (~~22~~23) and our choice of ϵ_0. There are few observations to constrain precise values of either of these parameters, although the primary contribution of iron oxide to measured aerosol radiative absorption offers an indirect constraint. The accreted fraction is ~~presumably~~probably insensitive to a range of R. A larger prescribed value would distribute the accreted iron oxide over fewer particles, while a smaller value would result in accretions within more particles. The accreted fraction of iron oxides in our model is presumably more sensitive to the prescribed partitioning of crystalline and accreted forms according to Eq. (~~22~~23) that is a heuristic attempt to represent the effect of soil weathering.

The fraction of quartz and phyllosilicates containing iron oxide accretions compared to the total dust mass is shown in Fig. ~~16~~15c and d, respectively. This fraction is largest in regions enriched in iron oxides, but also where the fractions of the host minerals are large, according to Eq. (~~26~~27). The total fractional mass of dust particles containing accretions is largest downwind of soils enriched in iron oxides (Fig. ~~16~~15e). The global mass fraction is 34.60 %. We can calculate the effective mixing fraction of iron oxide to the total particle mass as $\frac{1.82}{34.60+1.82} = 0.04997$ that can be compared to our chosen value of $R = 0.05$. The

discrepancy originates within regions of iron oxide-rich soils, where the accreted fraction, given by Eq. (~~24~~25), is so large that there is an insufficient supply of other minerals available for mixing (necessitating the minimum operator as an upper bound in Eq. ~~29~~30). The small difference between the prescribed value of R and its effective value indicates that the exhaustion of other minerals available to host accretions occurs at only a few locations.

We carried out additional experiments to illustrate the effect of our model assumptions for iron oxides and its mixtures (Table 9, and Figs. S16 and S17 in the Supplement). The introduction of iron oxides at clay sizes following Nickovic et al. (2012) results in global iron oxide mass that is five times larger compared to the SMF-NoClayFe experiment that emits iron oxides only at silt sizes following Claquin et al. (1999). This contrast results from the large fraction of clay particles in the wet-sieved soil characterized by Claquin et al. (1999) and the correspondingly large ~~clay emission~~emission of iron oxides at clay sizes.

The effect of accretions is shown by contrasting the AMF and AMF-NoFeAcc experiments. The iron oxide mass at clay sizes is nearly identical in the two experiments because removal of this particle size is dominated by wet deposition that is independent of particle density. However, at larger silt sizes, whose concentration is more vulnerable to removal by gravitational settling, the AMF experiment with accretions has a global iron oxide mass that is larger by 40 %.

4.5 Evaluation at Tinfou, ~~Morroco~~Morocco

~~A detailed~~An extensive comparison of the model to observations is ~~presented in~~deferred to a companion article (Perlwitz et al., 2015), where we use a global compilation of measurements from almost sixty studies. ~~In the present study, we compare the mineral fractions of the AMF and the SMF surface concentration to measurements at Tinfou, Morroco (Figs. 17 and 18). While we have used these measurements to distribute the emitted mass of each mineral within the silt size range, the observed fractions of surface concentration are not prescribed within our model. The model concentration is affected by local emission, but also by advection from other sources, and processes such as turbulent mixing and deposition. Therefore, the observed fractions of surface concentration are a collective test of these~~

model processes, along with the accuracy of the MMTHere, we compare to measurements only at Tinfou, Morocco, where the mineral fractions are characterized in exceptional detail (Kandler et al., 2009). These measurements demonstrate how processes represented by the AMF method (such as reaggregation) lead to improved agreement, but also show the limitations of other model assumptions, identifying the need for future model development.

Figure 17**16** shows the fractional contribution of each mineral to surface concentration. (Smectite is omitted, because it is not measuredCalculation of the observed mineral fractions is described in the Supplement.) These fractions sum to unity atwithin each size bin, so that comparison to measurements shows each model's ability to reproduce the fractional contribution of minerals within separate size classes. In the SMF experiment, phyllosilicates are missing from all silt-size bins, as are feldspar and gypsum from the clay-size binsat clay sizes; both are contrary to measurements. The AMF method improves the representation of these mineralsphyllosilicate comparison through reaggregation that restores phyllosilicatesthis mineral to the silt range and brittle fragmentation that creates feldspar and gypsum at clay sizes. Another distinctive feature of the SMF experiment is the strong overestimation of the quartz fraction at silt sizes. This is largely corrected by the AMF method that increases the phyllosilicate fraction of emitted silt at the expense of quartz. This is shown by the AMF fractions calculated with $\gamma = 3.5$, where enhanced reaggregation at silt sizes leads to an additional increase of phyllosilicates and a reduction of quartz. The AMF method overestimates the kaolinite fraction at all sizes. The common error ofBoth the AMF and SMF experiments overestimate kaolinite at clay sizes, and this common error suggests that the kaolinite fraction may beis overestimated by the MMT ,(although other processes like transport can contribute to the error). The AMF method also overestimates the kaolinite fraction at silt sizes. The AMF kaolinite fraction at this size is sensitive to its prescribed MMT fraction at clay sizes due to reaggregation, as shown by the increased error for $\gamma = 3.5$.

Feldspar is the exceptional mineral where the SMF fraction is more realistic at all silt sizes. The AMF experiment underestimates the measured feldspar fraction, although it predicts a non-zero fraction at clay sizes in contrast to the SMF experiment. In the companion article, we show that the AMF feldspar fraction is generally in better agreement at other

locations. Both methods underestimate the iron oxide fraction, and the discrepancy of the SMF value increases with particle diameter ~~due to the absence of internal mixtures~~. The relatively large density of the pure crystalline form enhances gravitational removal, reducing the particle lifetime as diameter increases. In contrast, the internal mixtures present only in the AMF experiment are removed more slowly, reproducing the measured weak dependence of the iron oxide fraction upon particle size.

Figure ~~18~~**17** shows mineral fractions, but without separate normalization within each size bin. That is, the fractions sum to unity over all minerals and all sizes. Fidelity in comparison to the measurements at Tinfou depends additionally upon the ability of each experiment to reproduce the measured size distribution ~~.~~ (rather than just the mineral fractions within each individual size category that are presented in Fig. **16**). Note that we apportion the emitted silt using only the *normalized* volume distribution measured at Tinfou, so that the comparison in Fig. **17** depends additionally upon the calculated magnitude of emission at the contributing sources.

The SMF experiment strongly overestimates the ~~clay size fractions~~mineral fractions at clay sizes due to its relatively large emission at this size (Fig. 8). In contrast, the AMF fractions are closer to the measured values ~~due to their smaller emitted clay fraction~~. The most consistent error in the AMF experiment is an underestimate of each mineral fraction within the largest size category. This behavior is partly the result of using measurements ~~of surface concentration~~after transport from the source to distribute the emitted mass within the silt size bins according to Eq. (~~17~~18). The emitted size distribution is modified by deposition, which preferentially removes the largest particles by gravitational settling. We try to limit the influence of deposition by using ~~the aerosol size distribution measured~~measurements during times of high ~~surface~~number concentration when emission is presumably recent. However, the use of ~~concentration~~measurements after transport will inevitably lead to a negative bias at the largest sizes that future model versions will have to address.

~~The measurements at Tinfou are exceptional among the literature for their range of characterization, but Kandler et al. (2009) note that feldspar and the phyllosilicates are difficult to distinguish, resulting in these minerals being assigned the same fractional~~

distribution of mass with respect to size (Fig. 4).Feldspar and the phyllosilicates are difficult to distinguish within single particles using X-ray diffraction (XRD) due to the small sample mass, so Kandler et al. (2009) assign the same volume fraction to each mineral within each size category (Fig. 4). Measurements of elemental composition (their Fig. 14) suggest that the mass of feldspar may increaseincreases relative to phyllosilicates at larger silt sizes. This would not narrow the discrepancy of the AMF fractions at these sizes (since the refined measurements would also modify the prescribed size distribution of silt in all our experiments according to Eq. 17). However, theThe uncertain distinction between the measured size distributions of feldspar and phyllosilicates has implications forinfluences the transport of both minerals. An increase of feldspar at larger sizes (with a corresponding decrease at smaller sizes due to theour normalization of the size distribution) would confine this mineral more closely to its source region. Conversely, a decrease of phyllosilicates at larger sizes would correspond to greater abundance and dispersaltransport at smaller sizes with corresponding impacts upon global climate, for example, through ice nucleation (Hoose et al., 2008). This uncertainty has implications for global climate because both minerals are hypothesized to be effective sites for ice nucleation (Hoose et al., 2008; Atkinson et al., 2013). We will revisit the effects of this uncertainty of the mineral size distributionsthe uncertain size distribution of both minerals in the companion article (Perlwitz et al., 2015).

5 Conclusions

Aerosol mineral composition depends upon the composition of the parent soil and its size fractionation during mobilization. Soil mineral fractions have been estimated by Claquin et al. (1999) using atlases of arid soil type and soil texture by Claquin et al. (1999). However, thesederived from measurements following wet sieving. These authors identify the additionalremaining challenge of accounting for the effect of wet sieving in both atlases that alters the soildestruction of soil aggregates during wet sieving that results in contrasts

between the particle size distribution ~~by breaking aggregates~~of both the soil and the emitted aerosols.

We have proposed ~~an empirical~~a heuristic method to reconstruct the ~~mineral fractions in~~size distribution of mineral aggregates that are emitted from the undisturbed soil that is subject to wind erosion. We assume that some of the emitted silt-size particles ~~originated in~~correspond to the clay-sized fraction of the wet-sieved soil (Eq. ~~11~~13), whose mineral fractions are estimated by Claquin et al. (1999). ~~We also account for subsequent distintegration during emission by imposing fractions of clay and silt-sized particles based upon size-resolved measurements of emission(cf. Kok, 2011b).~~Size-resolved measurements of emission provide the distribution of far-travelled particles, whose diameters are below 20 µm (cf. Kok, 2011b). We extend the emitted distribution to diameters as large as 50 µm to correspond to the size range of the soil mineral fractions, using the normalized volume distribution derived from concentration measurements after transport to Tinfou, Morocco (Kandler et al., 2009).

In addition, we create an additional class of iron oxide aerosol that is a small impurity embedded within other minerals, allowing it to travel farther than in its pure crystalline state. We assume that these impurities are least frequent in soils rich in iron oxides (as a result of the assumed effect of weathering ~~to create~~that creates pure iron oxide crystals). Nonetheless, the abundance of iron oxide in these soils means that the absolute value of iron oxides in accretions is large. ~~We assume that iron oxides contribute 5 % to the combined particle mass. The remainder is transported in pure crytalline form and falls out quickly due to its higher density, so total global iron oxide fraction is just under 2 %.~~We assume that iron oxides contribute 5 % to the combined particle mass, with the remainder transported as pure crystals that fall out quickly due to their higher density. The resulting global mass fraction of iron oxides that combines accreted and pure forms is just under 2 %, a value that we suggest is insensitive to the assumed mass fraction of this mineral in accreted form. Our treatment of iron oxides is constrained by relatively few observations and ~~subject to~~worthy of more precise future treatments. ~~Nonetheless, modeling~~Modeling of aerosol iron is impor-

tant for its influence upon several climate processes, including aerosol radiative forcing and marine photosynthesis that modulates atmospheric carbon dioxide.

These extensions define our AMF experiment. In contrast, the SMF experiment serves as a control whose ~~emitted size distribution~~size distribution of the emitted mineral fractions is taken directly from that of the wet-sieved soil and excludes iron accretions. For both experiments, we calculate the regional distribution of minerals using the NASA GISS ModelE2, whose dust size categories range in diameter from 0.1 to 32 µm.

Emission of clay-sized particles is much smaller in the AMF experiment, due to ~~the empricial~~an observational constraint upon the emitted size distribution. This has implications for long-range transport. Both the SMF and AMF have identical global emission (by construction), but the column load and surface concentration are much lower in the latter experiment, because the particles are larger. Nonetheless, the emission of clay minerals (i.e. phyllosilicates) is only slightly smaller in the AMF experiment. This is a consequence of reaggregation of the wet-sieved soil that results in a substantial fraction of phyllosilicate particles at silt sizes.

In companion articles (Perlwitz et al., 2015; Pérez García-Pando et al., 2015), we compare the AMF and SMF experiments to measurements. In the present article, our comparison is limited to the mineral fractions of surface concentration ~~measured~~derived from measurements at Tinfou, Morocco (Kandler et al., 2009). These show a majority of the phyllosilicate (or "clay" mineral) mass at silt sizes, consistent with our AMF method. ~~In~~ Kandler et al. (2009) note the difficulty of distinguishing phyllosilicates from feldspar in single particle samples due to their limited mass. For this reason, the volume fractions of these two minerals in each size bin are assumed to be identical (cf. Fig. 1). However, these minerals can be distinguished in larger size-integrated samples that reveal comparable masses of each mineral (Kandler et al., 2009). This demonstrates that the presense of phyllosilicate aerosols at diameters larger than 2 µm cannot be the result of misattribution of feldspar (because the phyllosilicate mass below this diameter is only a small fraction of the total). The existence of silt-sized phyllosilicates is corroborated by multiple independent

measurements (Leinen et al., 1994; Arnold et al., 1998; Reid et al., 2003; Alastuey et al., 2005; Jeong and Nousiainen, 2014).

Both experiments predict comparable fractions of quartz at Tinfou, in spite of the substantially greater silt-sized emission of ~~this~~the AMF method compared to the SMF~~, both experiments predict comparable fractions of quartz~~. This agreement is the result of the reaggregation of clay minerals that reduces the quartz fraction at silt sizes in the undispersed soil prior to emission. This reduction occurs because the total silt emission ~~of~~summed over all minerals is fixed by our empirical constraint Eq. (12). The ~~reduction~~comparative reduction of quartz in the SMF experiment also occurs because we account for the larger characteristic size of ~~quartz~~this mineral in the parent soil compared to other minerals. The ~~aerosol size distribution measured by Kandler et al. (2009)~~size distribution of quartz aerosols measured at Tinfou suggests that a disproportionate amount of quartz ~~at silt sizes is beyond the size range that~~ is at diameters that are too large to be dispersed far from the source. This shows the value of measurements that can distinguish ~~potential differences among the mineral size distributions . We have noted how the~~contrasts between the size distributions of different minerals. The distinction between the size distributions of phyllosilicates and feldspar have implications for long-range transport and climate impacts like ice nucleation (Hoose et al., 2008; Atkinson et al., 2013).

In general, our ~~empirical reconstruction of the undispersed~~reconstruction of emitted aggregates from the wet-sieved soil allows us to shift clay-sized phyllosilicates ~~in the wet-sieved soil~~ toward silt sizes where they are observed and maintain realistic fractions of quartz, despite the observed size distribution of ~~the emitted aerosol~~emission that is heavily biased toward silt sizes. We have made little effort to find the optimal amount of reaggregation. Instead, we are developing a more physically based model of reaggregation and brittle fragmentation that extends studies by Kok (2011b) and Scanza et al. (2015), while addressing certain inconsistencies of our present semi-empirical approach. ~~(~~For example, we presently reaggregate minerals in proportion to s_c, the local fraction of clay-sized particles given by the soil texture atlas, but assume a uniform fraction of clay-sized emission according to Eq. (~~9~~10) that is independent of this texture. ~~)~~ More generally, we will take

advantage of more recent estimates of soil mineral ~~fraction~~fractions (Journet et al., 2014) that use additional measurements to extend the method of Claquin et al. (1999). Singular soil environments like the Bodélé Depression and littoral margins of Lake Chad, where concentrations of diatomite and other constituents derived from biological processes are large, present an additional challenge that results from their significant contribution to global dust emission (Washington et al., 2009).

Appendix A:

Here we use the assumptions in Sect. 2.2.2 to derive the mass fraction of the iron oxide mixture given by Eq. (~~29~~30), along with the remaining mass fractions of iron oxides (Eq. ~~30~~31) and mineral n (Eq. ~~31~~32) in their pure unmixed state.

We have assumed that accreted iron oxides contribute fraction R to the total mass of the particle mixture via Eq. (~~25~~26). For small enough prescribed fractions of accretion ($R \ll 1$), there will be an insufficient amount of the other mineral to combine with the amount of iron oxides specified by Eq. (~~24~~25). This follows from Eq. (~~18~~19):

$$\underline{da}^{\mathsf{mix}}_{n,k} \leq \underline{da}_{n,k}, \tag{A1}$$

so that from Eq. (~~25~~26):

$$\underline{da}^{\mathsf{mix}}_{\mathsf{Fe}|n,k} \leq \frac{R}{1-R}\underline{da}_{n,k}. \tag{A2}$$

In general,

$$\underline{da}^{\mathsf{mix}}_{\mathsf{Fe}|n,k} = \min\left[(1-\underline{da}_{\mathsf{Fe},k})\underline{da}_{\mathsf{Fe},k}\frac{\underline{da}_{n,k}}{\underline{\bar{a}}_k}, \frac{R}{1-R}\underline{da}_{n,k}\right]. \tag{A3}$$

Then, the emitted mass fraction of the prognostic variable comprised of mineral n and iron oxides is:

$$\underline{d}\underline{a}^{\text{mix}}_{n,k} + \underline{d}\underline{a}^{\text{mix}}_{\text{Fe}|n,k} = \min\left[\frac{(1-\underline{d}\underline{a}_{\text{Fe},k})\underline{d}\underline{a}_{\text{Fe},k}}{R}\frac{\underline{d}\underline{a}_{n,k}}{\overline{\underline{d}\underline{a}}_k}, \frac{\underline{d}\underline{a}_{n,k}}{1-R}\right] \tag{29} (30)$$

Again, ~~$d_{\text{Fe},k}$ and $d_{n,k}$~~ $a_{\text{Fe},k}$ and $a_{n,k}$ that are inputs to Eqs. A3) and (~~29~~30) are given by Eqs. (~~12~~11)–(~~15~~16) and (~~17~~18).

The pure or unmixed mass fraction of each mineral can be derived from Eq. A3). Using Eqs. (~~18~~19) and (~~25~~26) it can be shown that:

$$\underline{d}\underline{a}^{\text{pure}}_{n,k} = \underline{d}\underline{a}_{n,k} - \left(\frac{1-R}{R}\right)\underline{d}\underline{a}^{\text{mix}}_{\text{Fe}|n,k}, \tag{31} (32)$$

and:

$$\begin{aligned}\underline{d}\underline{a}^{\text{pure}}_{\text{Fe},k} &= \underline{d}\underline{a}_{\text{Fe},k} - \sum_{n\neq\text{iron oxide}} \underline{d}\underline{a}^{\text{mix}}_{\text{Fe}|n,k} \\ &= \underline{d}\underline{a}_{\text{Fe},k} - \min\left[\left(1-\underline{d}\underline{a}_{\text{Fe},k}\right)\underline{d}\underline{a}_{\text{Fe},k}, \frac{R}{1-R}\sum_{n\neq\text{iron oxide}}\underline{d}\underline{a}_{n,k}\right]\end{aligned} \tag{A4}$$

so that:

$$\underline{d}\underline{a}^{\text{pure}}_{\text{Fe},k} = \underline{d}\underline{a}_{\text{Fe},k} - \min\left[\left(1-\underline{d}\underline{a}_{\text{Fe},k}\right)\underline{d}\underline{a}_{\text{Fe},k}, \frac{R}{1-R}\overline{\underline{d}\underline{a}}_k\right]. \tag{30} (31)$$

For the case where the mass fraction of the emitted iron oxides is small enough, so that:

$$\left(1-\underline{d}\underline{a}_{\text{Fe},k}\right)\underline{d}\underline{a}_{\text{Fe},k} \leq \frac{R}{1-R}\overline{\underline{d}\underline{a}}_k, \tag{A5}$$

all the iron oxides available for mixing can be combined with the other minerals, and Eq. (~~30~~31) reduces to Eq. (~~23~~24).

The Supplement related to this article is available online at doi:10.5194/acpd-0-1-2015-supplement.

Acknowledgements. We thank Paul Ginoux, Konrad Kandler, Natalie Mahowald, Sergio Rodríguez and Rachel Scanza for helpful conversations. This article was improved by the thoughtful comments of Yves Balkanski, Jasper Kok and two additional reviewers. This research was supported by the National Science Foundation (ATM-01-24258), the Department of Energy (DE-SC0006713), the NASA Modeling, Analysis and Prediction Program and the Ministry of Economy and Competitiveness of Spain through the POLLINDUST project (CGL2011-26259). NCEP Reanalysis winds were provided by the Physical Sciences Division at the National Oceanic and Atmospheric Administration Earth System Research Laboratory via http://www.esrl.noaa.gov/psd/. Computational resources were provided by the NASA High-End Computing (HEC) Program through the NASA Center for Climate Simulation (NCCS) at Goddard Space Flight Center. The ~~data file with the mineral fractions at emission~~ emitted mineral fractions for the AMF method at ~~a~~native resolution of $5' \times 5'$ latitude by longitude ~~is available online~~are available at the website of the NASA Goddard Institute for Space Studies: http://data.giss.nasa.gov/mineralfrac/.

References

Alastuey, A., Querol, X., Castillo, S., Escudero, M., Avila, A., Cuevas, E., Torres, C., Romero, P.-M., Exposito, F., García, O., Diaz, J. P., Van Dingenen, R., and Putaud, J. P.: Characterisation of TSP and PM2.5 at Izaña and Sta. Cruz de Tenerife (Canary Islands, Spain) during a Saharan Dust Episode (July 2002), Atmos. Environ., 39, 4715–4728, doi:10.1016/j.atmosenv.2005.04.018, http://dx.doi.org/10.1016/j.atmosenv.2005.04.018, 2005.

Albani, S., Mahowald, N. M., Perry, A. T., Scanza, R. A., Zender, C. S., Heavens, N. G., Maggi, V., Kok, J. F., and Otto-Bliesner, B. L.: Improved dust representation in the Community Atmosphere Model, J. Adv. Model. Earth Sys., 6, 541–570, doi:10.1002/2013MS000279, http://dx.doi.org/10.1002/2013MS000279, 2014.

Alfaro, S. C. and Gomes, L.: Modeling mineral aerosol production by wind erosion: Emission intensities and aerosol size distributions in source areas., J. Geophys. Res., 106, 18 075–18 084, doi:10.1029/2000JD900339, http://dx.doi.org/10.1029/2000JD900339, 2001.

Arnold, E., Merrill, J., Leinen, M., and King, J.: The effect of source area and atmospheric transport on mineral aerosol collected over the North Pacific Ocean, Global and Planetary Change, 18, 137–159, doi:10.1016/S0921-8181(98)00013-7, http://dx.doi.org/10.1016/S0921-8181(98)00013-7, 1998.

Atkinson, J. D., Murray, B. J., Woodhouse, M. T., Whale, T. F., Baustian, K. J., Carslaw, K. S., Dobbie, S., O'Sullivan, D., and Malkin, T. L.: The importance of feldspar for ice nucleation by mineral dust in mixed-phase clouds, Nature, 498, 355–358, doi:10.1038/nature12278, http://dx.doi.org/10.1038/nature12278, 2013.

Baker, A. R., Laskina, O., and Grassian, V. H.: Processing and Ageing in the Atmosphere, in: Mineral Dust: A Key Player in the Earth System, edited by Knippertz, P. and Stuut, J.-B. W., chap. 4, pp. 75–92, Springer Netherlands, Dordrecht, Heidelberg, New York, London, doi:10.1007/978-94-017-8978-3_4, http://link.springer.com/chapter/10.1007%2F978-94-017-8978-3_4, 2014.

Balkanski, Y., Schulz, M., Claquin, T., and Guibert, S.: Reevaluation of Mineral aerosol radiative forcings suggests a better agreement with satellite and AERONET data, Atmos. Chem. Phys., 7, 81–95, doi:10.5194/acp-7-81-2007, http://dx.doi.org/10.5194/acp-7-81-2007, 2007.

Bauer, S. E. and Koch, D.: Impact of heterogeneous sulfate formation at mineral dust surfaces on aerosol loads and radiative forcing in the Goddard Institute for Space Studies general circulation model, J. Geophys. Res., 110, D17202, doi:10.1029/2005JD005870, http://dx.doi.org/10.1029/2005JD005870, 2005.

Bian, H. and Zender, C. S.: Mineral dust and global tropospheric chemistry: Relative roles of photolysis and heterogeneous uptake, J. Geophys. Res., 108, 4672, doi:10.1029/2002JD003143, http://dx.doi.org/10.1029/2002JD003143, 2003.

Bian, H., Prather, M. J., and Takemura, T.: Tropospheric aerosol impacts on trace gas budgets through photolysis, J. Geophys. Res., 108, 4242, doi:10.1029/2002JD002743, http://dx.doi.org/10.1029/2002JD002743, 2003.

Cakmur, R. V., Miller, R. L., and Torres, O.: Incorporating the effect of small-scale circulations upon dust emission in an atmospheric general circulation model, J. Geophys. Res., 109, D07201, doi:10.1029/2003JD004067, http://dx.doi.org/10.1029/2003JD004067, 2004.

Cakmur, R. V., Miller, R. L., Perlwitz, J., Geogdzhayev, I. V., Ginoux, P., Koch, D., Kohfeld, K. E., Tegen, I., and Zender, C. S.: Constraining the magnitude of the global dust cycle by minimizing the difference between a model and observations, J. Geophys. Res., 111, D06207, doi:10.1029/2005JD005791, http://dx.doi.org/10.1029/2005JD005791, 2006.

Caquineau, S., Gaudichet, A., Gomes, L., Magonthier, M., and Chatenet, B.: Saharan dust: Clay ratio as a relevant tracer to assess the origin of soil-derived aerosols, Geophys. Res. Lett., 25, 983–986, doi:10.1029/98GL00569, http://dx.doi.org/10.1029/98GL00569, 1998.

Carlson, T. N. and Prospero, J. M.: The Large-Scale Movement of Saharan Air Outbreaks over the Northern Equatorial Atlantic, J. Appl. Meteorol., 11, 283–297, doi:10.1175/1520-0450(1972)011<0283:TLSMOS>2.0.CO;2, http://dx.doi.org/10.1175/1520-0450(1972)011<0283:TLSMOS>2.0.CO;2, 1972.

Chatenet, B., Marticorena, B., Gomes, L., and Bergametti, G.: Assessing the microped size distributions of desert soils erodible by wind, Sedimentology, 43, 901–911, doi:10.1111/j.1365-3091.1996.tb01509.x, http://dx.doi.org/10.1111/j.1365-3091.1996.tb01509.x, 1996.

Chen, H., Navea, J. G., Young, M. A., and Grassian, V. H.: Heterogeneous photochemistry of trace atmospheric gases with components of mineral dust aerosol, J. Phys. Chem. A, 115, 490–499, doi:10.1021/jp110164j, http://dx.doi.org/10.1021/jp110164j, 2011.

Chesworth, W., ed.: Encyclopedia of soil science, Encylopedia of Earth Sciences Series, Springer, Dordrecht, Berlin, Heidelberg, New York, doi:10.1007/978-1-4020-3995-9, http://www.springer.com/environment/soil+science/book/978-1-4020-3994-2, 2008.

Choate, L. M., Ranville, J. F., Bunge, A. L., and Macalady, D. L.: Dermally adhered soil: 2. Reconstruction of dry-sieve particle-size distributions from wet-sieve data, Integrated Environmental Assessment and Management, 2, 385–390, doi:10.1002/ieam.5630020410, http://dx.doi.org/10.1002/ieam.5630020410, 2006.

Claquin, T., Schulz, M., and Balkanski, Y. J.: Modeling the mineralogy of atmospheric dust sources, J. Geophys. Res., 104, 22,243–22,256, doi:10.1029/1999JD900416, http://dx.doi.org/10.1029/1999JD900416, 1999.

d'Almeida, G. A. and Schütz, L.: Number, Mass and Volume Distributions of Mineral Aerosol and Soils of the Sahara, J. Clim. Appl. Meteorol., 22, 233–243, doi:10.1175/1520-0450(1983)022<0233:NMAVDO>2.0.CO;2, http://dx.doi.org/10.1175/1520-0450(1983)022<0233:NMAVDO>2.0.CO;2, 1983.

Deboudt, K., Gloter, A., Mussi, A., and Flament, P.: Red-ox speciation and mixing state of iron in individual African dust particles, J. Geophys. Res., 117, D12307, doi:10.1029/2011JD017298, http://dx.doi.org/10.1029/2011JD017298, 2012.

DeMott, P. J., Sassen, K., Poellot, M. R., Baumgardner, D., Rogers, D. C., Brooks, S. D., Prenni, A. J., and Kreidenweis, S. M.: African dust aerosols as atmospheric ice nuclei, Geophys. Res. Lett., 30, 1732, doi:10.1029/2003GL017410, http://dx.doi.org/10.1029/2003GL017410, 2003.

Dentener, F. J., Carmichael, G. R., Zhang, Y., Lelieveld, J., and Crutzen, P. J.: Role of mineral aerosol as a reactive surface in the global troposphere, J. Geophys. Res., 101, 22,869–22,889, doi:10.1029/96JD01818, http://dx.doi.org/10.1029/96JD01818, 1996.

FAO: Digital Soil Map of the World and Derived Soil Properties, Food and Agriculture Organization, Rome, Italy, 1995.

FAO: Digital Soil Map of the World, Food and Agriculture Organization, Rome, Italy, 2007.

FAO/IIASA/ISRIC/ISSCAS/JRC: Harmonized World Soil Database (version 1.2), FAO, Rome, Italy and IIASA, Laxenburg, Austria, http://webarchive.iiasa.ac.at/Research/LUC/External-World-soil-database/HTML/HWSD_Data.html?sb=4, last access date: 24 January 2013, 2012.

Feingold, G., Cotton, W. R., Kreidenweis, S. M., and Davis, J. T.: The Impact of Giant Cloud Condensation Nuclei on Drizzle Formation in Stratocumulus: Implications for Cloud Radiative Properties, J. Atmos. Sci., 56, 4100–4117, doi:10.1175/1520-0469(1999)056<4100:TIOGCC>2.0.CO;2, http://dx.doi.org/10.1175/1520-0469(1999)056<4100:TIOGCC>2.0.CO;2, 1999.

Frinak, E. K., Mashburn, C. D., Tolbert, M. A., and Toon, O. B.: Infrared characterization of water uptake by low-temperature Na-montmorillonite: Implications for Earth and Mars, J. Geophys. Res., 110, D09308, doi:10.1029/2004JD005647, http://dx.doi.org/10.1029/2004JD005647, 2005.

Gillette, D. A.: On the production of soil wind erosion aerosols having the potential for long range transport, J. Rech. Atmos, 8, 735–744, 1974.

Gillette, D. A., Blifford Jr, I. H., and Fenster, C. R.: Measurements of aerosol size distributions and vertical fluxes of aerosols on land subject to wind erosion, Journal of Applied Meteorology, 11, 977–987, doi:10.1175/1520-0450(1972)011<0977:MOASDA>2.0.CO;2, http://dx.doi.org/10.1175/1520-0450(1972)011<0977:MOASDA>2.0.CO;2, 1972.

Gillette, D. A., Blifford JR., I. H., and Fryrear, D. W.: The Influence of Wind Velocity on the Size Distributions of Aerosols Generated by the Wind Erosion of Soils, J. Geophys. Res., 79, 4068–4075, doi:10.1029/JC079i027p04068, http://dx.doi.org/10.1029/JC079i027p04068, 1974.

Ginoux, P., Chin, M., Tegen, I., Prospero, J. M., Holben, B., Dubovik, O., and Lin, S.-J.: Sources and distributions of dust aerosols simulated with the GOCART model, J. Geophys. Res., 106, 20,255–20,273, doi:10.1029/2000JD000053, http://dx.doi.org/10.1029/2000JD000053, 2001.

Glaccum, R. A. and Prospero, J. M.: Saharan aerosols over the tropical North Atlantic – Mineralogy, Marine Geology, 37, 295–321, doi:10.1016/0025-3227(80)90107-3, http://dx.doi.org/10.1016/0025-3227(80)90107-3, 1980.

Goldstein, H., Reynolds, R., Reheis, M., Yount, J., Lamothe, P., Roberts, H., and McGeehin, J.: Particle Size, CaCO3, Chemical, Magnetic, and Age Data from Surficial Deposits in and around Canyonlands National Park, Utah, Open-file report 2005-1186, U.S. Geological Survey, Reston, Virginia, http://pubs.usgs.gov/of/2005/1186, last access date: 8 September 2014, 2005.

Goodman, A. L., Underwood, G. M., and Grassian, V. H.: A laboratory study of the heterogeneous reaction of nitric acid on calcium carbonate particles, J. Geophys. Res., 105, 29,053–29,064, doi:10.1029/2000JD900396, http://dx.doi.org/10.1029/2000JD900396, 2000.

Grini, A., Zender, C. S., and Colarco, P. R.: Saltation Sandblasting behavior during mineral dust aerosol production, Geophys. Res. Lett, 29, 1868, doi:10.1029/2002GL015248, http://dx.doi.org/10.1029/2002GL015248, 2002.

Hatch, C. D., Gierlus, K. M., Schuttlefield, J. D., and Grassian, V. H.: Water adsorption and cloud condensation nuclei activity of calcite and calcite coated with model humic and fulvic acids, Atmos. Environ., 42, 5672–5684, doi:10.1016/j.atmosenv.2008.03.005, http://dx.doi.org/10.1016/j.atmosenv.2008.03.005, 2008.

Hatch, C. D., Greenaway, A. L., Christie, M. J., and Baltrusaitis, J.: Water adsorption constrained Frenkel-Halsey-Hill adsorption activation theory: Montmorillonite and illite, Atmos. Environ., 87, 26–33, doi:10.1016/j.atmosenv.2013.12.040, http://dx.doi.org/10.1016/j.atmosenv.2013.12.040, 2014.

Hoose, C. and Möhler, O.: Heterogeneous ice nucleation on atmospheric aerosols: a review of results from laboratory experiments, Atmos. Chem. Phys., 12, 9817–9854, doi:10.5194/acp-12-9817-2012, http://dx.doi.org/10.5194/acp-12-9817-2012, 2012.

Hoose, C., Lohmann, U., Erdin, R., and Tegen, I.: The global influence of dust mineralogical composition on heterogeneous ice nucleation in mixed-phase clouds, Environ. Res. Lett., 3, 14 pp, doi:10.1088/1748-9326/3/2/025003, http://iopscience.iop.org/1748-9326/3/2/025003/, 2008.

~~Huneeus, N., Schulz, M., Balkanski, Y., Griesfeller, J., Prospero, J., Kinne, S., Bauer, S., Boucher, O., Chin, M., Dentener, F., Diehl, T., Easter, R., Fillmore, D., Ghan, S., Ginoux, P., Grini, A., Horowitz, L., Koch, D., Krol, M. C., Landing, W., Liu, X., Mahowald, N., Miller, R., Morcrette, J.-J., Myhre, G., Penner, J., Perlwitz, J., Stier, P., Takemura, T., and Zender, C. S.: Global dust model intercomparison in AeroCom phase I, Atmos. Chem. Phys., 11, 7781–7816, doi:10.5194/acp-11-7781-2011, http://dx.doi.org/10.5194/acp-11-7781-2011, 2011.~~

Ito, A.: Contrasting the effect of iron mobilization on soluble iron deposition to the ocean in the Northern and Southern Hemispheres, J. Meteorol. Soc. Japan, 90A, 167–188, doi:10.2151/jmsj.2012-A09, http://dx.doi.org/10.2151/jmsj.2012-A09, 2012.

Iversen, J. D. and White, B. R.: Saltation threshold on Earth, Mars and Venus, Sedimentology, 29, 111–119, doi:10.1111/j.1365-3091.1982.tb01713.x, http://dx.doi.org/10.1111/j.1365-3091.1982.tb01713.x, 1982a.

Iversen, J. D., Greeley, R., and Pollack, J. B.: Windblown dust on Earth, Mars and Venus, J. Atmos. Sci., 33, 2425–2429, doi:10.1175/1520-0469(1976)033<2425:WDOEMA>2.0.CO;2, http://dx.doi.org/10.1175/1520-0469(1976)033<2425:WDOEMA>2.0.CO;2, 1976.

Jeong, G. Y.: Bulk and single-particle mineralogy of Asian dust and a comparison with its source soils, J. Geophys. Res., 113, D02208, doi:10.1029/2007JD008606, http://dx.doi.org/10.1029/2007JD008606, 2008.

Jeong, G. Y. and Nousiainen, T.: TEM analysis of the internal structures and mineralogy of Asian dust particles and the implications for optical modeling, Atmos. Chem. Phys., 14, 7233–7254, doi:10.5194/acp-14-7233-2014, http://dx.doi.org/10.5194/acp-14-7233-2014, 2014.

Jickells, T. D., An, Z. S., Andersen, K. K., Baker, A. R., Bergametti, G., Brooks, N., Cao, J. J., Boyd, P. W., Duce, R. A., Hunter, K. A., Kawahata, H., Kubilay, N., laRoche, J., Liss, P. S., Mahowald, P. S. N., Prospero, J. M., Ridgwell, A. J., Tegen, I., and Torres, R.: Global Iron Connections Between Desert Dust, Ocean Biogeochemistry, and Climate, Science, 308, 67–71, doi:10.1126/science.1105959, http://dx.doi.org/10.1126/science.1105959, 2005.

Johnson, D. B.: The Role of Giant and Ultragiant Aerosol Particles in Warm Rain Initiation, J. Atmos. Sci., 39, 448–460, doi:10.1175/1520-0469(1982)039<0448:TROGAU>2.0.CO;2, http://dx.doi.org/10.1175/1520-0469(1982)039<0448:TROGAU>2.0.CO;2, 1982.

Journet, E., Desboeufs, K. V., Caquineau, S., and Colin, J.-L.: Mineralogy as a critical factor of dust iron solubility, Geophys. Res. Lett., 35, L07805, doi:10.1029/2007GL031589, http://dx.doi.org/10.1029/2007GL031589, 2008.

Journet, E., Balkanski, Y., and Harrison, S. P.: A new data set of soil mineralogy for dust-cycle modeling, Atmos. Chem. Phys., 14, 3801–3816, doi:10.5194/acp-14-3801-2014, http://dx.doi.org/10.5194/acp-14-3801-2014, 2014.

Kalnay, E., Kanamitsu, M., Kistler, R., Collins, W., Deaven, D., Gandin, L., Iredell, M., Saha, S., White, G., Woollen, J., Zhu, Y., Leetmaa, A., Reynolds, R., Chelliah, M., Ebisuzaki, W., Higgins, W., Janowiak, J., Mo, K. C., Ropelewski, C., Wang, J., Jenne, R., and Joseph, D.: The NCEP/NCAR 40-Year Reanalysis Project, Bull. Amer. Meteor. Soc., 77, 437–471, doi:10.1175/1520-0477(1996)077<0437:TNYRP>2.0.CO;2, 1996.

Kandler, K., Benker, N., Bundke, U., Cuevas, E., Ebert, M., Knippertz, P., Rodríguez, S., Schütz, L., and Weinbruch, S.: Chemical composition and complex refractive index of Saharan Min-

eral Dust at Izanã, Tenerife (Spain) derived by electron microscopy, Atmospheric Environment, 41, 8058–8074, doi:10.1016/j.atmosenv.2007.06.047, http://dx.doi.org/10.1016/j.atmosenv.2007.06.047, 2007.

Kandler, K., Schütz, L., Deutscher, C., Ebert, M., Hofmann, H., Jäckel, S., Jaenicke, R., Knippertz, P., Lieke, K., Massling, A., Petzold, A., Schladitz, A., Weinzierl, B., Wiedensohler, A., Zorn, S., and Weinbruch, S.: Size distribution, mass concentration, chemical and mineralogical composition and derived optical parameters of the boundary layer aerosol at Tinfou, Morocco, during SAMUM 2006, Tellus B, 61, 32–50, doi:10.1111/j.1600-0889.2008.00385.x, http://dx.doi.org/10.1111/j.1600-0889.2008.00385.x, 2009.

Kandler, K., Schütz, L., Jäckel, S., Lieke, K., Emmel, C., Müller-Ebert, D., Ebert, M., Scheuvens, D., Schladitz, A., Šegvić, B., Wiedensohler, A., and Weinbruch, S.: Ground-based off-line aerosol measurements at Praia, Cape Verde, during the Saharan Mineral Dust Experiment: microphysical properties and mineralogy, Tellus B, 63, 459–474, doi:10.1111/j.1600-0889.2011.00550.x, http://dx.doi.org/10.1111/j.1600-0889.2011.00550.x, 2011.

Kelly, J. T., Chuang, C. C., and Wexler, A. S.: Influence of dust composition on cloud droplet formation, Atmos. Environ., 41, 2904–2916, doi:10.1016/j.atmosenv.2006.12.008, http://dx.doi.org/10.1016/j.atmosenv.2006.12.008, 2007.

Koch, D., Jacob, D., Tegen, I., Rind, D., and Chin, M.: Tropospheric sulfur simulation and sulfate direct radiative forcing in the Goddard Institute for Space Studies general circulation model, J. Geophys. Res., 104, 23,799–23,822, doi:10.1029/1999JD900248, http://dx.doi.org/10.1029/1999JD900248, 1999.

Kok, J. F.: Does the size distribution of mineral dust aerosols depend on the wind speed at emission?, Atmos. Chem. Phys, 11, 10 149–10 156, doi:10.5194/acp-11-10149-2011, http://www.atmos-chem-phys.net/11/10149/2011/acp-11-10149-2011.html, 2011a.

Kok, J. F.: A scaling theory for the size distribution of emitted dust aerosols suggests climate models underestimate the size of the global dust cycle, PNAS, 108, 1016–1021, doi:10.1073/pnas.1014798108, http://www.pnas.org/content/108/3/1016, 2011b.

Koven, C. D. and Fung, I.: Inferring dust composition from wavelength-dependent absorption in Aerosol Robotic Network (AERONET) data, J. Geophys. Res., 111, D14205, doi:10.1029/2005JD006678, http://dx.doi.org/10.1029/2005JD006678, 2006.

Krueger, B. J., Grassian, V. H., Cowin, J. P., and Laskin, A.: Heterogeneous chemistry of individual mineral dust particles from different dust source regions: the importance of particle mineralogy,

Atmos. Environ., 38, 6253–6261, doi:10.1016/j.atmosenv.2004.07.010, http://dx.doi.org/10.1016/j.atmosenv.2004.07.010, 2004.

Lafon, S., Sokolik, I. N., Rajot, J. L., Caquineau, S., and Gaudichet, A.: Characterization of iron oxides in mineral dust aerosols: Implications for light absorption, J. Geophys. Res., 111, D21207, doi:10.1029/2005JD007016, http://dx.doi.org/10.1029/2005JD007016, 2006.

Laurent, B., Marticorena, B., Bergametti, G., Léon, J. F., and Mahowald, N. M.: Modeling mineral dust emissions from the Sahara desert using new surface properties and soil database, Journal of Geophysical Research: Atmospheres (1984–2012), 113, D14218, doi:10.1029/2007JD009484, http://dx.doi.org/10.1029/2007JD009484, 2008.

Leinen, M., Prospero, J. M., Arnold, E., and Blank, M.: Mineralogy of aeolian dust reaching the North Pacific Ocean 1. Sampling and analysis, J. Geophys. Res., 99, 21,017–21,023, doi:10.1029/94JD01735, http://dx.doi.org/10.1029/94JD01735, 1994.

Li, J. and Osada, K.: Preferential settling of elongated mineral dust particles in the atmosphere, Geophys. Res. Lett., 34, doi:10.1029/2007gl030262, http://dx.doi.org/10.1029/2007GL030262, 2007.

Lieke, K., Kandler, K., Scheuvens, D., Emmel, C., Von Glahn, C., Petzold, A., Weinzierl, B., Veira, A., Ebert, M., Weinbruch, S., and Schütz, L.: Particle chemical properties in the vertical column based on aircraft observations in the vicinity of Cape Verde Islands, Tellus B, 63, 497–511, doi:10.1111/j.1600-0889.2011.00553.x, http://dx.doi.org/10.1111/j.1600-0889.2011.00553.x, 2011.

Ma, Q., Liu, Y., Liua, C., and He, H.: Heterogeneous reaction of acetic acid on MgO, α-Al_2O_3, and $CaCO_3$ and the effect on the hygroscopic behaviour of these particles, Phys. Chem. Chem. Phys., 14, 8403–8409, doi:10.1039/C2CP40510E, http://dx.doi.org/10.1039/C2CP40510E, 2012.

Maher, B., Prospero, J., Mackie, D., Gaiero, D., Hesse, P., and Balkanski, Y.: Global connections between aeolian dust, climate and ocean biogeochemistry at the present day and at the last glacial maximum, Earth-Science Reviews, 99, 61–97, doi:10.1016/j.earscirev.2009.12.001, http://dx.doi.org/10.1016/j.earscirev.2009.12.001, 2010.

Marticorena, B.: Dust Production Mechanisms, in: Mineral Dust: A Key Player in the Earth System, edited by Knippertz, P. and Stuut, J.-B., chap. 5, pp. 93–120, Springer Netherlands, Dordrecht, Heidelberg, New York, London, doi:10.1007/978-94-017-8978-3_5, http://dx.doi.org/10.1007/978-94-017-8978-3_5, 2014.

Marticorena, B., Bergametti, G., Gillette, D., and Belnap, J.: Factors controlling threshold friction velocity in semiarid and arid areas of the United States, J. Geophys. Res., 102, 23 277–23 287, doi:10.1029/97JD01303, http://dx.doi.org/10.1029/97JD01303, 1997.

Matsuki, A., Schwarzenboeck, A., Venzac, H., Laj, P., Crumeyrolle, S., and Gomes, L.: Cloud processing of mineral dust: direct comparison of cloud residual and clear sky particles during AMMA aircraft campaign in summer 2006, Atmos. Chem. Phys., 10, 1057–1069, doi:10.5194/acp-10-1057-2010, http://dx.doi.org/10.5194/acp-10-1057-2010, 2010.

McFadden, L. D. and Hendricks, D. M.: Changes in the content and composition of pedogenic iron oxyhydroxides in a chronosequence of soils in southern California, Quaternary Research, 23, 189–204, doi:10.1016/0033-5894(85)90028-6, http://dx.doi.org/10.1016/0033-5894(85)90028-6, 1985.

McTainsh, G. H., Lynch, A. W., and Hales, R.: Particle-size analysis of aeolian dusts, soils and sediments in very small quantities using a Coulter Multisizer, Earth Surf. Process. Landforms, 22, 1207–1216, doi:10.1002/(SICI)1096-9837(199724)22:13<1207::AID-ESP820>3.0.CO;2-K, http://onlinelibrary.wiley.com/doi/10.1002/%28SICI%291096-9837%28199724%2922:13%3C1207::AID-ESP820%3E3.0.CO;2-K/abstract, 1997.

Mei, F., Zhang, X., Lu, H., Shen, Z., and Wang, Y.: Characterization of MASDs of surface soils in north China and its influence on estimating dust emission, Chin. Sci. Bull., 49, 2169–2176, doi:10.1007/BF03185784, http://dx.doi.org/10.1007/BF03185784, 2004.

Miller, R. L., Tegen, I., and Perlwitz, J.: Surface radiative forcing by soil dust aerosols and the hydrologic cycle, J. Geophys. Res., 109, D04203, doi:10.1029/2003JD004085, http://dx.doi.org/10.1029/2003JD004085, 2004.

Miller, R. L., Cakmur, R. V., Perlwitz, J., Geogdzhayev, I. V., Ginoux, P., Koch, D., Kohfeld, K. E., Prigent, C., Ruedy, R., Schmidt, G. A., and Tegen, I.: Mineral dust aerosols in the NASA Goddard Institute for Space Sciences ModelE atmospheric general circulation model, J. Geophys. Res., 111, D06208, doi:10.1029/2005JD005796, http://dx.doi.org/10.1029/2005JD005796, 2006.

Miller, R. L., Knippertz, P., Pérez García-Pando, C., Perlwitz, J. P., and Tegen, I.: Impact of Dust Radiative Forcing upon Climate, in: Mineral Dust: A Key Player in the Earth System, edited by Knippertz, P. and Stuut, J.-B. W., chap. 13, pp. 327–357, Springer Netherlands, Dordrecht, Heidelberg, New York, London, doi:10.1007/978-94-017-8978-3_13, http://dx.doi.org/10.1007/978-94-017-8978-3_13, 2014.

Moosmüller, H., Engelbrecht, J. P., Skiba, M., Frey, G., Chakrabarty, R. K., and Arnott, W. P.: Single Scattering Albedo of Fine Mineral Dust Aerosols Controlled by Iron Concentration, J. Geophys. Res., 117, D11210, doi:10.1029/2011JD016909, http://dx.doi.org/10.1029/2011JD016909, 2012.

Murray, B. J., O'Sullivan, D., Atkinson, J. D., and Webb, M. E.: Ice nucleation by particles immersed in supercooled cloud droplets, Chem. Soc. Rev., 41, 6519–6554, doi:10.1039/C2CS35200A, http://dx.doi.org/10.1039/C2CS35200A, 2012.

Nickovic, S., Vukovic, A., Vujadinovic, M., Djurdjevic, V., and Pejanovic, G.: Technical Note: High-resolution mineralogical database of dust-productive soils for atmospheric dust modeling, Atmos. Chem. Phys., 12, 845–855, doi:10.5194/acp-12-845-2012, http://dx.doi.org/10.5194/acp-12-845-2012, 2012.

NRCS Soil Survey Staff: U.S. General Soil Map (STATSGO), Natural Resources Conservation Service, United States Department of Agriculture, http://sdmdataaccess.nrcs.usda.gov/, last access date: 11 April 2013, 2012.

Pérez García-Pando, C., Stanton, M. C., Diggle, P. J., Trzaska, S., Miller, R. L., Perlwitz, J. P., Baldasano, J. M., Cuevas, E., Ceccato, P., Yaka, P., and Thomson, M. C.: Soil Dust Aerosols and Wind as Predictors of Seasonal Meningitis Incidence in Niger, Environ. Health Perspect., 122, 679–686, doi:10.1289/ehp.1306640, http://dx.doi.org/10.1289/ehp.1306640, 2014a.

Pérez García-Pando, C., Thomson, M. C., Stanton, M. C., Diggle, P. J., Hopson, T., Pandya, R., Miller, R. L., and Hugonnet, S.: Meningitis and climate: from science to practice, Earth Perspectives, 1, 1–15, doi:10.1186/2194-6434-1-14, http://dx.doi.org/10.1186/2194-6434-1-14, 2014b.

Pérez García-Pando, C., Perlwitz, J. P., Miller, R. L., and Rodriguez, S.: Predicting the mineral composition of dust aerosols: Insights from elemental composition measurements at the Izaña Observatory, Geophys. Res. Lett., (in preparation), 2015.

Perlwitz, J. and Miller, R. L.: Cloud cover increase with increasing aerosol absorptivity: A counterexample to the conventional semidirect aerosol effect, J. Geophys. Res., 115, D08203, doi:10.1029/2009JD012637, http://dx.doi.org/10.1029/2009JD012637, 2010.

Perlwitz, J. P., Pérez García-Pando, C., and Miller, R. L.: Predicting the mineral composition of dust aerosols. Part II: Model evaluation and identification of key processes with observations, Atmos. Chem. Phys. Discuss., 15, 3577–3672, doi:10.5194/acpd-15-3577-2015, http://www.atmos-chem-phys-discuss.net/15/3577/2015/acpd-15-3577-2015.html, 2015.

Prather, M. J.: Numerical Advection by Conservation of Second-Order Moments, J. Geophys. Res., 91, 6671–6681, doi:10.1029/JD091iD06p06671, http://dx.doi.org/10.1029/JD091iD06p06671, 1986.

Prigent, C., Tegen, I., Aires, F., Marticorena, B., and Zribi, M.: Estimation of the aerodynamic roughness length in arid and semi-arid regions over the globe with the ERS scatterometer, J. Geophys. Res., 110, D09205, doi:10.1029/2004JD005370, http://dx.doi.org/10.1029/2004JD005370, 2005.

Rayner, N. A., Parker, D. E., Horton, E. B., Folland, C. K., Alexander, L. V., Rowell, D. P., Kent, E. C., and Kaplan, A.: Global analyses of sea surface temperature, sea ice, and night marine air temperature since the late nineteenth century, J. Geophys. Res., 108, 4407, doi:10.1029/2002JD002670, http://dx.doi.org/10.1029/2002JD002670, 2003.

Redmond, H. E., Dial, K. D., and Thompson, J. E.: Light scattering and absorption by wind blown dust: Theory, measurement, and recent data, Aeolian Research, 2, 5–26, doi:10.1016/j.aeolia.2009.09.002, http://dx.doi.org/10.1016/j.aeolia.2009.09.002, 2010.

Reid, E. A., Reid, J. S., Meier, M. M., Dunlap, M. R., Cliff, S. S., Broumas, A., Perry, K., and Maring, H.: Characterization of African dust transported to Puerto Rico by individual particle and size segregated bulk analysis, J. Geophys. Res., 108, 22 pp., doi:10.1029/2002JD002935, http://dx.doi.org/10.1029/2002JD002935, 2003.

Reynolds, C. A., Jackson, T. J., and Rawls, W. J.: Estimating soil water-holding capacities by linking the Food and Agriculture Organization Soil map of the world with global pedon databases and continuous pedotransfer functions, Water Resources Research, 36, 3653–3662, doi:10.1029/2000WR900130, http://dx.doi.org/10.1029/2000WR900130, 2000.

Rodríguez, S., Alastuey, A., Alonso-Pérez, S., Querol, X., Cuevas, E., Abreu-Afonso, J., Viana, M., Pérez, N., Pandolfi, M., and de la Rosa, J.: Transport of desert dust mixed with North African industrial pollutants in the subtropical Saharan Air Layer, Atmos. Chem. Phys., 11, 6,663–6,685, doi:10.5194/acp-11-6663-2011, http://www.atmos-chem-phys.net/11/6663/2011/acp-11-6663-2011.html, 2011.

Rubasinghege, G., Ogden, S., Baltrusaitis, J., and Grassian, V. H.: Heterogeneous Uptake and Adsorption of Gas-Phase Formic Acid on Oxide and Clay Particle Surfaces: The Roles of Surface Hydroxyl Groups and Adsorbed Water in Formic Acid Adsorption and the Impact of Formic Acid Adsorption on Water Uptake, J. Phys. Chem. A, 117, 11,316–11,327, doi:10.1021/jp408169w, http://dx.doi.org/10.1021/jp408169w, 2013.

Russell, L. M., Maria, S. F., and Myneni, S. C. B.: Mapping organic coatings on atmospheric particles, Geophys. Res. Lett, 29, 1779, doi:10.1029/2002GL014874, http://dx.doi.org/10.1029/2002GL014874, 2002.

Sassen, K.: Indirect climate forcing over the western US from Asian dust storms, Geophys. Res. Lett., 29, 1465, doi:10.1029/2001GL014051, http://dx.doi.org/10.1029/2001GL014051, 2002.

Scanza, R. A., Mahowald, N., Ghan, S., Zender, C. S., Kok, J. F., Liu, X., Zhang, Y., and Albani, S.: Modeling dust as component minerals in the Community Atmosphere Model: development of framework and impact on radiative forcing, Atmos. Chem. Phys, 15, 537–561, doi:10.5194/acp-15-537-2015, http://www.atmos-chem-phys.net/15/537/2015/acp-15-537-2015.html, 2015.

Scheuvens, D. and Kandler, K.: On Composition, Morphology, and Size Distribution of Airborne Mineral Dust, in: Mineral Dust: A Key Player in the Earth System, edited by Knippertz, P. and Stuut, J.-B., chap. 2, pp. 15–49, Springer Netherlands, Dordrecht, Heidelberg, New York, London, doi:10.1007/978-94-017-8978-3_2, http://dx.doi.org/10.1007/978-94-017-8978-3_2, 2014.

Scheuvens, D., Kandler, K., Küpper, M., Lieke, K., Zorn, S., Ebert, M., Schütz, L., and Weinbruch, S.: Individual-particle analysis of airborne dust samples collected over Morocco in 2006 during SAMUM 1, Tellus B, 63, 512–530, doi:10.1111/j.1600-0889.2011.00554.x, http://dx.doi.org/10.1111/j.1600-0889.2011.00554.x, 2011.

Schmidt, G. A., Ruedy, R., Hansen, J. E., Aleinov, I., Bell, N., Bauer, M., Bauer, S., Cairns, B., Canuto, V., Ye Cheng, A. D., Faluvegi, G., Friend, A. D., Hall, T. M., Hu, Y., Kelley, M., Kiang, N. Y., Koch, D., Andy A. Lacis, J. L., Lo, K. K., Miller, R. L., Nazarenko, L., Oinas, V., Perlwitz, J., Rind, J. P. D., Romanou, A., Gary L. Russell, M. S., Shindell, D. T., Stone, P. H., Sun, S., Tausnev, N., Thresher, D., , and Yao, M.-S.: Present-Day Atmospheric Simulations Using GISS ModelE: Comparison to In Situ, Satellite, and Reanalysis Data, J. Climate, 19, 153–192, doi:10.1175/JCLI3612.1, http://dx.doi.org/10.1175/JCLI3612.1, 2006.

Schmidt, G. A., Kelley, M., Nazarenko, L., Ruedy, R., Russell, G. L., Aleinov, I., Bauer, M., Bauer, S. E., Bhat, M. K., Bleck, R., Canuto, V., Chen, Y.-H., Cheng, Y., Clune, T. L., Del Genio, A., de Fainchtein, R., Faluvegi, G., Hansen, J. E., Healy, R. J., Kiang, N. Y., Koch, D., Lacis, A. A., LeGrande, A. N., Lerner, J., Lo, K. K., Matthews, E. E., Menon, S., Miller, R. L., Oinas, V., Oloso, A. O., Perlwitz, J. P., Puma, M. J., Putman, W. M., Rind, D., Romanou, A., Sato, M., Shindell, D. T., Sun, S., Syed, R. A., Tausnev, N., Tsigaridis, K., Unger, N., Voulgarakis, A., Yao, M.-S., and Zhang, J.: Configuration and assessment of the GISS ModelE2 contributions to the CMIP5 archive, J. Adv. Model. Earth Sys., 6, 141–184, doi:10.1002/2013MS000265, http://dx.doi.org/10.1002/2013MS000265, 2014.

Schulz, M., Prospero, J. M., Baker, A. R., Dentener, F., Ickes, L., Liss, P. S., Mahowald, N. M., Nickovic, S., Pérez García-Pando, C., Rodríguez, S., Sarin, M., Tegen, I., and Duce, R. A.: Atmospheric Transport and Deposition of Mineral Dust to the Ocean: Implications for Research Needs, Environ. Sci. Technol., 46, 10 390–10 404, doi:10.1021/es300073u, http://dx.doi.org/10.1021/es300073u, 2012.

Seifert, P., Ansmann, A., Mattis, I., Wandinger, U., Tesche, M., Engelmann, R., Müller, D., Pérez, C., and Haustein, K.: Saharan dust and heterogeneous ice formation: Eleven years of cloud observations at a central European EARLINET site, Journal of Geophysical Research: Atmospheres (1984–2012), 115, D20201, doi:10.1029/2009JD013222, http://dx.doi.org/10.1029/2009JD013222, 2010.

Shangguan, W., Dai, Y., Duan, Q., Liu, B., and Yuan, H.: A global soil data set for earth system modeling, J. Adv. Model. Earth Syst., 6, 249–263, doi:10.1002/2013MS000293, http://dx.doi.org/10.1002/2013MS000293, 2014.

Shao, Y.: A model for mineral dust emission, J. Geophys. Res., 106, 20 239–20 254, doi:10.1029/2001JD900171, http://dx.doi.org/10.1029/2001JD900171, 2001.

Shao, Y. and Lu, H.: A simple expression for wind erosion threshold friction velocity, J. Geophys. Res., 105, 22 437, doi:10.1029/2000jd900304, http://dx.doi.org/10.1029/2000JD900304, 2000.

Shao, Y., Raupach, M. R., and Findlater, P. A.: Effect of Saltation Bombardment on the Entrainment of Dust by Wind, J. Geophys. Res., 98, 12,719–12,726, doi:10.1029/93JD00396, http://dx.doi.org/10.1029/93JD00396, 1993.

Shao, Y., Raupach, M. R., and Leys, J. F.: A model for predicting aeolian sand drift and dust entrainment on scales from paddock to region, Aust. J. Soil Res., 34, 309–342, doi:10.1071/SR9960309, http://dx.doi.org/10.1071/SR9960309, 1996.

Shao, Y., Ishizuka, M., Mikami, M., and Leys, J. F.: Parameterization of size-resolved dust emission and validation with measurements, J. Geophys. Res., 116, D08203, doi:10.1029/2010JD014527, http://dx.doi.org/10.1029/2010JD014527, 2011.

Shi, Z., Krom, M. D., Jickells, T. D., Bonneville, S., Carslaw, K. S., Mihalopoulos, N., Baker, A. R., and Benning, L. G.: Impacts on iron solubility in the mineral dust by processes in the source region and the atmosphere: A review, Aeolian Research, 5, 21–42, doi:10.1016/j.aeolia.2012.03.001, http://dx.doi.org/10.1016/j.aeolia.2012.03.001, 2012.

Shi, Z. B., Woodhouse, M. T., Carslaw, K. S., Krom, M. D., Mann, G. W., Baker, A. R., Savov, I., Fones, G. R., Brooks, B., Drake, N., Jickells, T. D., and Benning, L. G.: Minor effect of physical size sorting on iron solubility of transported mineral dust, Atmos. Chem. Phys., 11, 8459–8469, doi:10.5194/acp-11-8459-2011, http://dx.doi.org/10.5194/acp-11-8459-2011, 2011.

Sokolik, I. N. and Toon, O. B.: Direct radiative forcing by anthropogenic airborne mineral aerosols, Nature, 381, 681–683, doi:10.1038/381681a0, http://dx.doi.org/10.1038/381681a0, 1996.

Sokolik, I. N. and Toon, O. B.: Incorporation of mineralogical composition into models of the radiative properties of mineral aerosol from UV to IR wavelengths, J. Geophys. Res., 104, 9423–9444, doi:10.1029/1998JD200048, http://dx.doi.org/10.1029/1998JD200048, 1999.

Sow, M., Alfaro, S. C., Rajot, J. L., and Marticorena, B.: Size resolved dust emission fluxes measured in Niger during 3 dust storms of the AMMA experiment, Atmos. Chem. Phys., 9, 3881–3891, doi:10.5194/acp-9-3881-2009, http://dx.doi.org/10.5194/acp-9-3881-2009, 2009.

Sullivan, R. C., Guazzotti, S. A., Sodeman, D. A., Tang, Y., Carmichael, G. R., and Prather, K. A.: Mineral dust is a sink for chlorine in the marine boundary layer, Atmos. Environ., 41, 7166–7179, doi:10.1016/j.atmosenv.2007.05.047, http://dx.doi.org/10.1016/j.atmosenv.2007.05.047, 2007.

Takahashi, Y., Higashi, M., Furukawa, T., and Mitsunobu, S.: Change of iron species and iron solubility in Asian dust during the long-range transport from western China to Japan, Atmos. Chem. Phys., 11, 11 237–11 252, doi:10.5194/acp-11-11237-2011, http://dx.doi.org/10.5194/acp-11-11237-2011, 2011.

Tegen, I. and Fung, I.: Modeling of mineral dust in the atmosphere: Sources, transport, and optical thickness, J. Geophys. Res., 99, 22,897–22,914, doi:10.1029/94JD01928, http://dx.doi.org/10.1029/94JD01928, 1994.

Tegen, I., Hollrig, P., Chin, M., Fung, I., Jacob, D., and Penner, J.: Contribution of different aerosol species to the global aerosol extinction optical thickness: Estimates from model results, J. Geophys. Res., 102, 23,895–23,915, doi:10.1029/97JD01864, http://dx.doi.org/10.1029/97JD01864, 1997.

Turner, D. D.: Ground-based infrared retrievals of optical depth, effective radius, and composition of airborne mineral dust above the Sahel, J. Geophys. Res., 113, D00E03, doi:10.1029/2008JD010054, http://dx.doi.org/10.1029/2008JD010054, 2008.

Twohy, C. H., Kreidenweis, S. M., Eidhammer, T., Browell, E. V., Heymsfield, A. J., Bansemer, A. R., Anderson, B. E., Chen, G., Ismail, S., DeMott, P. J., and Heever, S. C. V. D.: Saharan dust particles nucleate droplets in eastern Atlantic clouds, Geophys. Res. Lett., 36, L01807, doi:10.1029/2008GL035846, http://dx.doi.org/10.1029/2008GL035846, 2009.

Usher, C. R., Michel, A. E., Stec, D., and Grassian, V. H.: Laboratory studies of ozone uptake on processed mineral dust, Atmos. Environ., 37, 5337–5347, doi:10.1016/j.atmosenv.2003.09.014, http://www.sciencedirect.com/science/article/pii/S1352231003007556, 2003.

Wagner, R., Ajtai, T., Kandler, K., Lieke, K., Linke, C., Müller, T., Schnaiter, M., and Vragel, M.: Complex refractive indices of Saharan dust samples at visible and near UV wavelengths: a

laboratory study, Atmos. Chem. Phys., 12, 2491–2512, doi:10.5194/acp-12-2491-2012, http://dx.doi.org/10.5194/acp-12-2491-2012, 2012.

Washington, R., Bouet, C., Cautenet, G., Mackenzie, E., Ashpole, I., Engelstaedter, S., Lizcano, G., Henderson, G. M., Schepanski, K., and Tegen, I.: Dust as a tipping element: the Bodélé Depression, Chad, Proceedings of the National Academy of Sciences, 106, 20 564–20 571, doi:10.1073/pnas.0711850106, http://dx.doi.org/10.1073/pnas.0711850106, 2009.

Webb, R. S., Rosenzweig, C. E., and Levine, E. R.: Specifying land surface characteristics in general circulation models: Soil profile data set and derived water-holding capacities, Global Biogeochemical Cycles, 7, 97–108, doi:10.1029/92GB01822, http://dx.doi.org/10.1029/92GB01822, 1993.

Wesely, M. L. and Hicks, B. B.: Some factors that affect the deposition rates of sulfur dioxide and similar gases on vegetation, J. Air Pollut. Control Assoc., 27, 1110–1116, doi:10.1080/00022470.1977.10470534, http://dx.doi.org/10.1080/00022470.1977.10470534, 1977.

Yakobi-Hancock, J. D., Ladino, L. A., and Abbatt, J. P. D.: Feldspar minerals as efficient deposition ice nuclei, Atmos. Chem. Phys., 13, 11,175–11,185, doi:10.5194/acp-13-11175-2013, http://dx.doi.org/10.5194/acp-13-11175-2013, 2013.

Zimmermann, F., Weinbruch, S., Schütz, L., Hofmann, H., Ebert, M., Kandler, K., and Worringen, A.: Ice nucleation properties of the most abundant mineral dust phases, J. Geophys. Res., 113, D23204, doi:10.1029/2008JD010655, http://dx.doi.org/10.1029/2008JD010655, 2008.

Table 1. Datasets used in this study.

Name and Reference	Description
Mean Mineralogical Table (MMT) (Claquin et al., 1999)	Mineral fractions of clay and silt soil particles for 25 FAO arid soil types. The MMT was expanded with 3 additional soil types (Yermosols, Haplic Yermosols and Xerosols) whose mineral fractions were extrapolated by Nickovic et al. (2012) from similar types.
Digital Soil Map of the World (DMSW) (FAO, 2007; FAO/IIASA/ISRIC/ISSCAS/JRC, 2012) www.fao.org/geonetwork/srv/en/metadata.show?id=14116	Geographical distribution of 137 soil types with a resolution of $5' \times 5'$ latitude by longitude. The MMT uses 28 arid soil types to assign mineral fractions to the clay and silt-sized fractions of the soil.
Hybrid STATSGO/FAO (FAO/IIASA/ISRIC/ISSCAS/JRC, 2012; NRCS Soil Survey Staff, 2012) www.ral.ucar.edu/research/land/technology/lsm.php	Geographical distribution of soil texture classes (see Table 3). The FAO global soil texture maps at $5' \times 5'$ latitude by longitude are remapped onto a global $30'' \times 30''$ latitude by longitude grid. Within Contiguous United States (CONUS), the soil texture is replaced by the $30'' \times 30''$ STATSGO data.
Dust and mineral measurements at Tinfou, Morocco (Kandler et al., 2009)	Measurements of dust number and fractional mineral volume for 10 size bins extending to $250\,\mu m$ at Tinfou, Morocco during the SAMUM campaign in 2006.

Table 2. Minerals represented in ~~ModelE~~ModelE2. Closed circles (●) denote minerals identified in wet-sieved soils by Claquin et al. (1999). Stars (⋆) denote iron oxide extrapolated to clay sizes by Nickovic et al. (2012). Open circles (○) denote minerals restored to silt sizes that were disaggregrated by wet sieving. Triangles (▷) denote minerals introduced at clay sizes as suggested by measurements at Tinfou, Morocco during SAMUM (Kandler et al., 2009).

Mineral	Disturbed soil		Undisturbed soil &dust	
	Clay	Silt	Clay	Silt
Illite	●		●	○
Kaolinite	●		●	○
Smectite	●		●	○
Quartz	●	●	●	●
Carbonates	●	●	●	●
Gypsum		●	▷	●
Feldspar		●	▷	●
Iron Oxides	⋆	●	⋆	●

Table 3. Soil texture classes with sand, silt, and clay percentages, and clay (s^c) and silt (s^s) mass fractions (relative to clay plus silt) in the Hybrid STATSGO/FAO soil texture data base that are used for the derivation of the mineral fractions.

Class	Texture	Sand (%)	Silt (%)	Clay (%)	s^c	s^s
1	Sand	92	5	3	0.38	0.62
2	Loamy Sand	82	12	6	0.33	0.67
3	Sandy Loam	58	32	10	0.24	0.76
4	Silt Loam	17	70	13	0.16	0.84
5	Silt	10	85	5	0.06	0.94
6	Loam	43	39	18	0.32	0.68
7	Sandy Clay Loam	58	15	27	0.64	0.36
8	Silty Clay Loam	10	56	34	0.38	0.62
9	Clay Loam	32	34	34	0.5	0.5
10	Sandy Clay	52	6	42	0.88	0.12
11	Silty Clay	6	47	47	0.5	0.5
12	Clay	22	20	58	0.74	0.26

Table 4. Size categories for dust transported in ~~ModelE~~ModelE2. k-index is subscript denoting the particle size of the soil and emitted mass fractions. Note that the sixth size category (comprised of the largest particles) is not transported, and exists solely to match the diameter range corresponding to the MMT.

Diameter (μm)	k-index
Clay	
0.1–2	1
Silt	
2–4	2
4–8	3
8–16	4
16–32	5
32–50	6

Table 5. List of symbols used to represent mass fractions of soil and emitted minerals (Sect. 2.2.1).

~~a~~ α	soil type
~~b~~ β	soil texture
s^{c}	mass fraction of clay-sized soil particles relative to total clay and silt (Table 3)
s^{s}	mass fraction of silt-sized soil particles relative to total clay and silt (Table 3)
f_n^{c}	mass fraction of soil mineral n (relative to clay-sized minerals)
f_n^{n}	mass fraction of soil mineral n (relative to silt-sized minerals)
s_n^{c}	mass fraction of soil mineral n at clay sizes
s_n^{s}	mass fraction of soil mineral n at silt sizes
~~d^{c}~~ a^{c}	mass fraction of emitted clay-sized dust
~~d^{s}~~ a^{s}	mass fraction of emitted silt-sized dust
~~d_n^{c}~~ a_n^{c}	mass fraction of emitted mineral n at clay sizes
~~d_n^{s}~~ a_n^{s}	mass fraction of emitted mineral n at silt sizes
~~$a_{n,k}^{\mathsf{s}}$~~	mass fraction of emitted mineral n within the silt size category k (for $k = 2, \ldots 6$)
γ	parameter controlling reaggregation of emitted silt particles from wet-sieved clay particles
η	parameter related to reaggregation
~~ψ_n~~	ratio of the emitted clay-sized mass fraction to the emitted silt fraction for feldspar and gypsum
$m_{n,k}$	mass fraction of mineral n within size category k (normalized using only silt sizes)

Table 6. List of symbols used to represent mixtures of iron oxide and other minerals (Sect. 2.2.2).

~~$d_{n,k}$~~ $a_{n,k}$	mass fraction of mineral n in size class k ($a_{n,1} = a^{\mathsf{c}}_n$, $a_{n,k} = a^{\mathsf{s}}_{n,k}$ for $k = 2, \ldots 6$)
~~$d^{\mathsf{pure}}_{n,k}$~~ $a^{\mathsf{pure}}_{n,k}$	mass fraction of uncombined mineral n in size class k (excluding iron oxide)
~~$d^{\mathsf{mix}}_{n,k}$~~ $a^{\mathsf{mix}}_{n,k}$	mass fraction of mineral n with mixed with iron oxide
~~$d_{\mathsf{Fe},k}$~~ $a_{\mathsf{Fe},k}$	mass fraction of iron oxide in size class k
~~$d^{\mathsf{pure}}_{\mathsf{Fe},k}$~~ $a^{\mathsf{pure}}_{\mathsf{Fe},k}$	mass fraction of pure crystalline iron oxide k
~~$d^{\mathsf{mix}}_{\mathsf{Fe},k}$~~ $a^{\mathsf{mix}}_{\mathsf{Fe},k}$	mass fraction of iron oxide mixed with other minerals
~~$d^{\mathsf{mix}}_{\mathsf{Fe}\|n,k}$~~ $a^{\mathsf{mix}}_{\mathsf{Fe}\|n,k}$	mass fraction of iron oxide mixed with mineral n
ϵ	fraction of iron oxide not available for mixing
ϵ_0	Coefficient of proportionality between ~~$d_{\mathsf{Fe},k}$~~ $a_{\mathsf{Fe},k}$ and ϵ
R	fraction of mixed particle mass contributed by iron oxide
~~$\overline{d}_k$~~ $\overline{a}_k$	mass fraction of all non-iron oxide minerals in size class k

Table 7. Globally averaged dust emission, load and lifetime. The number in parentheses is one SD of interannual variability

	SMF		AMF	
Emission [Tg a^{-1}]				
Clay (0–2 µm)	920		44	
Silt (2–16 µm)	657		1049	
Total (<16 µm)	1577	($\pm$70)	1094	($\pm$49)
Silt (16–32 µm)	647		1131	
Total (<32 µm)	2224	($\pm$100)	2224	($\pm$100)
Load [Tg]				
Clay (0–2 µm)	14.60		0.71	
Silt (2–16 µm)	4.66		7.31	
Total (<16 µm)	19.26	($\pm$0.73)	8.02	($\pm$0.29)
Silt (16–32 µm)	0.46		0.81	
Total (<32 µm)	19.72	($\pm$0.74)	8.83	($\pm$0.31)
Lifetime (<16 µm) [d]				
Emission	4.45		2.68	
Wet Deposition	8.35		8.87	
Gravitational Settling	19.05		5.07	
Turbubulent Deposition	20.44		16.35	
Lifetime (<32 µm) [d]				
Emission	3.24		1.45	
Wet Deposition	8.41		9.08	
Gravitational Settling	7.40		1.98	
Turbubulent Deposition	19.23		14.01	

Table 8. Mineral densities in $10^3\,\mathrm{kg\,m^{-3}}$. The densities of illite and smectite are an average of their individual values, since they are often found interleaved. Feldspar density is taken from plagioclase. The iron oxide density is an average of hematite and goethite. The densities were taken from http://www.mindat.org and http://www.webmineral.com.

Mineral	Density
Illite	2.57
Kaolinite	2.63
Smectite	2.57
Calcite	2.71
Quartz	2.67
Feldspar	2.68
Iron oxides	4.77

Table 9. List of experiments. (SD = size distribution)

Experiment Name	Comment
SMF	Control (no reaggregation; emitted SD from local soil texture)
AMF	Default reaggregation parameter ($\gamma = 2$); emitted SD from measurements
AMF ($\gamma = 0$)	No reaggregation
AMF ($\gamma = 3.5$)	Increased reaggregation
AMF-NoFeAcc	No internal mixtures of iron oxide with other minerals ($\gamma = 2$)
SMF-NoClayFe	No clay-sized iron oxide

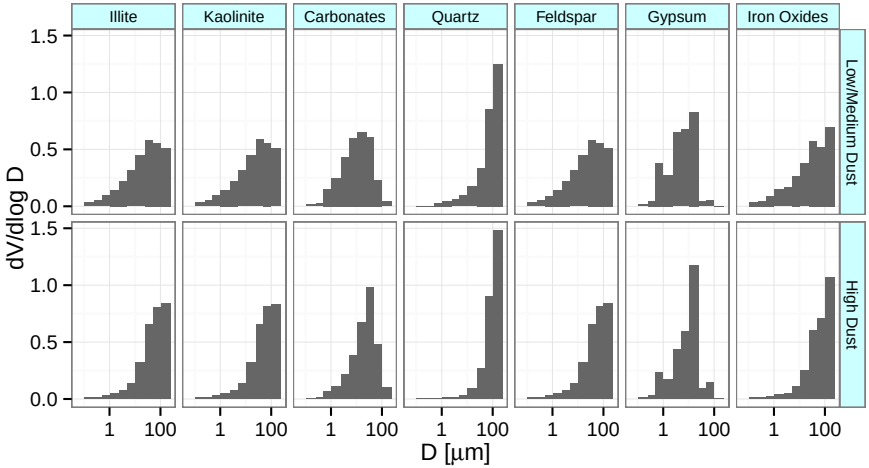

Figure 1. Volume distribution of minerals with respect to particle diameter, calculated ~~from~~as described in the Supplement, using size-resolved ~~measurements of~~ dust number and volume fraction measured by Kandler et al. (2009). ~~(Phyllosilicates and feldspar are assumed by that study to have identical volume fractions due to the similar measurement properties of these minerals.)~~ The size bins correspond to the following range of particle diameter (µm): 0.1–0.25; 0.25–0.5; 0.5–1.0; 1.0–2.5; 2.5–5.0; 5.0–10.0; 10.0–25.0; 25.0–50.0; 50.0–100.0.; 100.0–250.0. Upper panel: low/medium dust concentration; lower panel: high dust concentration. The size distribution is normalized so that the total volume is unity for each mineral.

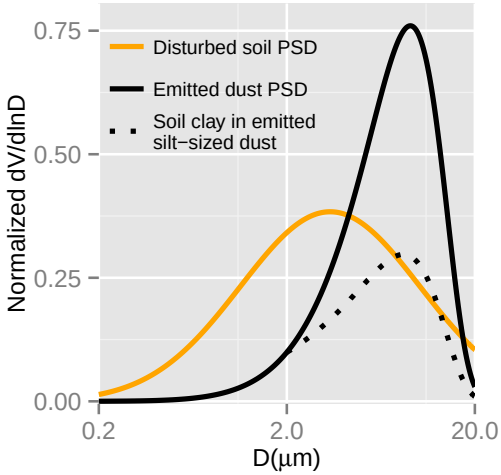

Figure 2. Size distribution of emitted dust (black line) derived from Eq. (~~1~~2) with $\lambda = 12\,\mu\text{m}$ (Kok, 2011b). The orange curve describes the arid dispersed soil used in the calculation of $U(D)$ in Eq. (~~1~~2), and is represented by a monomodal log-normal distribution with a volume median diameter of 3.4 µm and geometric SD of 3.0. Both curves are and normalized over the range 0–20 µm. The dotted line represents the contribution of dispersed soil clay particles to silt-sized dust aggregates calculated with Eq. (~~1~~2) and in this example contributes 45 % of the emitted silt.

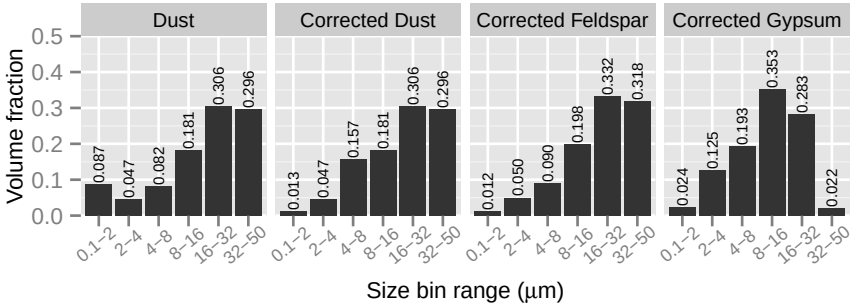

Figure 3. (From left to right) Distribution of dust volume calculated ~~from measurements~~ by ~~Kandler et al. (2009)~~summing minerals in Fig. 1; same but with corrected ratio of clay to silt (up to 20 μm) using Eq. (~~1~~2) (cf. Kok, 2011b); distribution of feldspar volume ~~calculated from measurements by Kandler et al. (2009)~~in Fig. 1, but with same correction based on Kok (2011b); same for gypsum. Each distribution is projected onto the ~~ModelE~~ ModelE2 transport bins (Table 4). A fifth "virtual" transport bin for diameters between 32 and 50 μm is added so that the total diameter range corresponds to that of the MMT. Each distribution is normalized over the entire diameter range.

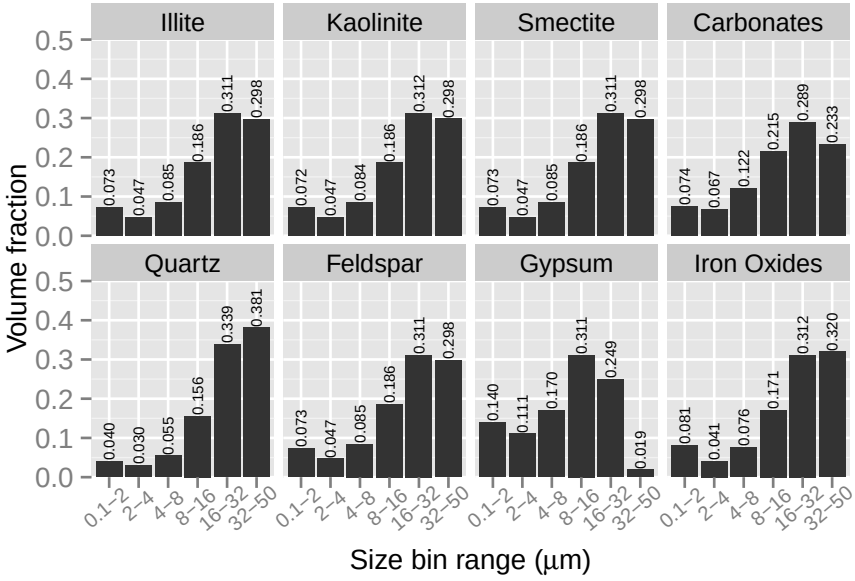

Figure 4. Fractional distribution of volume within the ~~ModelE~~ModelE2 size bins for the minerals in Table 2, calculated ~~from measurements~~ by ~~Kandler et al. (2009)~~interpolating the distributions in Fig. 1. A fifth "virtual" transport bin for diameters between 32 and 50 µm is added so that the total diameter range corresponds to that of the MMT. The distribution of each mineral is normalized separately over the entire diameter range.

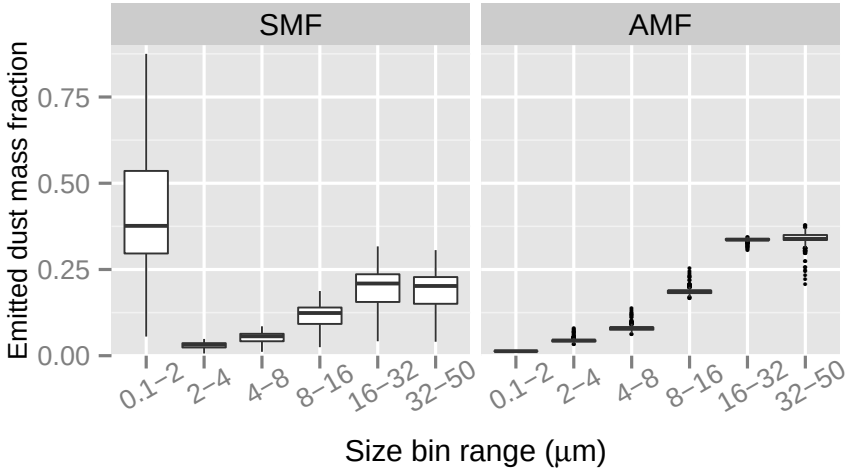

Figure 5. The distribution of the emitted dust ~~volume~~mass fraction ~~over the ModelE~~at each ModelE2 size ~~bins~~bin for the soil mineral fraction (SMF) method (left) and the aerosol mineral fraction (AMF) method (right). Within each size bin, the box plots ~~depict variations related~~depicts the distribution with respect to the combinations of the 12 soil ~~texture~~textures and the 28 arid soil types included in the MMT. For each combination, the sum over all sizes is one. At each bin, each combination within the distribution is weighted by the total emission (~~at~~summed over all sizes) to emphasize prolific sources. Each box shows the range in which the central 50 % of the data fall. The box borders show the first and third quartiles and the crossbar shows the median. Outliers exceeding the quartile values by more than a factor of 1.5, the interquartile distance, are marked as points. Note that only diameters below 32 μm are transported by the model.

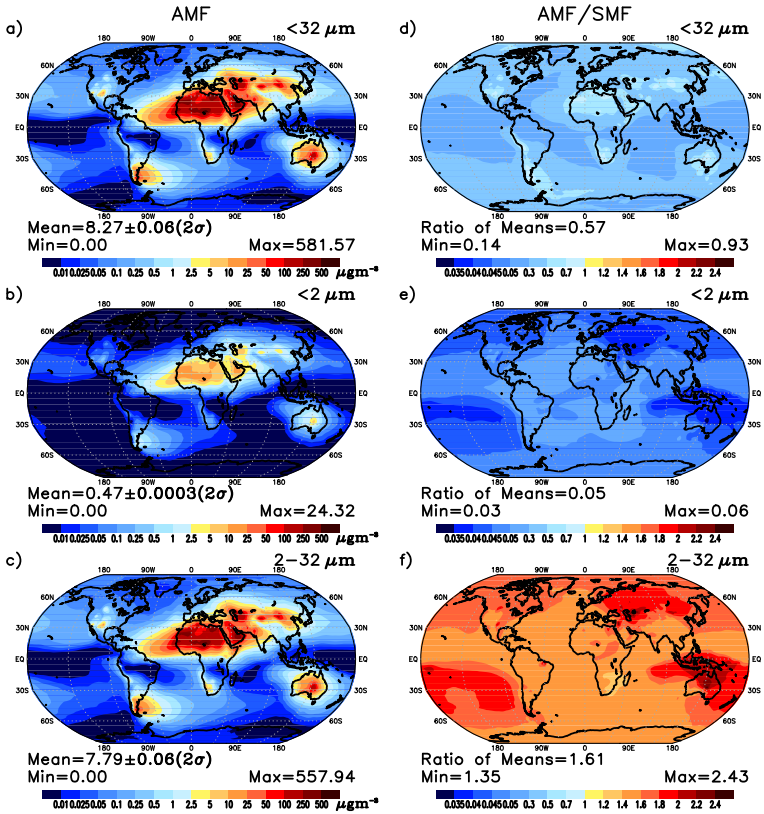

Figure 6. (Left panels) Annual-average surface concentration (summed over all minerals) for the AMF method and (right panels) the ratio of the AMF and SMF concentrations for: **(a, d)** total dust; **(b, e)** clay-sized dust; and **(c, f)** silt-sized dust.

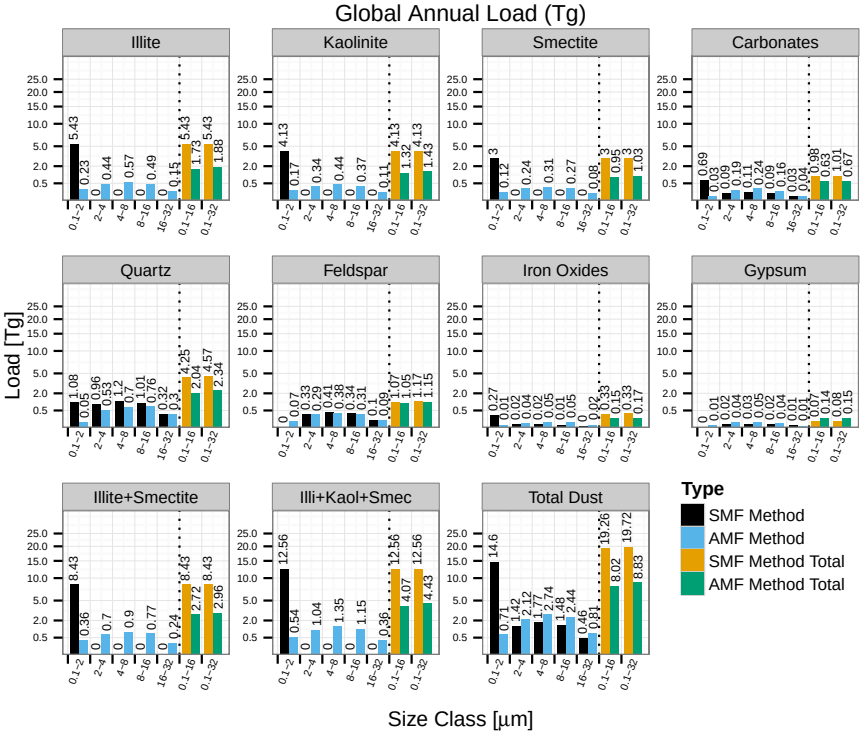

Figure 7. Global annual load (Tg) for the AMF and SMF experiments.

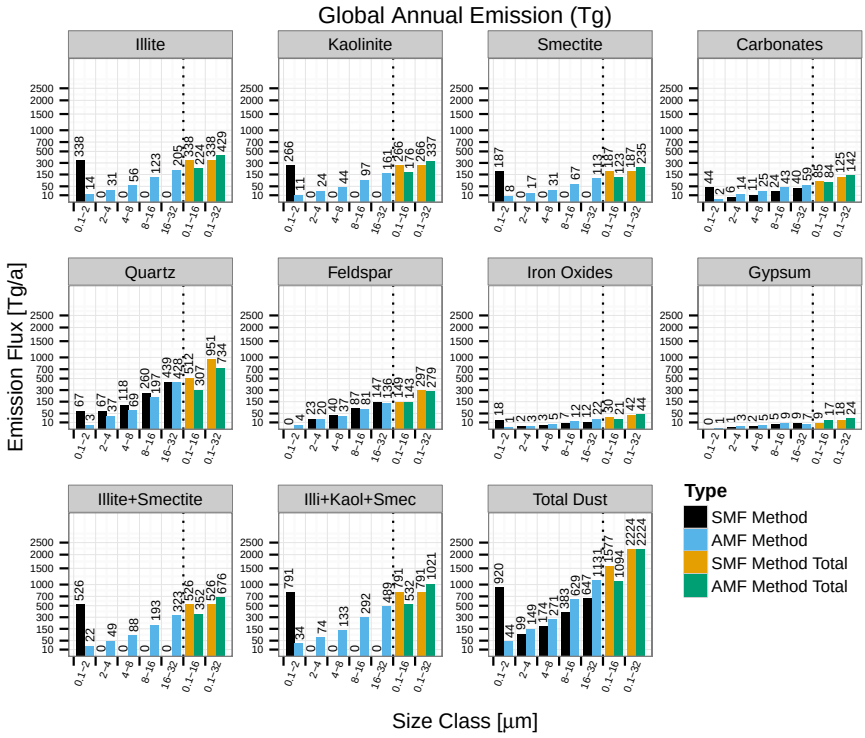

Figure 8. Global annual emission (Tg) for the AMF and SMF experiments.

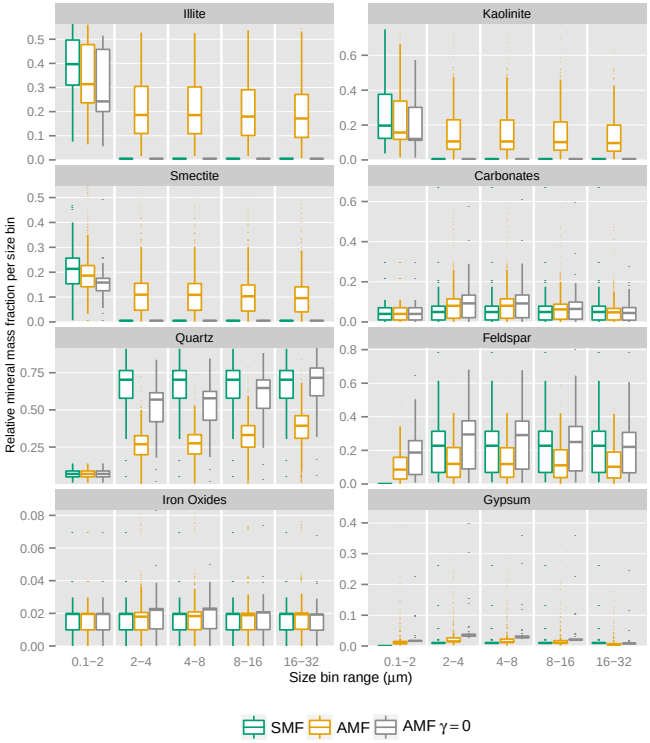

Figure 9. ~~Relative~~The distribution of the emitted mass fraction of each mineral ~~in~~at each ModelE2 size bin for the soil mineral fraction (SMF) method (~~left panels~~green)~~and~~ , the aerosol mineral fraction (AMF) method (orange), and the AMF method with $\gamma = 0$ (black). The box plots are constructed as in Fig. 5, but the emitted mineral fractions sum to unity within each *separate* size bin, to identify the mineral making the largest contribution to emission at that size.

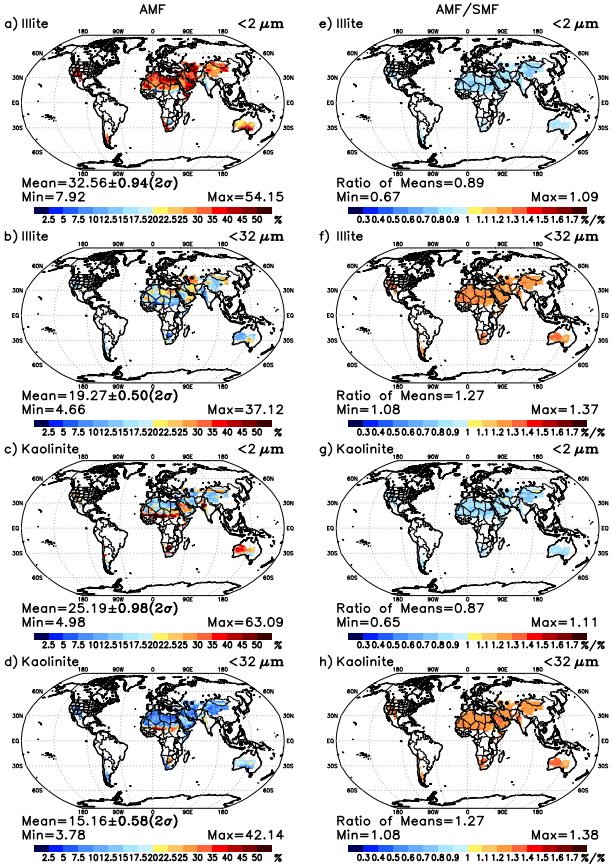

Figure 10. ~~**Figure 11.**~~ Annual-average fraction of emission of **(a, b)** illite and **(c, d)** kaolinite at clay and all sizes for the aerosol mineral fraction (AMF) method. The right column shows the ratio of fractional emission for the AMF and soil mineral fraction (SMF) methods for **(e, f)** illite and **(g, h)** kaolinite.

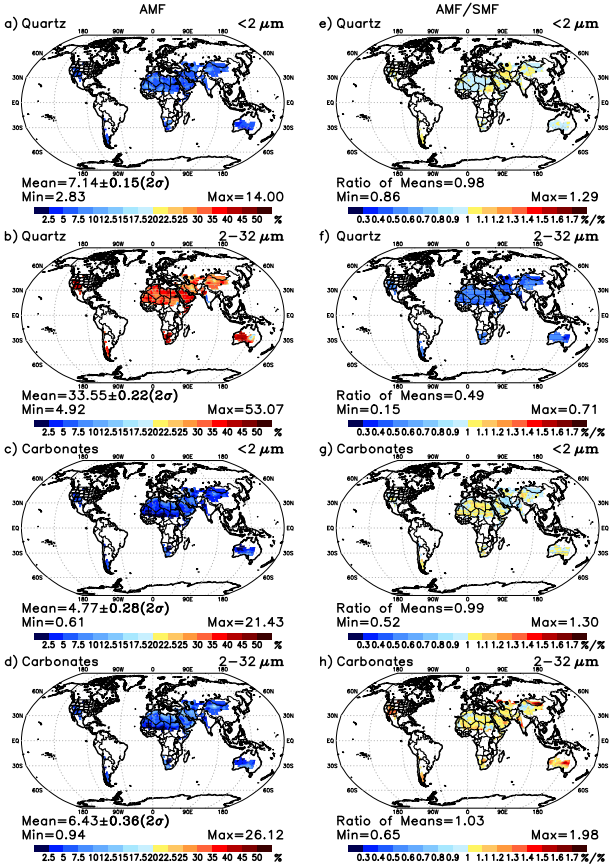

Figure 11. ~~**Figure 12.**~~ Fractional emission as in Fig. ~~11~~**10** but for clay and silt-sized quartz and carbonates.

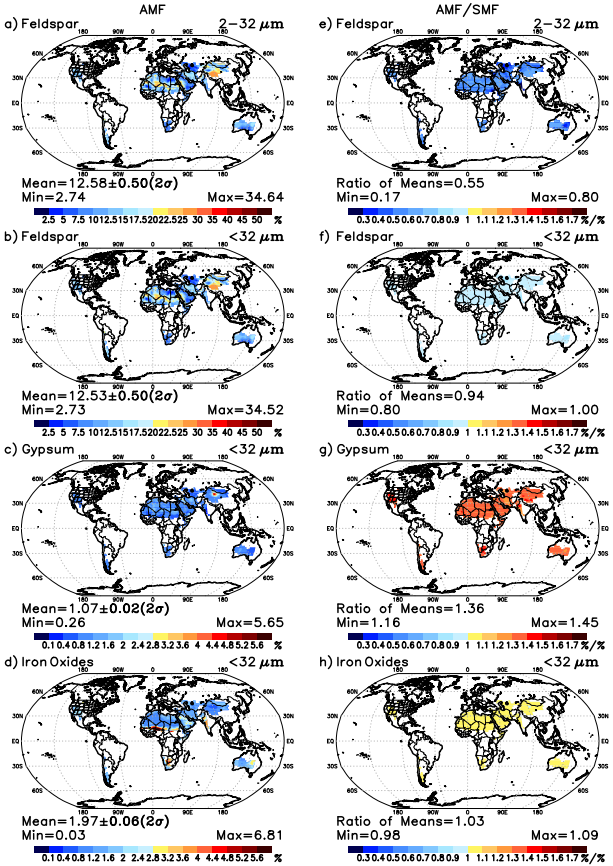

Figure 12. ~~**Figure 13.**~~ Fractional emission as in Fig. ~~11~~10 but for feldspar (silt-sized and total), gypsum and iron oxides.

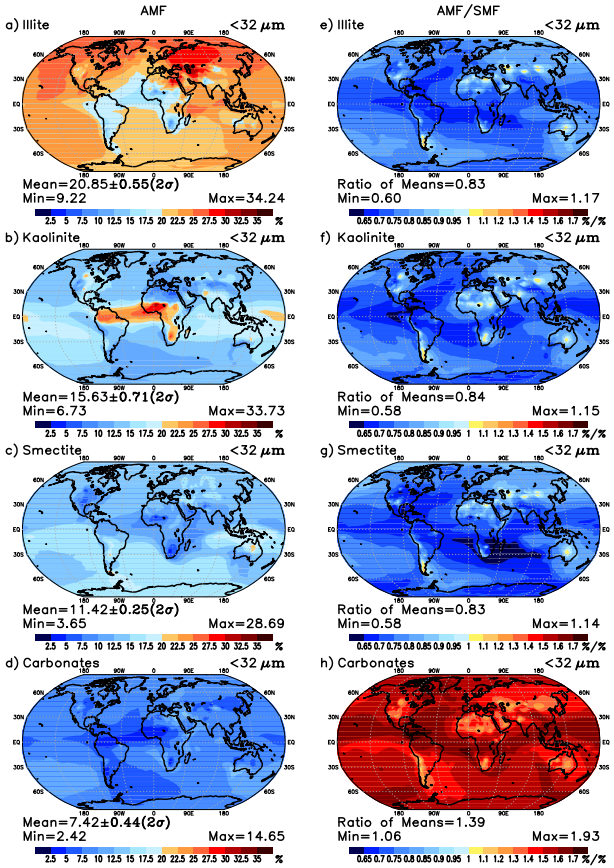

Figure 13. ~~**Figure 14.**~~ Annual-average fraction of surface concentration for **(a)** illite, **(b)** kaolinite, **(c)** smectite, and **(d)** carbonates for the AMF method. The right column shows the ratio between the AMF and the SMF fractions for **(e)** illite, **(f)** kaolinite, **(g)** smectite, and **(h)** carbonates.

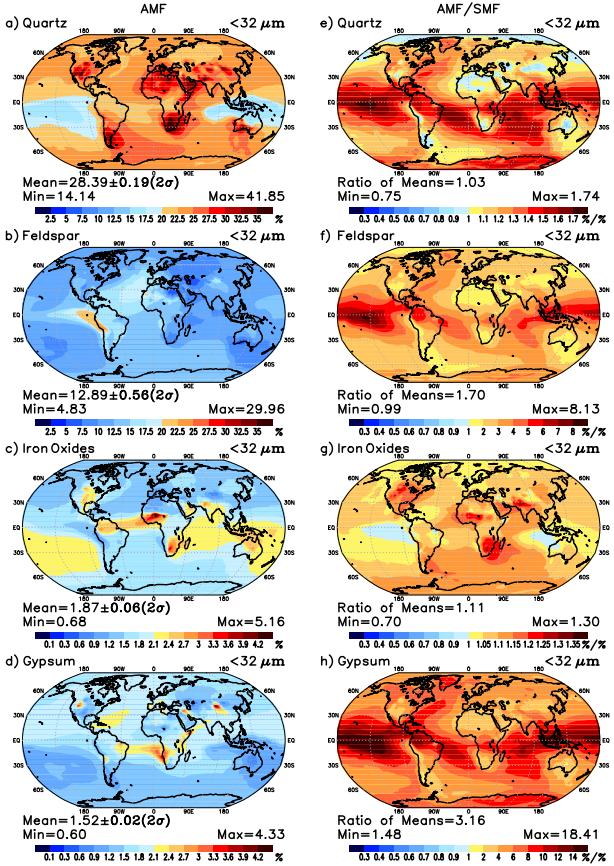

Figure 14. ~~**Figure 15.**~~ Fractional surface concentration as in Fig. ~~14~~13 but for **(a, e)** quartz, **(b, f)** feldspar, **(c, g)** iron oxides, and **(d, h)** gypsum. Note that the color scale varies among panels to represent regional variations in mineral fractions.

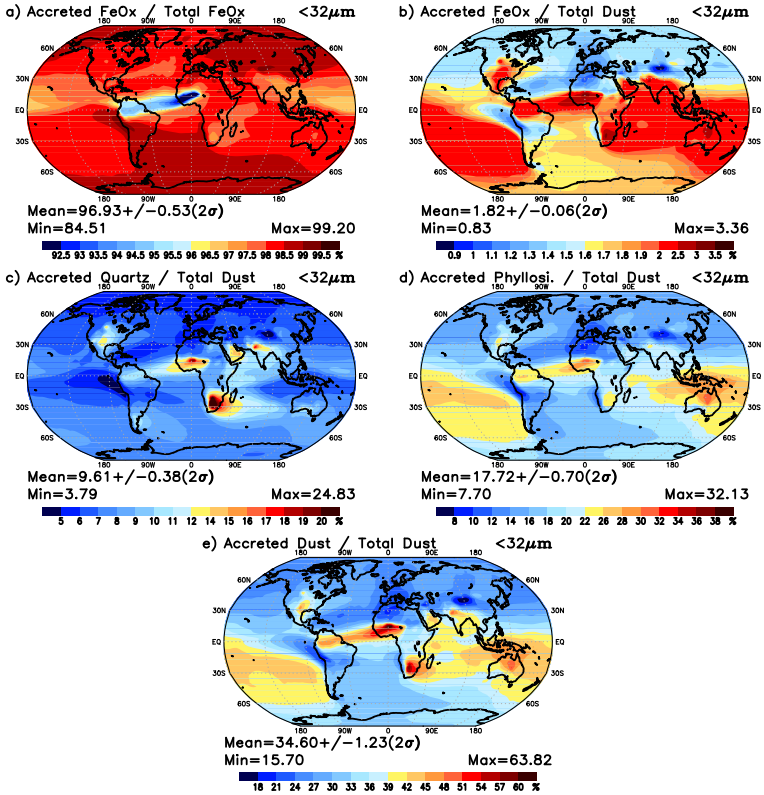

Figure 15. ~~**Figure 16.**~~ Annual-average column mass fraction of **(a)** accreted iron oxide relative to total iron oxide, and (relative to total dust) accreted **(b)** iron oxide, **(c)** quartz, **(d)** phyllosilicate (illite + kaolinite + smectite) and **(e)** dust.

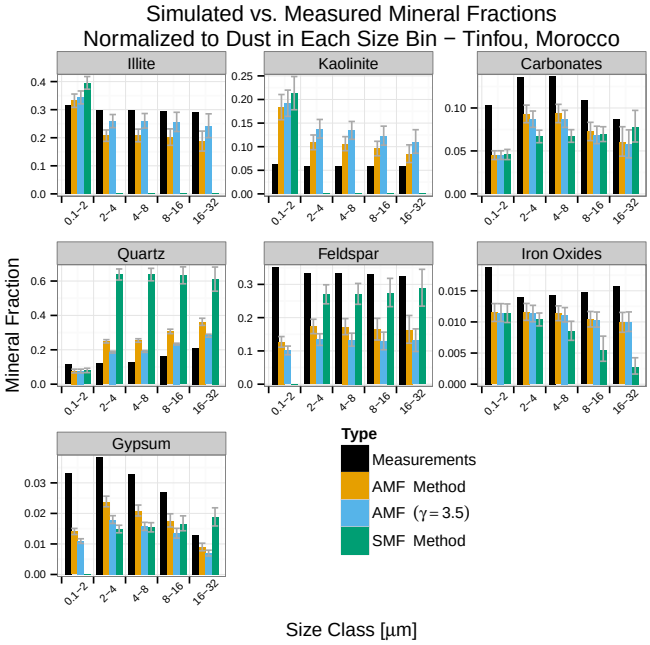

Figure 16. ~~**Figure 17.**~~ Mineral fractions of surface concentration relative to total dust concentration. Values at Tinfou, Morocco ~~. Measured values~~ are calculated from volume fractions of minerals and number of total dust particles provided by Kandler et al. (2009) along with mineral densities from Table 8, as described in the Supplement. Model values are from the SMF, AMF and AMF ($\gamma = 3.5$) experiments. The sum of mineral fractions within each size bin equals 1. Smectite is not included as it is not distinguished by the measurements. The uncertainty bars correspond to two standard errors.

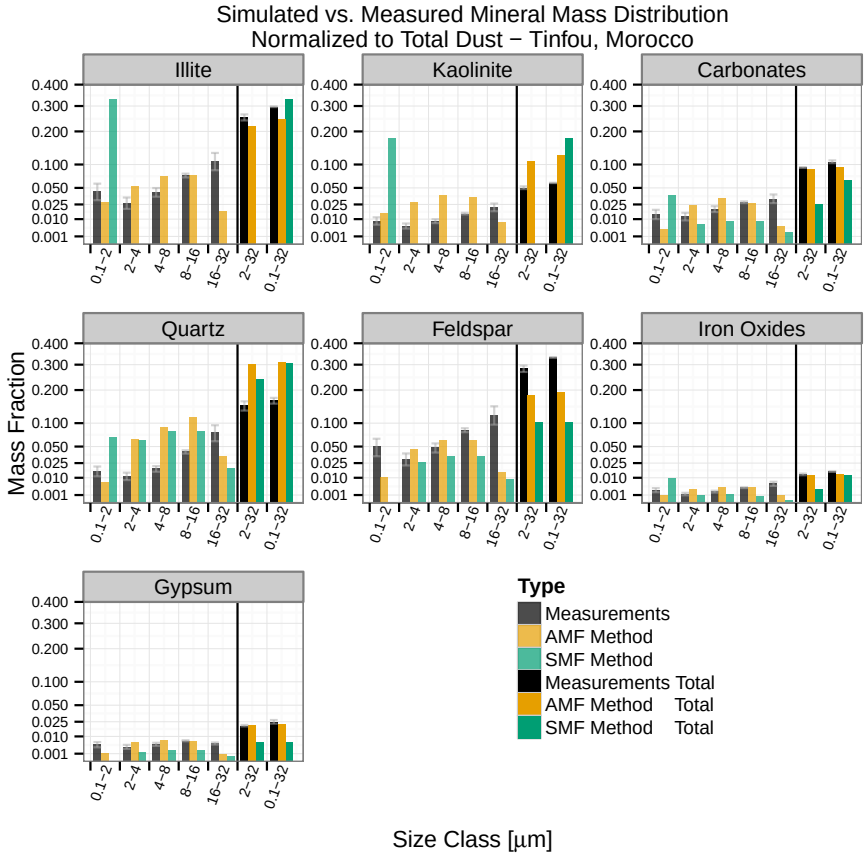

Figure 17. ~~**Figure 18.**~~ Same as Fig. ~~17~~16 but the mineral fractions are relative to the total dust concentration, so that the sum over all mineral fractions and all size bins equals 1.